NUMERICAL SIMULATION OF NONLINEAR WAVES AND SHIP MOTIONS

by

JOHN R. FITZ-CLARKE

B.A.Sc., University of British Columbia (1983)

A THESIS SUBMITTED IN PARTIAL FULFILMENT OF

THE REQUIREMENTS FOR THE DEGREE OF

MASTER OF APPLIED SCIENCE

in

FACULTY OF GRADUATE STUDIES

Department of Mechanical Engineering

We accept this thesis as conforming

to the required standard

UNIVERSITY OF BRITISH COLUMBIA

October, 1986

In presenting this thesis in partial fulfilment of the requirements for an advanced degree at the UNIVERSITY OF BRITISH COLUMBIA, I agree that the Library shall make it freely available for reference and study. I further agree that permission for extensive copying of this thesis for scholarly purposes may be granted by the Head of my Department or by his or her representatives. It is understood that copying or publication of this thesis for financial gain shall not be allowed without my written permission.

Department of Mechanical Engineering

UNIVERSITY OF BRITISH COLUMBIA
2075 Wesbrook Place
Vancouver, Canada
V6T 1W5

Date: October, 1986

ABSTRACT

A numerical method is presented for simulating the behaviour of large amplitude nonlinear free surface waves including wave breaking. Various initial conditions are given and the subsequent surface profiles are calculated by a time stepping simulation. The flow field is solved as a boundary value problem for the velocity potential using a complex variable method based on the Cauchy integral theorem. Waves of varying shape, height, and length are investigated to determine the parameters necessary for wave breaking and the resulting fluid velocities. The technique has proven to be very accurate and stable.

The method is extended to predict the motions of a two dimensional floating body in large amplitude seas accounting for non-linear effects and fluid-body interaction. The presence of singularities at the free surface intersection points was found to severely limit accuracy of the solution and attempts to overcome this problem are discussed. An extension to handle three dimensional ships is also described.

Table of Contents

LIST OF FIGURES

NOMENCLATURE

a_x, a_y = body acceleration

a_{ij} = real part of matrix element

b_{ij} = imaginary part of matrix element

c = phase velocity of wave

C = contour of integration

d = water depth

E_K = kinetic energy

E_P = potential energy

E_t = total energy

F_x, F_y = body forces

g = gravitation constant

G = centre of gravity of body

H = wave height

h_{ij} = real matrix

I = mass moment of inertia of body

k = wave number = $2\pi/L$

L = wave length

m = body mass

M = body moment about G

$\hat{n}$ = normal unit vector

N = total number of elements

NB = number of bottom elements

NH = number of hull elements

NS = number of free surface elements

NV = number of vertical side elements

P = fluid pressure

Q = volume flow rate per unit width

R = radius from G to body surface

s = arc length running variable

t = time

Δt = time step interval

T = wave period

t_B = time to wave breaking

u = horizontal fluid velocity

u_G = horizontal body velocity

v = vertical fluid velocity

v_G = vertical body velocity

V_n = normal component of body velocity

$\forall$ = volume

w = complex fluid velocity = u-iv

w^* = complex conjugate of w

x = horizontal distance

Δx = element size

y = vertical distance

z = complex spatial coordinate = x+iy

α = included angle at node

β = complex potential = $\phi+i\psi$

ϕ = velocity potential

ψ = stream function

Γ_{ij} = complex influence coefficient

ρ = fluid density

θ = roll angle

η = wave elevation above still water

Λ_{ij} = influence coefficient

Π_{ij} = influence coefficient

ω = angular frequency = $2\pi/T$

Ω = fluid domain

ACKNOWLEDGEMENT

The author would like to extend sincere thanks to his supervisor Dr. Sander M. Calisal for patient guidance throughout the course of this work. The author would also like to express his gratitude to the British Columbia Science Council and the Defence Research Establishment Atlantic, Halifax for financial support which made this work possible.

1. INTRODUCTION

1.1 INTRODUCTION

Despite advances in ship design, small vessels are still no match for rough seas and capsizings continue to occur each year with the loss of lives and property. Fundamental to reducing the risk of such tradgedies is a better understanding of the kinematics and dynamics of extreme waves and the resulting forces and response of a vessel to them.

Capsizing of a vessel may occur due to any of several phenomena including extreme rolling in beam seas, roll excited by a near-resonant encounter frequency while underway in following or quartering seas (the Mathieu effect), or broaching or pitch-poling involving steep overtaking stern waves and loss of directional stability. These phenomena frequently result in water on deck and subsequent downflooding of deck openings. Model experiments of fishing boats carried out at the B.C. Research Ocean Engineering Centre have demonstrated that extreme roll capsizing in beam seas is very unlikely for a vessel loaded within the recommended limits. No such capsizings have been observed in the basin under extensive tests involving large amplitude regular wave conditions [26]. The presence of breaking waves in the vicinity of the vessel, however, can lead to very large additional forces from the plunging jet impacting on the side, possibly sufficient to cause

capsizing. Fishermen who have survived accidents have occasionally reported being hit by "freak waves", that is one or more waves unusually larger than those in the normal preceding sea state. Such anomalous waves have indeed been documented (figure 1) and may have contributed as well to unwitnessed accidents. The present work concentrates on examining the motions of a vessel in extreme beam seas.

Current stability criteria are usually based on quasi-static definitions involving the metacentric height and critical roll angles in calm water. These rules are largely empirical and become somewhat meaningless in dynamic conditions encountered in the real sea, especially where large steep waves are involved. More recently, efforts have been made to define stability in terms of dynamic parameters but much work remains to be done. Occasionally model tests are performed when experience with a particular design is lacking, however, such tests are expensive and time consuming, and frequently limited by facility size and equipment.

The theoretical analysis of wave and body motions provides important insight into the fundamental processes involved and permits estimates of dynamic behaviour in conditions that cannot readily be tested. In addition, the relative effects of the different governing parameters can be seen and assessed in theoretical models whereas in actual model tests the influence of contributing effects usually cannot readily be decomposed.

1.2 LITERATURE SURVEY

1.2.1 WAVE SOLUTIONS

Analytical solutions to free surface waves have been developed to a fairly high degree beginning with the classical linearized theory of Airy. Stokes (1847) developed a perturbation expansion to extend the solution to finite amplitude steady waves and calculated the third order correction. To date many higher order solutions have been calculated, more recently using a computer to perform the coefficient arithmetic as by Schwartz (1974) in an attempt to find the elusive highest possible steady progressive wave. Other nonlinear theories have been developed including Dean's stream function theory for intermediate and deep water and cnoidal theory for shallow water. Each method has its limitations and the most appropriate depends on the intended application. Sarpkaya and Isaacson (1981) provide an overview of these and other wave theories.

Progress in transient wave behaviour has so far required numerical simulation on a computer. The first attempt was a marker and cell solution to the incompressible Navier Stokes equations carried out by Harlow in 1965 at the Los Alamos Laboratories. The method required unrealistically high viscosity to compensate for numerical instability and accuracy was poor. Chan and Street (1970) improved the grid adjustments and achieved a reasonable simulation of a solitary wave on a beach up to the point where the free

surface became vertical. On a separate front, Longuet-Higgins and Cokelet (1976) concentrated on the inviscid solution using a potential flow boundary integral method based on Green's theorem to simulate one wavelength of a periodic deep water breaking wave, again up to a vertical face. Further applications of their work may be found in Longuet-Higgins (1977). Vinje and Brevig (1980) extended the solution by developing a complex variable boundary integral method based on the Cauchy theorem to simulate the complete breaking wave in finite water depth including overturning of the crest. Vinje and Brevig (1981a) describe how the method might be used to numerically estimate breaking wave forces on a fixed object and some experiments to measure such forces are presented in Kjeldsen and Myrhaug (1979), and Kjeldsen (1981).

1.2.2 BODY MOTIONS

Calculation of floating body motions poses a very difficult mathematical problem owing to the complexity and nonlinearity of the governing equations. Korvin-Kroukovsky (1955) presented the coupled equations of body motion for the six degrees of freedom, however, analytical determination of forces, added masses, and damping coefficients were only crudely possible in idealized cases. Analytical solutions developed to date have invariably required some form of linearization, where body and free surface boundary conditions are applied on fixed surfaces

and body geometries are simple shapes such as circular cylinders or spheres. Examples include MacCamy (1964), Ursell (1964), Lee (1969), and Maskell and Ursell (1970). Wehausen (1971) gives an overview of these and other formulations, and additional references. Applications of these methods are, of course, limited to periodic small amplitude waves and motions. Numerical panel methods based on Green's theorem have been used by Kim (1966), and Garrison (1975) to handle the linearized, steady harmonic motions of arbitrarily shaped bodies.

The methods described so far are frequency-domain techniques which predict the response in regular monochromatic waves. For the more general wave conditions a transfer function can be constructed and used to obtain a frequency spectrum of motions given an input spectrum of the sea state. Statistical quantities can then be estimated. These techniques are necessarily linear, yet can provide reasonable results in waves that are not too large, and are widely used in practice. Details may be found in Bhattacharyya (1979) and Newman (1980).

The calculation of transient nonlinear motions again requires application of a numerical time-stepping simulation from given initial conditions. Examples include Faltinsen (1977), Chapman (1979), and Isaacson (1982). Vinje and Brevig (1981b,c) extended their nonlinear wave simulation technique to include the presence of an arbitrary two dimensional floating body and describe its application to a

heaving cylinder. Greenhow, Brevig, and Taylor (1982) applied the method to study the extreme motions of a rotating wave energy device, however, free surface behaviour near the body had to be specified empirically. Very few quantitative results of body motion simulations have been presented in the literature making comparisons with previous work difficult. Several problems have yet to be overcome involving the choice of initial conditions and the presence of singular points where the body intersects the free surface. This thesis addresses these problems, and various attempts to handle them are discussed.

1.3 OBJECTIVES

A theoretical model for predicting ship motions must solve for the coupled body motions and fluid behaviour. An exact solution including small scale fluid motions and viscous effects is beyond the state of the art and various approximations must be made to keep the mathematics tractible and within the capacity of available computing resources. The usual assumptions are that the fluid is incompressible and inviscid and thus satisfies Laplace's equation for a velocity potential.

The first task in the present work is to develop a numerical technique for solving Laplace's equation and calculating the velocity potential in a general two dimensional fluid domain under arbitrary boundary conditions using a complex variable boundary integral method. This

Laplace solving routine is then used to calculate the fluid velocities of a free surface wave at discrete time intervals and allow a time-stepping simulation of the behaviour of an arbitrary wave up to and including breaking. The effect of different initial wave conditions can then be assessed to establish a domain of dependence of breaking waves and the detailed kinematics of the flow development. Finally, the wave simulation technique is extended to permit the inclusion of an arbitrary two dimensional body on the free surface. Fluid velocities and pressures are calculated around the body at each time step to determine the resulting hydrodynamic forces. The equations of rigid body motion are then integrated at each time step to calculate a time history of the nonlinear body response in the wave field.

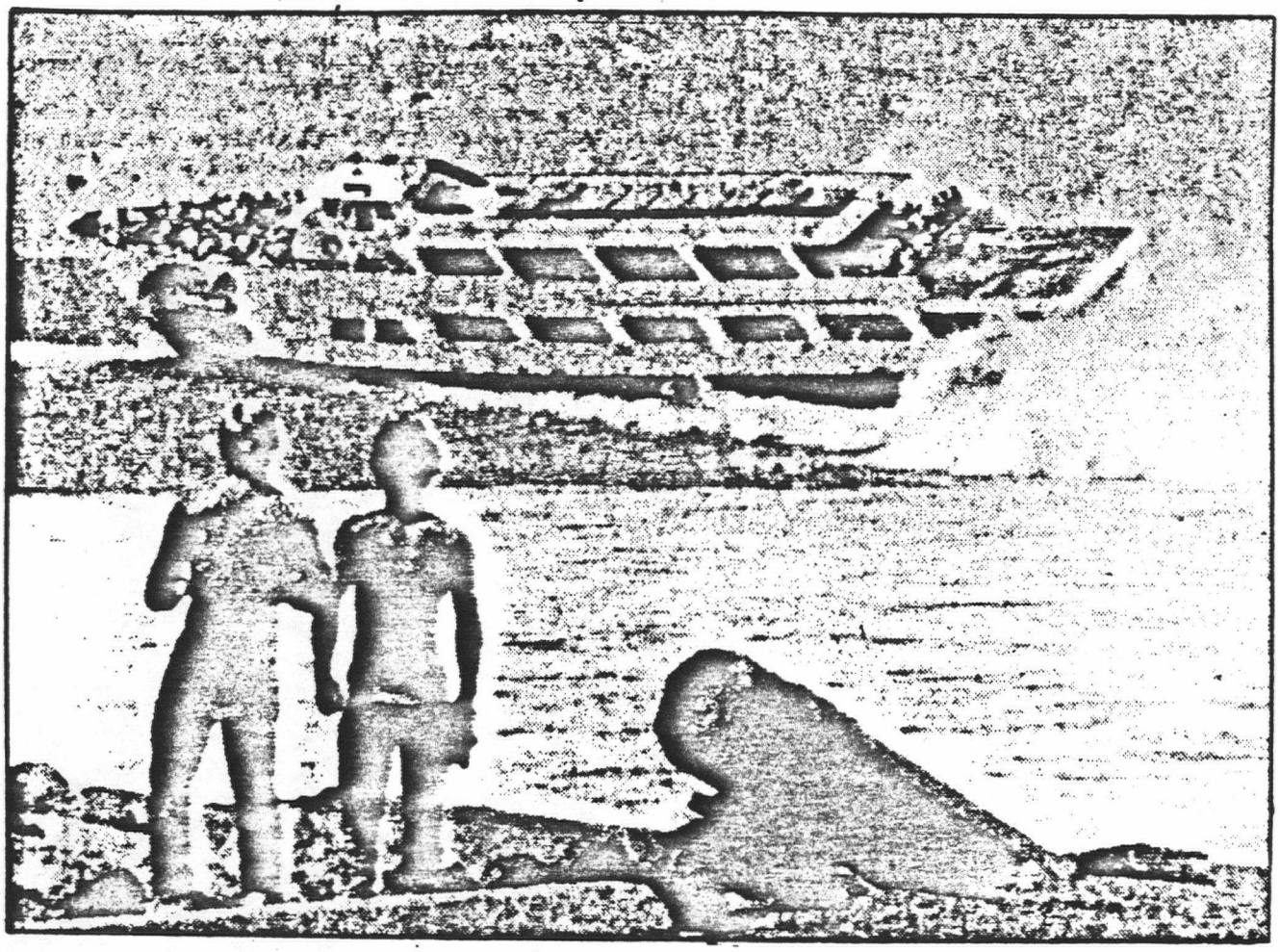

Figure 1. Tour ship being buffetted by "freak waves".

2. POTENTIAL FLOW SOLUTION

2.1 INTRODUCTION

The exact calculation of an arbitrary flow field including viscous and turbulent effects is an extremely difficult task due to the complexity of the governing Navier-Stokes equations and can only be done in very limited cases. In general, one must make assumptions that simplify the problem and permit a tractible mathematical solution. The usual assumptions are that the fluid is incompressible and irrotational, the latter a consequence of neglecting the effects of viscosity. These two conditions dictate that the flow field satisfies Laplace's equation

$$\nabla^2\phi = 0 \tag{2.1}$$

or in Cartesian coordinates

$$\frac{\partial^2\phi}{\partial x^2} + \frac{\partial^2\phi}{\partial y^2} = 0$$

for a scalar velocity potential ϕ. Velocities are then found as the gradient of ϕ. The problem is completed by specifying the appropriate boundary conditions and solving the resulting boundary value problem.

Analytical solutions to (2.1) are possible in many cases using classical methods such as separation of variables, linear superposition of sources and vortices, perturbation methods, and conformal mappings, however, for transient problems involving complicated geometries and boundary conditions one must resort to a numerical

procedure. Several numerical methods have been developed over the years to solve Laplace's equation including the traditional finite difference and finite element methods which solve for the potential along a grid of discrete interior points. More recently, attention has turned to boundary integral methods which have the powerful advantage that the values of ϕ and an orthogonal function are calculated only on the domain boundary. The problem is thereby reduced by one dimension allowing much greater resolution for a given computational effort. Element generation is also greatly simplified. Furthermore, in many problems of fluid dynamics one is interested only in the fluid velocities and pressures at the boundary. The interior flow field can be found if desired knowing only the boundary values, however, this is usually of little practical interest.

The method used in this work is a complex variable boundary integral method based on the Cauchy integral theorem.

2.2 CAUCHY INTEGRAL METHOD

2.2.1 FORMULATION

The objective of the numerical procedure is to obtain ϕ values around the contour C, however, this alone is insufficient to determine velocities at the boundary since differentiaton along C provides only the tangential

velocity. The normal component must also be determined, consequently one must evaluate an orthogonal function along the boundary as well. Green's function approaches carry out the calculations for ϕ and $\partial\phi/\partial n$, while the current approach solves for the velocity potential ϕ and the stream function ψ. The normal velocity at the boundary can then be found by differentiating ψ along the contour since, by the Cauchy-Riemann property,

$$\frac{\partial \psi}{\partial s} = \frac{\partial \phi}{\partial n}$$

The stream function can also be shown to satisfy Lapalace's equation

$$\nabla^2 \psi = 0$$

hence both ϕ and ψ are harmonic functions. By defining a complex potential

$$\beta = \phi + i\psi$$

the problem reduces to one of finding the function β that is analytic in the domain Ω of the complex plane z=x+iy, and satisfies the boundary conditions of ϕ or ψ given.

Since β is required to be analytic, it must satisfy the well-known Cauchy integral theorem [9]

$$\oint_C \frac{\beta}{z-z_0}\, dz = 0 \qquad (2.2)$$

provided z_0 is outside the contour C. If z_0 is allowed to

approach C in the limit, this equation becomes

$$\oint_C \frac{\beta}{z-z_0}\,dz = i\,\alpha\,\beta(z_0)$$

with z_0 on C. Derivation of this expression can be found in Appendix I. β must be found that satisfies this integral equation.

To solve (2.2) numerically, the contour C is discretized into N linear elements bounded by nodal points at each end. The integral can then be represented as the sum of the integrals over each element

$$\sum_{j=1}^{N} \left\{ \int_{z_j}^{z_{j+1}} \frac{\beta}{z-z_0}\,dz \right\} = i\,\alpha\,\beta(z_0) \qquad (2.3)$$

A linear variation of β is assumed over each element (a higher order polynomial distribution could be used, however this has not been found necessary). Defining upper and lower nodal values as z_j, z_{j+1}, β_j, and β_{j+1} as in figure 3, the distribution of β on the element can be expressed as

$$\beta = \left(\frac{z-z_j}{z_{j+1}-z_j}\right)\beta_{j+1} + \left(\frac{z_{j+1}-z}{z_{j+1}-z_j}\right)\beta_j \qquad z_j \leqslant z \leqslant z_{j+1}$$

This expression is then substituted into the lefthand side of (2.3). β_j are constants so they can be removed from the integrals and the remaining kernel functions evaluated. After algebraic manipulation the integral equation (2.2) reduces to the linear equation

$$\sum_{j=1}^{N} \Gamma_j \beta_j = 0$$

By letting each node take on the value z_o in turn, one can obtain N complex equations for N unknown β

$$\sum_{j=1}^{N} \Gamma_{ij} \beta_j = 0 \qquad (2.4)$$

where the influence coefficients are

$$\Gamma_{ij} = \left(\frac{z_i - z_{j-1}}{z_j - z_{j-1}}\right) \ln \left(\frac{z_j - z_i}{z_{j-1} - z_i}\right) + \left(\frac{z_{j+1} - z_i}{z_{j+1} - z_j}\right) \ln \left(\frac{z_{j+1} - z_i}{z_j - z_i}\right)$$

$$= \left(\frac{z_{j+1} - z_{j-1}}{z_{j+1} - z_j}\right) \ln \left(\frac{z_{j+1} - z_{j-1}}{z_j - z_{j-1}}\right) \qquad i=j-1$$

$$= \ln \left(\frac{z_{j+1} - z_j}{z_{j-1} - z_j}\right) \qquad i=j$$

$$= \left(\frac{z_i - z_{j-1}}{z_j - z_{j-1}}\right) \ln \left(\frac{z_j - z_{j+1}}{z_{j-1} - z_{j+1}}\right) \qquad i=j+1$$

Details can be found in Appendix II. Care must be exercised in evaluating the term Γ_{ii} to avoid problems with the multiple-valued complex logarithm function as described in Appendix III.

2.2.2 BOUNDARY CONDITIONS

Since Laplace's equation is elliptic in nature, each point affects every other point and boundary conditions must be specified on all boundaries. Due to linearity, problems can also be handled where the boundary conditions on segments are linearly related such as being proportional or

equal by lumping together the unknown quantities appropriately in the final linear equations.

The solution of Laplace's equation is unique only to within an arbitrary constant. For example if $\beta(z)$ is a solution then so is $\beta(z) + \beta_0$ where β_0 is any constant. The numerical method does not generate this constant and thereby fix the unique solution, consequently the boundary conditions given must include contributions from both ϕ and ψ to eliminate any ambiguity.

2.2.3 SOLUTION

Defining $\Gamma_{ij}=a_{ij}+ib_{ij}$, equation (2.4) can be written as

$$\sum_{j=1}^{N} (a_{ij} + i\, b_{ij})(\phi_j + i\, \psi_j) = 0$$

with the real part

$$\sum_{j=1}^{N} (a_{ij}\phi_j - b_{ij}\psi_j) = 0$$

and the imaginary part

$$\sum_{j=1}^{N} (a_{ij}\psi_j + b_{ij}\phi_j) = 0$$

It is clear now that while there are N unknown quantities (either ϕ_j or ψ_j at each node) there are actually 2N real equations available. The problem is overspecified and one must make a choice as to which N equations to satisfy.

Selection of only the real parts provides a satisfactory solution, as does selection of only the imaginary parts, albeit slightly different, however an improved solution is possible if one selects the real part for equation i when ϕ_i is the unknown quantity and the imaginary part when ψ_i is unknown. Such selection will ensure that only the inhomogeneous integral equations are being chosen in each case and one would expect a more stable solution as a result. Recently, Schultz et al (1986) formulated a solution utilizing all 2N equations which are solved in a least squares sense, resulting in a further improvement.

The N selected equations contain the unknown values X_j as well as terms involving the known boundary conditions. If these latter terms are transposed to the righthand side and summed one obtains a set of N linear equations for N unknowns which can be solved in matrix form as

$$\sum_{j=1}^{N} h_{ij} X_j = g_j$$

The complete solution β_j is constructed by combining the calculated X_j with the known boundary conditions as shown in figure 5.

2.2.4 VELOCITIES

Once β has been calculated on the boundary, the velocitites can be determined as

$$w = u - iv = \frac{\partial \beta}{\partial z} \tag{2.5}$$

The derivative of a complex function is independent of direction so this differentiation can be carried out along the contour C. Since β has been assumed piecewise linear, $\partial\beta/\partial Z$ is discontinuous at the nodal points. A central difference scheme is used based on a Taylor series expansion of β about the point of evaluation. Details may be found in Appendix IV.

2.2.5 INTERIOR

The method presented allows calculation of β only on the boundary C. For practical purposes this is usually sufficient since often one is only intetrested in the velocities and pressures on the bounding surfaces. The interior flow field can be found however, if desired, by reapplying Cauchy's theorem as

$$\beta(z_k) = \frac{1}{2\pi i} \oint_C \frac{\beta}{z - z_k} \, dz$$

and

$$w(z_k) = \frac{1}{2\pi i} \oint_C \frac{\beta}{(z - z_k)^2} \, dz$$

The integrals here can again be evaluated numerically as linear sums involving the known nodal values β_j in a similar fashion as before resulting in equations of the form

$$\beta(z) = \sum_{j=1}^{N} \Lambda_{ij}\beta_j$$

and

$$w(z) = \sum_{j=1}^{N} \Pi_{ij}\beta_j$$

where the influence coefficients are functions of the contour geometry z_j. Interior values calculated as such are not used in the present work.

2.3 TEST CASE

The Cauchy integral method provides a powerful technique for solving an interior flow field that can be cast into the form of a mixed boundary value problem involving ϕ and ψ.

To test the method an example is chosen of uniform flow past a circular cylinder as in figure 5, the analytical solution of which is well known. The velocity potential can be shown to be

$$\beta(z) = U(z + \frac{R^2}{z})$$

with the origin at the centre of the cylinder, and the velocity

$$w(z) = U(1 - \frac{R^2}{z^2})$$

For the purpose of numerical solution, boundaries are placed in the fluid and assumed far enough away from the cylinder

that their effect is small. By symmetry, the numerical solution can be set up considering only the upper left quadrant as shown in figure 6. The upper boundary is assumed a streamline as is the midline axis with ψ_1 and ψ_2 chosen such that their difference equals the flow between the streamlines $Q = \psi_1 - \psi_2$. The righthand side is an equipotential line by symmetry, with ϕ chosen as an arbitrary constant. The lefthand side is assumed far enough upstream that uniform flow conditions prevail and ψ can be considered to vary linearly.

A test case has been run with R=1, L=5, H=5, and U=1. Elements are placed on the cylinder at 5° intervals with a total of 80 elements on the contour.

The calculated velocity potential and stream function are shown in figure 7 and agree well with the analytical solution. Velocities along the cylinder surface, calculated using the numerical differentiation technique described above are plotted in figure 8 along with the theoretical values. Agreement is generally good, with the discrepencies due primarily to the finite far field boundaries imposed in the numerical solution.

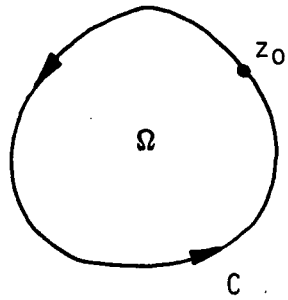

Figure 2. General fluid domain in complex plane.

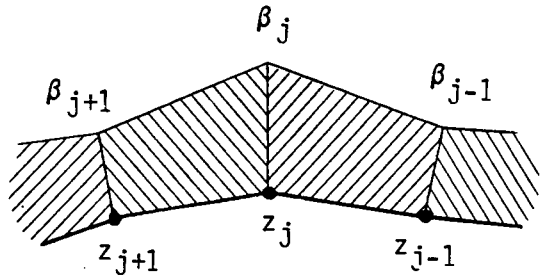

Figure 3. Distribution of complex potential on elements.

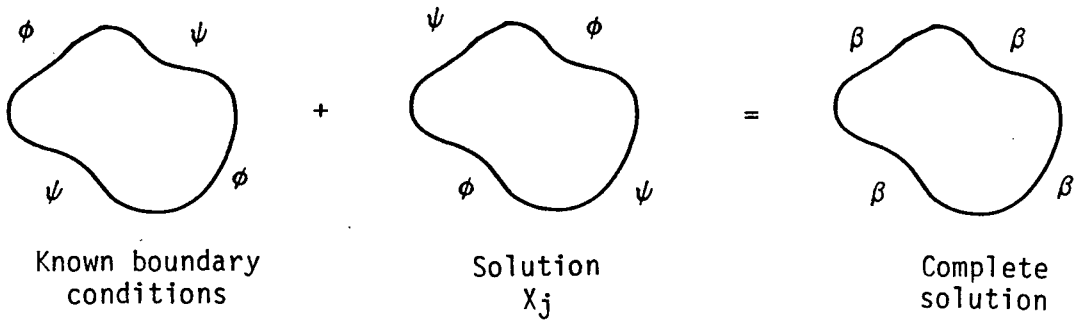

Figure 4. Final construction of complex potential solution on contour.

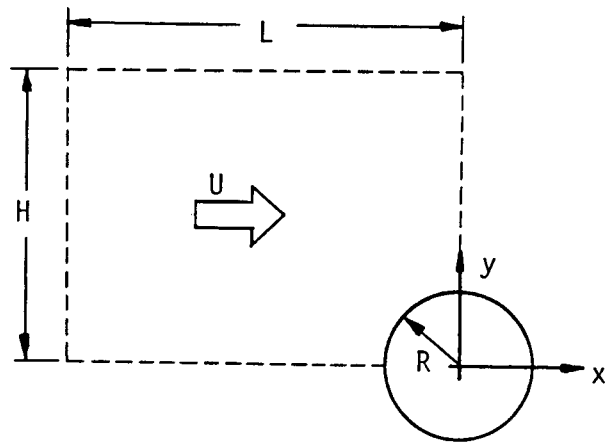

Figure 5. Test case of circular cylinder in uniform flow.

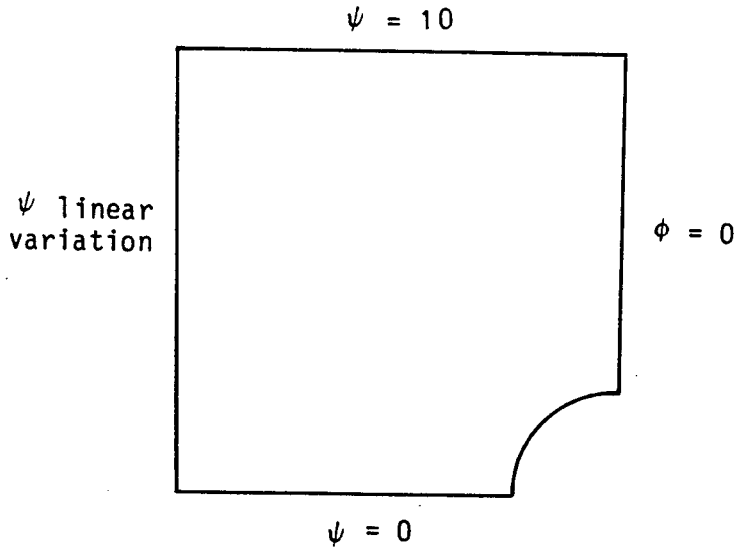

Figure 6. Geometry and boundary conditions for test case.

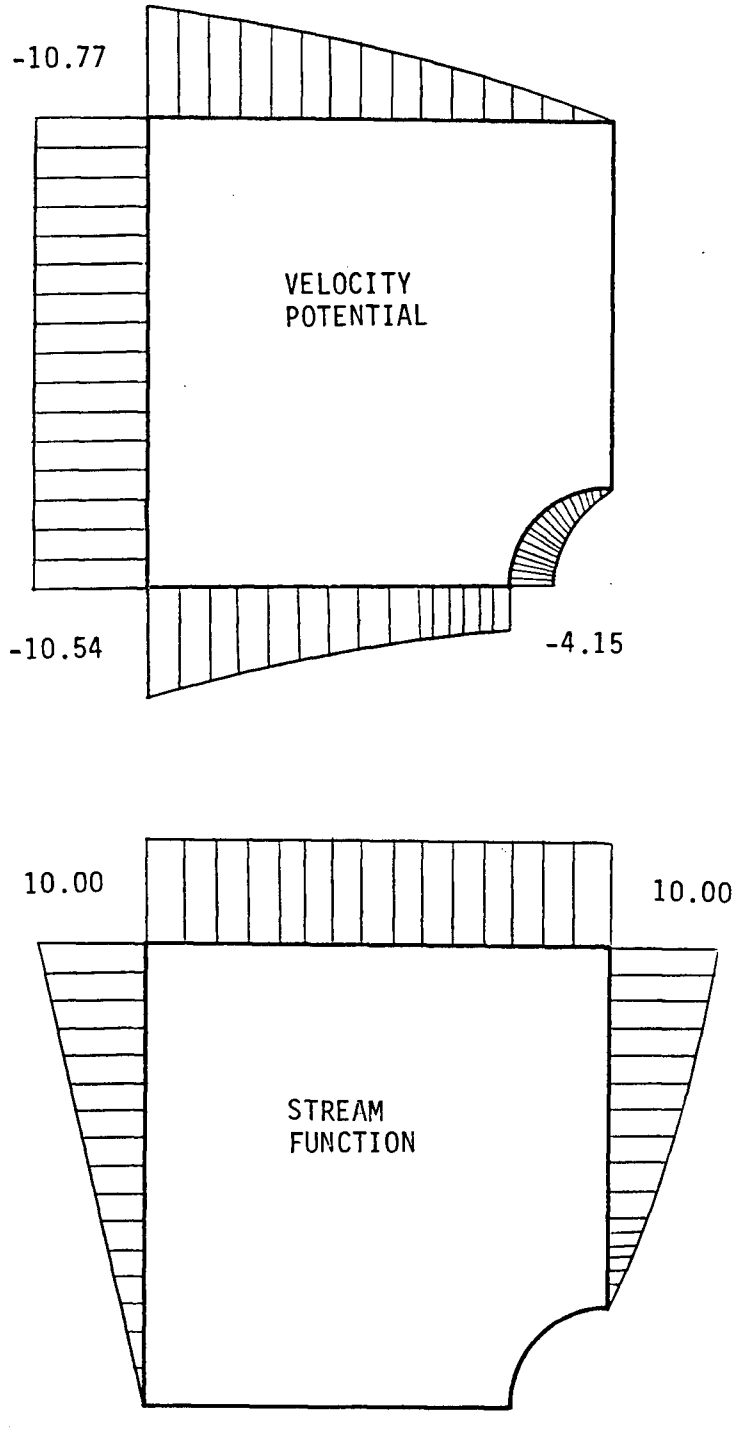

Figure 7. Velocity potential and stream function calculated in test case.

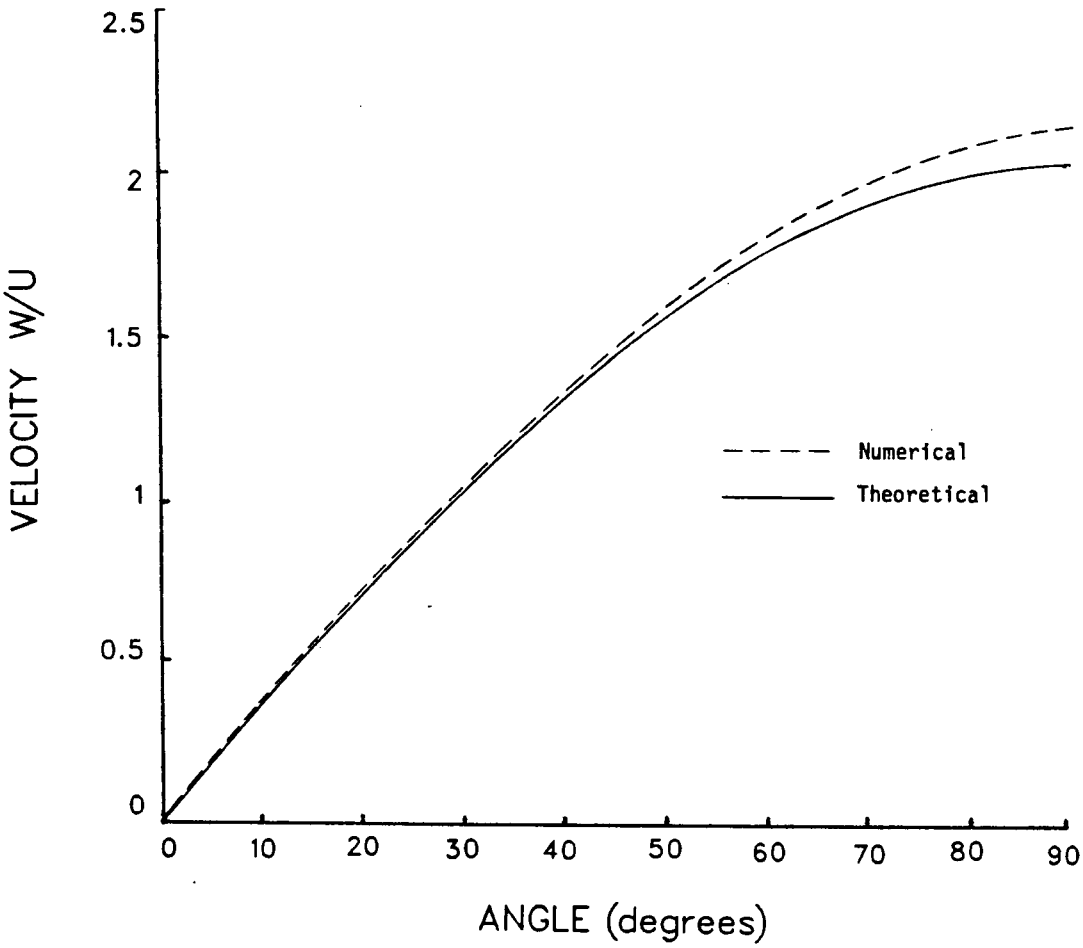

Figure 8. Comparison of numerical and theoretical solutions for velocity on cylinder surface. Angle is measured from forward stagnation point.

3. WAVE SIMULATION

3.1 INTRODUCTION

3.1.1 THE PROBLEM

A wave is considered of wavelength L, water depth d, and surface elevation $\eta(x,t)$ measured from the still water level. The wave is periodic of period T, and translates with a phase speed c as in figure 9. The fluid is considered incompressible and irrotational and again satisfies Laplace's equation

$$\frac{\partial^2\phi}{\partial x^2} + \frac{\partial^2\phi}{\partial y^2} = 0$$

subject to the following boundary conditions. The seabed is impermeable and therefore can have no normal velocity

$$\frac{\partial\phi}{\partial y} = 0 \qquad y = -d \qquad (3.1)$$

The free surface must satisfy a dynamic condition that Bernoulli's equation is obeyed

$$\frac{\partial\phi}{\partial t} + \frac{\rho}{2}\left[\left(\frac{\partial\phi}{\partial x}\right)^2 + \left(\frac{\partial\phi}{\partial y}\right)^2\right] + g\eta = f(t) \qquad y = \eta \qquad (3.2)$$

as well as a kinematic condition which states that surface fluid particles have velocities identical to the wave profile velocities

$$\frac{\partial\eta}{\partial t} + \left(\frac{\partial\phi}{\partial x}\right)\left(\frac{\partial\eta}{\partial x}\right) = \frac{\partial\phi}{\partial y} \qquad y = \eta \qquad (3.3)$$

If the wave is considered periodic in space then explicit

boundary conditions on the vertical control volume segments are unnecessary.

3.1.2 LINEAR WAVE THEORY

The problem defined above is very difficult to solve because the two free surface boundary conditions are nonlinear in ϕ and the surface elevation η is unknown a priori. The classical solution of Airy assumes the wave amplitude is small so the problem can be linearized. A sinusoidal surface is assumed

$$\eta = \frac{H}{2} \cos(kx-\omega t)$$

and the slope is considered small so the nonlinear terms are negligible.

The boundary conditions then reduce to

$$\frac{\partial \phi}{\partial t} + g\eta = 0 \qquad y = 0$$

and

$$\frac{\partial \phi}{\partial y} - \frac{\partial \eta}{\partial t} = 0 \qquad y = 0$$

Solution of the boundary value problem by separation of variables yields:

$$\phi = \frac{\pi H}{KT} \frac{\cosh k(y+d)}{\sinh kd} \sin(kx-\omega t)$$

$$C^2 = \frac{gL}{2\pi} \tanh(kd) \qquad (3.4)$$

3.1.3 STOKES WAVE THEORY

Early work by Stokes (1847) extended the analytical solution to include nonlinear effects by expanding variables in a perturbation series. Variables are expressed as

$$\phi = \varepsilon \phi_1 + \varepsilon^2 \phi_2 + \cdots$$

$$\eta = \varepsilon \eta_1 + \varepsilon^2 \eta_2 + \cdots$$

where ϵ is a small parameter of the order H/L. These expressions are substituted into equations (3.2) and (3.3), and terms of like order of magnitude are gathered yielding successively higher order solutions, linear theory providing the first approximation. Stokes originally calculated a third order solution, as the algebra quickly becomes involved. Skjelbreia and Hendrickson (1960) presented a Stokes fifth order solution of the form:

$$\eta = \sum_{n=1}^{5} \eta_n \cos(nKx)$$

$$\phi = \sum_{n=1}^{5} \phi_n \sin(nKx)$$

The effect of higher order terms is to sharpen the crests and flatten the troughs. The regions of validity of linear and higher order solutions can be seen in figure 10 from Sarpkaya and Isaacson (1981).

3.1.4 WAVES IN NATURE

Most ocean waves are generated by winds exerting shear on the sea surface forming small disturbances which then grow as a result of work done by aerodynamic forces. Steady periodic progressive waves have been well studied in theory, but probably exist only under ideal conditions. The real sea, by contrast, is very unsteady. More generally, real wave trains are irregular and undergo distortion over time due to amplitude and frequency dispersion effects. In addition, the real ocean is characterized by many intersecting wave trains from storms in different locations and from changes in wind speed and direction.

Wave breaking is a form of instability that can develop whenever the local energy density of the wave field exceeds some critical limit. Examples of when this may occur are when deep water waves overtake or collide raising the surface to unstable heights, or due to shoaling in shallow water. Winds may also induce shear forces at the wave crests.

Breaking waves are commonly classified as surging, spilling, or plunging as shown in figure 11. Surging breakers usually occur only on steeply sloped beaches and are not considered in the present work. Spilling and plunging breakers may occur in deep or shallow water, the resulting type depending on the available energy.

Spilling breakers are characterized by a sharpening of the wave crest until the forward face begins to curl over.

The ejected jet is weak and immediately succumbs to gravity, simply flowing down the forward face dissipating energy in viscous turbulence. This is the classic white cap. More dramatic are plunging breakers which contain much more energy and are able to eject a well defined jet ahead of the forward face resulting in the surface completely overturning on itself. The momentum of the plunging jet can be very large.

3.2 NUMERICAL SOLUTION

3.2.1 FORMULATION

The analytical theories described above suffer the severe restriction that they can handle only steady state symmetric waves. To overcome this limitation one must resort to a numerical time-stepping simulation of the wave from a given initial condition. The problem is solved as an initial value problem where equations (3.2) and (3.3) are integrated numerically in time and a boundary value problem for the potential field is solved at each time step to provide the right-hand side parameters. A control volume is considered consisting of a segment of the sea surface, the seabed, and vertical boundaries through the water column. This region is considered to be periodic in space furnishing the remaining necessary condition.

The seabed impermeability condition, equation (3.1), can be rewritten as the seabed being a streamline of

arbitrary constant value

$$\psi = 0$$

The free surface kinematic condition, expressed in terms of the material derivative, becomes

$$\frac{Dz}{Dt} = w^* \tag{3.5}$$

stating that the free surface particles move according to their fluid velocities, and the dynamic condition, equation (3.2), can be rewritten as

$$\frac{\partial \phi}{\partial t} = -\frac{ww^*}{2} - gy$$

or, as seen by the fluid particles,

$$\frac{D\phi}{Dt} = \frac{ww^*}{2} - gy \tag{3.6}$$

Equations (3.5) and (3.6) are evaluated at each time step to determine the new positions and potentials of the free surface nodes. Velocities are then determined as

$$w = \frac{\partial \beta}{\partial z}$$

following the procedure described in Chapter 2.

A flow chart for the time stepping algorithm is shown in figure 12.

3.2.2 CONSTRUCTION OF MATRIX

The control volume consists of one wavelength, with nodal points numbered as shown in figure 13. The free surface nodes, 1 to N2, have known values of ϕ and the real parts of equation (2.4) are selected here, while the seabed nodes, N3 to N4, have known values of ψ and the imaginary parts are chosen. The vertical boundaries, however, have both ϕ and ψ as unknowns, hence both the real and imaginary equations must be used for these points. When the collocation point z_0 is on the lefthand boundary, ϕ is considered to be the unknown quantity and the real equation is taken here. Similarly, on the righthand side ψ is considered as the unknown quantity and the imaginary equations are selected here. A set of N equations results for the N unknowns. An improvement can be made however by recognizing that 1 and N2 are the same point as are N3 and N4 allowing elimination of two unknowns. The actual equations used are given in Appendix V.

3.2.3 CHOICE OF INITIAL CONDITIONS

Initialization of the simulation requires starting values for the surface position $\eta(x)$ and surface velocity. The latter is achieved indirectly by specifying the velocity potential $\phi(x)$ as there is a one to one correspondence

between ϕ and w on the surface. Selection of ϕ to match a given velocity distribution, however, would be an inverse problem requiring either integration of the tangential velocity or trial and error.

3.2.4 TIME STEPPING PROCEDURE

Several standard numerical procedures were compared for integrating equations (3.5) and (3.6) with respect to time. The preliminary version of the simulation program used the single step Euler method which uses time derivative values at the present step to predict the new function values. This simple scheme yielded satisfactory results. Higher order methods were then tested for comparison beginning with a second order Heun method [2]. This method calculates derivatives at the current time and uses them to make an estimate of the values of z_i and ϕ_i after Δt where the derivatives are again calculated. An average of these derivative values before and after Δt is used to take the actual step forward in time. Specifically,

$$\phi'_{n+1} = \phi_n + \dot{\phi}_n \Delta t$$

$$z'_{n+1} = z_n + w^*_n \Delta t$$

$$\phi_{n+1} = \phi_n + [\dot{\phi}'_{n+1} + \dot{\phi}_n] \frac{\Delta t}{2}$$

$$z_{n+1} = z_n + [w^*_n + w'^*_{n+1}] \frac{\Delta t}{2}$$

where subscript n indicates current values and subscript n+1 refers to the new values of surface nodal points. This scheme provides a slight improvement over the single step Euler method and results in a very stable solution in terms of both smoothness and stationarity of energy as discussed in a later section.

To test the adequacy of the two step scheme test runs were then carried out using a fourth order Adams-Moulton predictor-corrector method [2]. Values from three previous steps are required and new values are predicted as a first approximation. New derivatives are then calculated and a correction made to obtain the actual time derivatives used to step forward. Specifically,

$$\dot{\phi}'_{n+1} = \frac{1}{24}(55\dot{\phi}_n - 59\dot{\phi}_{n-1} + 37\dot{\phi}_{n-2} - 9\dot{\phi}_{n-3})$$

$$w'_{n+1} = \frac{1}{24}(55w_n - 59w_{n-1} + 37w_{n-2} - 9w_{n-3})$$

$$\phi''_{n+1} = \phi_n + \dot{\phi}'_{n+1}\,\Delta t$$

$$z'_{n+1} = z_n + w'^{*}_{n+1}\,\Delta t$$

$$\dot{\phi}_{n+1} = \frac{1}{24}(9\dot{\phi}''_{n+1} + 19\dot{\phi}_n - 5\dot{\phi}_{n-1} + \dot{\phi}_{n-2})$$

$$w_{n+1} = \frac{1}{24}(9w''_{n+1} + 19w_n - 5w_{n-1} + \quad _{n-2})$$

$$\phi'_{n+1} = \phi_n + \dot{\phi}_n\,\Delta t$$

$$z'_{n+1} = z_n + w^{*}_n\,\Delta t$$

The results of the second order method have been found to be

virtually indistinguishible from those of the fourth order method. The latter requires more programming effort with the only possible advantage of increasing the permissible time step interval Δt, thereby reducing computational time. As will be shown in the next section, however, Δt is dictated by a numerical stability criterion. It is concluded that the two step integration scheme is sufficient and higher order techniques are not necessary. Each time step in the simulation as such requires two matrix solutions.

3.2.5 SEGMENT SIZE AND TIME STEP

Program perfomance depends on the segment size selected for the elements. Too few elements result in poor resolution and large errors while too many elements result in excessive computational time and the risk of numerical instability. The optimum number of elements selected depends somewhat on the situation.

A non-breaking wave with relatively low surface curvature can be simulated reasonably well with as few as 30 surface points for one wavelength. Fewer than this results in undesirable cusps in the regions of high curvature, most notably at the wave crest. Excessive errors in the calculated velocities follow with subsequent instability and breakdown. Breaking waves have regions of high curvature and therefore require more elements. Fortunately, nodal points tend to migrate into the crest region as the simulation proceeds, automatically providing better resolution here

where it is needed. Most breaking waves require about 60 surface elements. Occasionally more may be needed, especially in cases where the plunging jet is thin and the elliptical surface under the wave crest becomes poorly resolved due to nodal point migration away from this area. Such situations may require up to 100 surface elements. Simply increasing the number of surface elements, however, can lead to additional problems as the increasing element density in the crest region may result in nodes crossing over creating a multiply-connected fluid domain and immediate breakdown of the simulation. A solution to this problem would be to remove elements from the high density crest region to the more sparse trough region. This procedure would be useful if the detailed structure of the jet tip was being examined.

The number of elements recommended for the vertical boundary depends on the water depth. For deep water waves at least 15 should be used if elements are uniformly spaced, or 20 for higher waves. This number could be reduced slightly by using progressively larger elements as the depth increases. On the seabed 20 elements usually proves sufficient for deep water waves. In shallower water, however, where seabed velocities become significant, more elements are required with 30 being used typically. The greatest number of elements, therefore, are required for large amplitude shallow water breaking waves where N may be up to 180.

Once element sizes have been determined the time step interval Δt is selected according to the Courant stability criterion which states that a particle should not be permitted to move a distance greater than approximately the element size. This condition can be expressed roughly as

$$\frac{\Delta x}{\Delta t} < c$$

or

$$\frac{\Delta t}{T} < \frac{\Delta x}{L}$$

where Δx is the element size and c is the phase velocity of the wave. A convenient time step interval is selected following this criterion based on the initial element size. One further disadvantage of too many elements on the free surface apparent now is the smaller time step required and the resulting increase in computation time.

3.2.6 NUMERICAL ADJUSTMENTS

Several checks and adjustments of elements must be made at each time step to ensure smooth execution of the simulation. The vertical nodes are fixed points, however, the surface corner nodes 1 and N2 are free to move and will tend to stretch and compress the uppermost vertical element resulting in poor accuracy in this region. To overcome this problem the elements on the vertical boundary are evenly redistributed at each time step by dividing the vertical boundary length by the number of elements on the side.

Element size here then becomes $(d+\eta)/NV$. Failure to do so will usually result in "sawtooth" instabilities developing on the surface near the edges.

A similar problem results from excessive horizontal excursion of the surface corner points. The situation is compounded by nonlinear effects causing a gradual downstream migration of surface particles. If left unchecked the control volume will distort as shown in figure 14. A check of the region is made at each step and the corner points readjusted if necessary to ensure that they are always those closest to the vertical boundary. Surface nodal point indices are incremented if such a shift is required.

The simulation is very stable and smoothing of the surface has not been found necessary in most cases. Occasionally, altering initial element size slightly will correct rare unstable situations.

3.2.7 ENERGY

A wave contains kinetic energy due to fluid motion and potential energy due to displacement of the free surface. Under the assumption of zero viscosity in potential flow there is no mechanism for energy dissipation, and the total control volume energy

$$E_t = E_K + E_P$$

must in theory remain constant. Due to numerical approximations and computer roundoff errors, however, one

would expect a slight "numerical viscosity" to cause artificial changes in energy. A perfect solution should exhibit no such change, therefore, stationarity of the total energy provides an excellent assessment of simulation accuracy.

Kinetic energy can be expressed as

$$E_K = \frac{\rho}{2} \int\int_{\Omega} V^2 \, dV$$

which, by invoking Green's theorem, can be evaluated numerically as

$$E_K = \frac{\rho}{4} \sum_{i=1}^{N2} (\phi_i \psi_{i+1} - \phi_{i+1} \psi_i) \tag{3.7}$$

Potential energy is given by

$$E_P = \frac{\rho g}{2} \int_0^L \eta^2 \, dx \tag{3.8}$$

or numerically as

$$E_P = \frac{\rho g}{6} \sum_{i=1}^{N2} (x_i - x_{i+1})(y_{i+1} y_i + y_{i+1}^2 + y_i^2)$$

Derivation of these equations may be found in Appendix VI.

Linear theory predicts kinetic and potential energies are exactly equal, while nonlinear theories predict that the kinetic component is slightly larger. Breaking waves exhibit a shift from potential to kinetic energy as time proceeds.

3.2.8 COMPUTER SOLUTION

The wave simulation library developed consists of preprocessing programs for generating the various types of wave initial conditions which are then passed to the main simulation program. The primary output file provides all numerical values for each time step in formatted tables suitable for analysis. A secondary output file can be used for hard-copy plotting of the waves or animated display on a graphics terminal.

All programs were written in FORTRAN, and compiled and run on a VAX 11/750. Matrix solutions were obtained using standard Gaussian elimination with double precision variables used throughout. Required CPU times for different numbers of elements are shown in figure 15. CPU time for a single step increases roughly as N^2, however, as N increases a smaller Δt is required so CPU time actually increases by a power approaching N^3. Simulation of a typical breaking wave with N=120 requires about four hours.

3.3 RESULTS

The simulation procedure described provides a powerful tool for analysing the behaviour of arbitrary nonlinear waves under the assumptions described previously.

To test the accuracy of the simulation a Stokes fifth order wave was chosen. Linear wave theory predicts that fluid motions should be negligible below a depth of about $d/L = 0.5$ which is considered the transition between shallow

and deep water. Since Stokes theory is valid only for deep water, the sea bed was placed at a depth of d/L = 0.6 and negligible fluid motions were confirmed. The height ratio was selected to be H/L = 0.06 which can be seen from figure 10 to lie well within the region of validity of Stokes theory. As such, one would expect the wave to translate steadily with no deformation over time. Figure 16 shows the results of a simulation carried out using NS=60, NV=15, NB=20, L=100 feet, and Δt = 0.05 sec. The resulting surface profile after one wave period is shown superimposed on the initial wave. The simulation in this case is remarkably accurate showing little distinguishible difference after one period. Following three complete wave periods the wave still showed negligible distortion. Total control volume energy exhibited fluctuations of less than 0.1%. Figure 17 shows the trajectory over time of a typical nodal point representing a marked fluid particle. The nonlinear Stokes drift results in a net migration of fluid in the downwave direction. Net excursion at the surface in this case was x/L = 0.036 and increased with wave height.

Generation of a breaking wave requires an initial condition that is unstable. As discussed earlier this selection is somewhat arbitrary, and many waves would satisfy this criterion. To be specific, however, a particular class has been chosen of a cosine surface profile with ϕ from linear theory applied at the exact free surface. Such waves cannot remain steady in form and would be

expected to break if given sufficient initial height.

A deep water cosine wave was run with H/L = 0.06. In this case nonlinear effects were quite small and after two wave periods the only discernible change was a slight increase in the slope of the forward surface. Increasing the initial wave height to H/L = 0.10 produced a spilling breaker as shown in Figure 18. Fluid particle velocities at the wave crest reached the phase speed around this time. The horizontal acceleration of the fluid here was about 0.04 g and the vertical acceleration -0.22 g, having changed little from the initial condition. Acceleration in the forward direction was very small and fluid in the incipient jet would simply flow down the forward face of the wave under the influence of gravity. Further computation beyond this point is not possible as the nodal points at the crest fall inside the control volume producing a multiply connected region.

The results of a deep water cosine wave with H/L = 0.13 are shown in Figure 19. The initial energy in this case is much higher and a well defined plunging breaker results. The simulation in this case looked qualitatively identical to that presented in Vinje and Brevig (1980) for the same initial condition, however, no numerical results were given in their work. At the time of the forward face becoming vertical the horizontal fluid acceleration near the crest was 0.58 g while the vertical acceleration was -0.76 g. As the jet became well developed, the horizontal acceleration

at the tip dropped to near zero while the vertical acceleration approached -0.98 g characteristic of a pure gravity jet. For comparison, the same initial conditions were run in shallow water using d/L = 0.25. A spilling breaker of H/L = 0.10 is shown in figure 20 and is remarkably similar to the deep water case demonstrating that spilling is a local phenomenon and not very sensitive to water depth. As can be seen in figure 21 for the shallow water plunging breaker, the jet resulted in a greater fluid volume ejected at a slightly higher velocity.

Numerous wave simulations have been run using the deep water cosine initial conditions. Waves of small amplitude exhibit only a gradual sharpening of the crest over several wave periods. As the initial height ratio is increased, however, a transition from spilling to plunging behaviour occurs as shown in figure 22. Simulations terminate when velocities cannot be resolved in the jet tip region due to nodal point crossover or when the plunging jet touches the forward face.

Figure 23 shows the time course of maximum fluid velocities on the surface for deep water waves of increasing initial height ratios. Figure 24 shows the same thing for shallow water waves of depth ratio d/L = 0.25. Fluid velocities in the shallow water waves are greater for the same initial height ratios. Breaking wave jet velocities can approach twice the phase speed of the corresponding linear wave. For the plunging breakers these maximum velocities

tend to occur on the advancing top surface just above the jet tip and are directed almost horizontally as seen in figure 25. For the class of waves studied, breaking usually occurs in less than one wave period. The breaking limits indicated in figures 23 and 24 are not really well defined but indicate roughly a transition between the plunging jet touching the forward face and spilling breakers reaching the critical point where further computation is not possible due to problems in spatial or temporal resolution.

The energy histories for plunging breakers of H/L = 0.13 in deep and shallow water are shown in figures 26 and 27. At t = 0 the cosine initial condition has a kinetic component only slightly larger than the potential component. As the wave breaks, however, there is a transfer from potential to kinetic energy which becomes increasingly rapid as the plunging jet forms. The total energy remains nearly constant throughout most of the simulation showing a typical slight increase near termination due to imperfect resolution in the jet region.

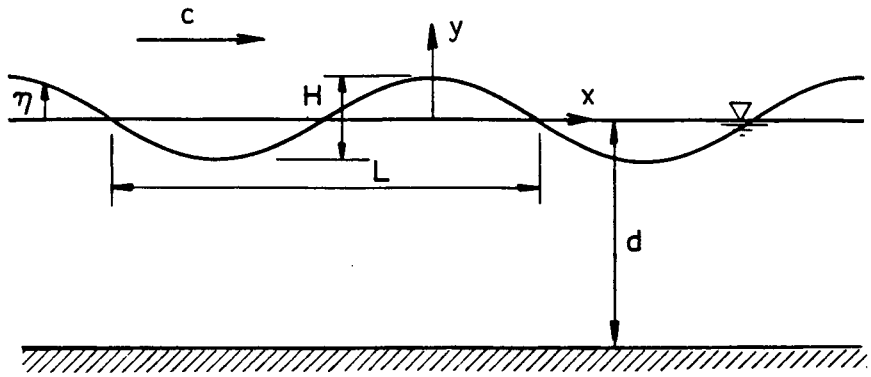

Figure 9. Definition of wave variables.

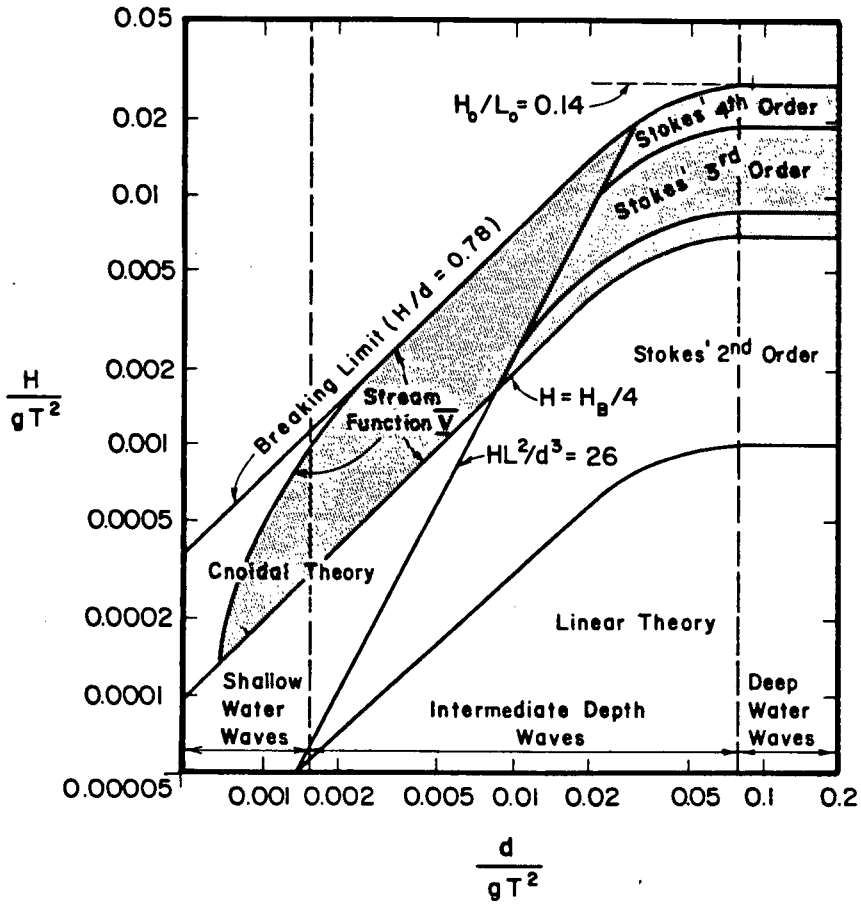

Figure 10. Regions of validity of wave theories (27).

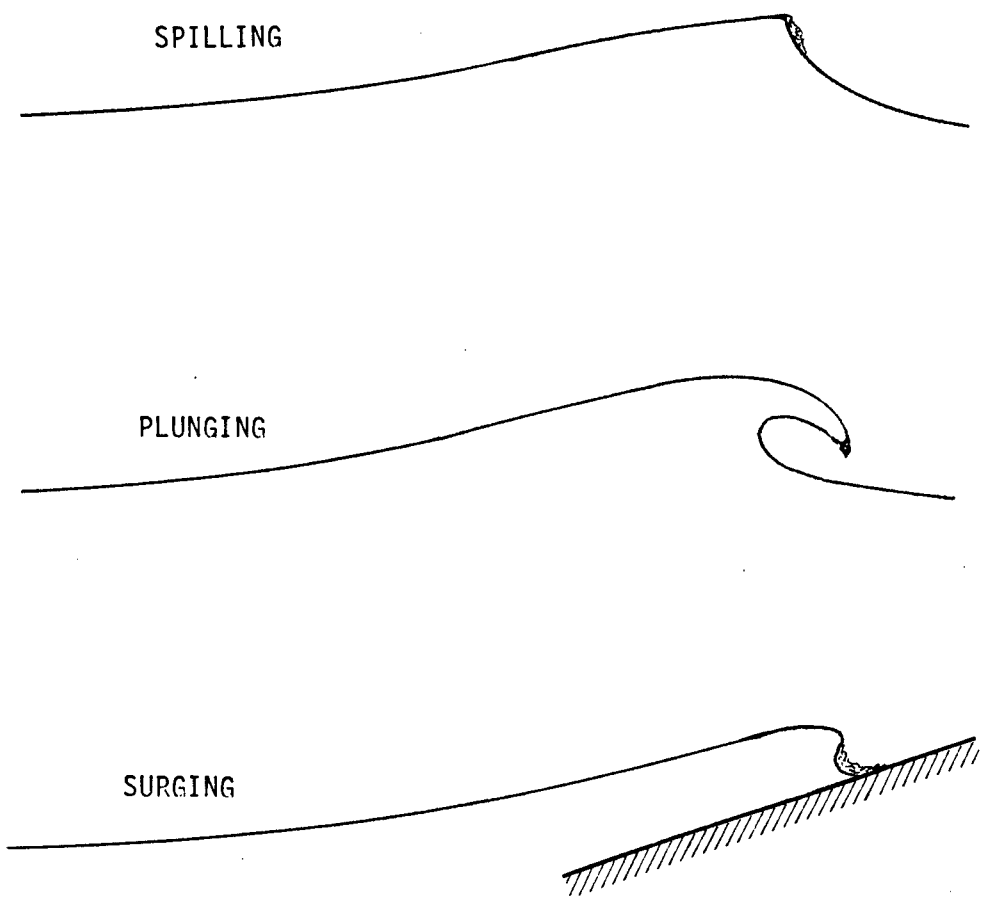

Figure 11. Classification of breaking waves.

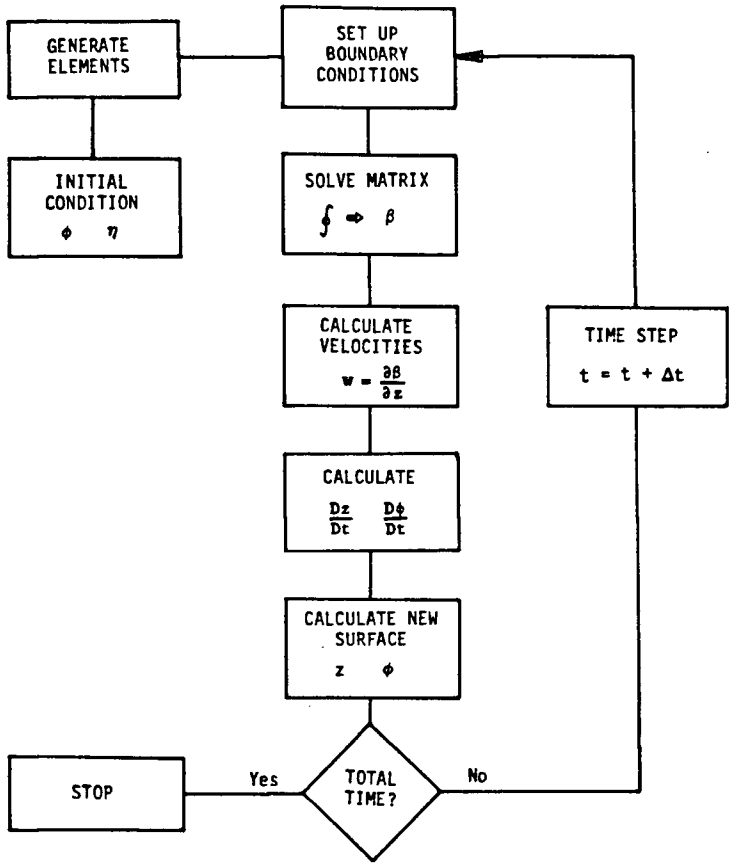

Figure 12. Flow chart of wave simulation algorithm.

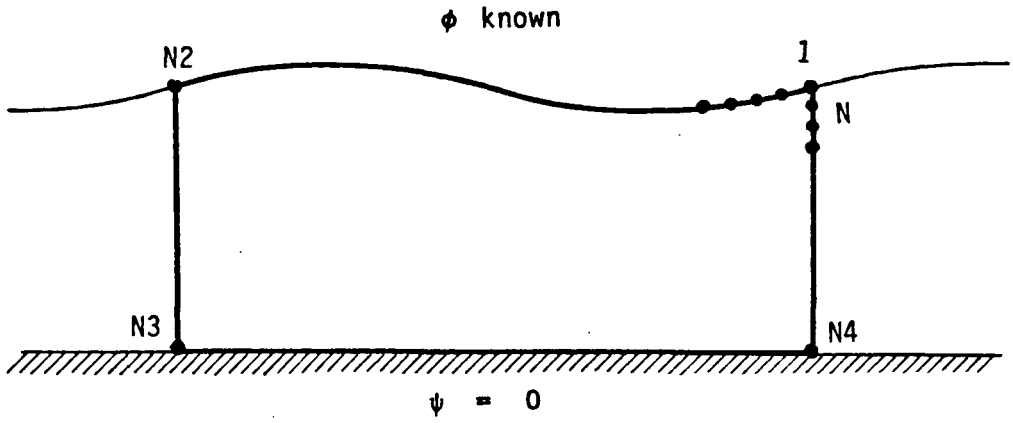

Figure 13. Definition of wave control volume.

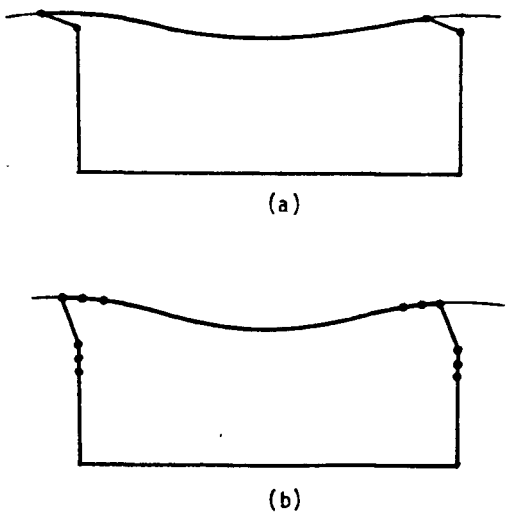

Figure 14. Two types of control volume distortion requiring nodal point adjustment: (a) horizontal drift, and (b) vertical stretch.

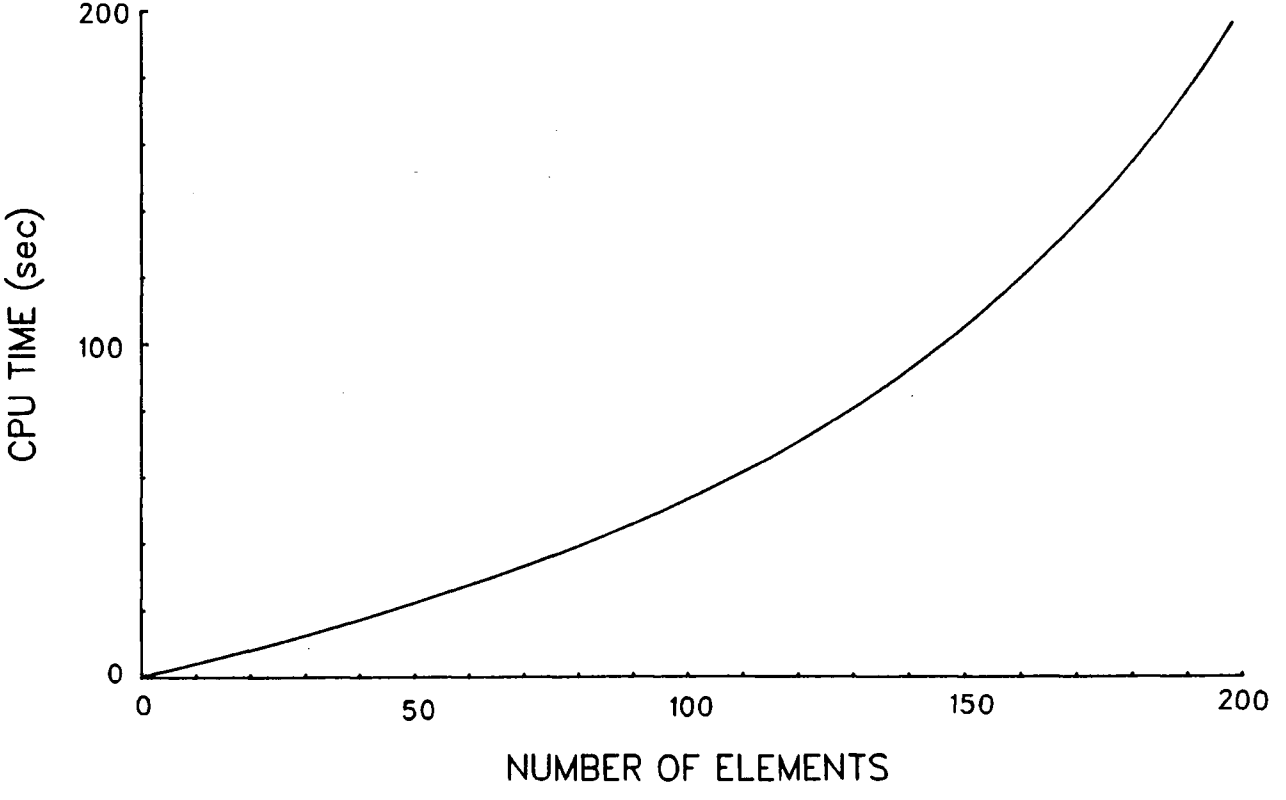

Figure 15. CPU time per step versus number of elements for wave simulation.

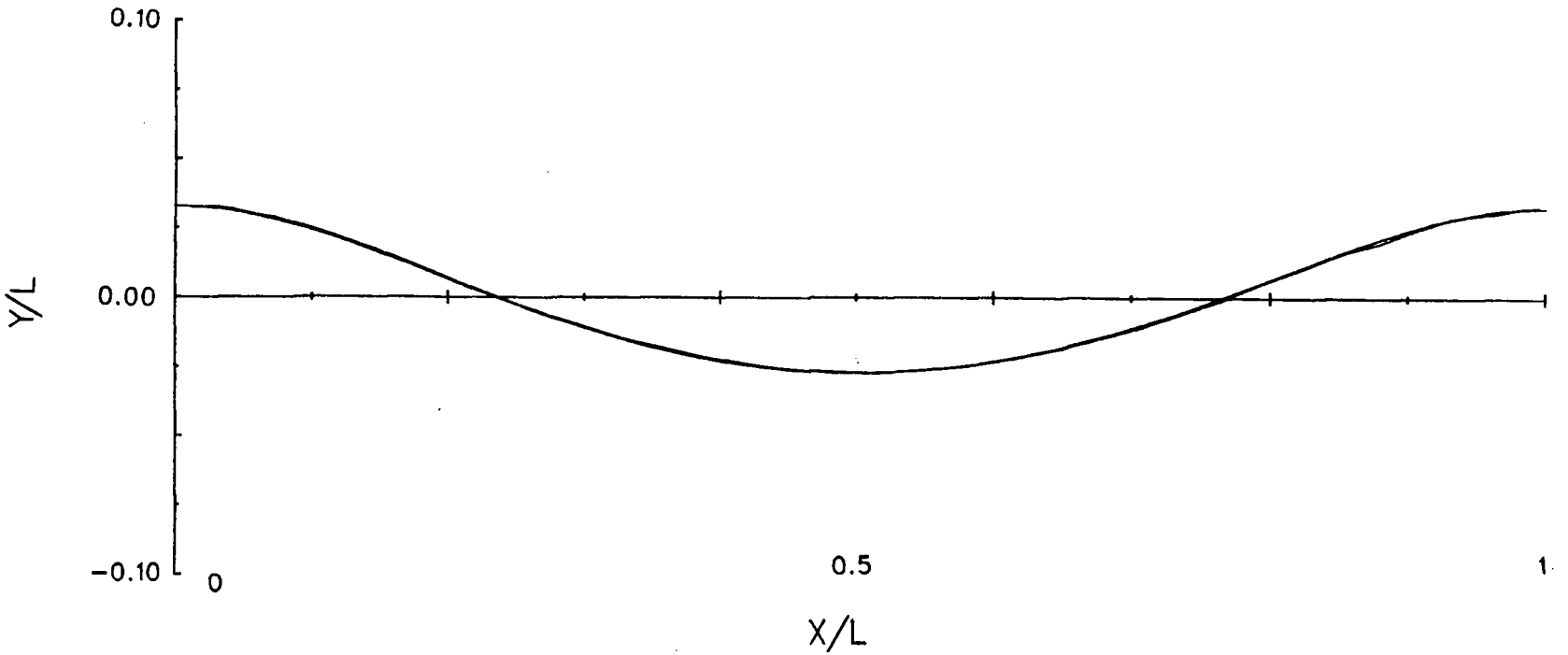

Figure 16. Translating Stokes fifth order wave of H/L = 0.06 simulated for one period and superposed on initial condition. Vertical scale has been doubled for clarity.

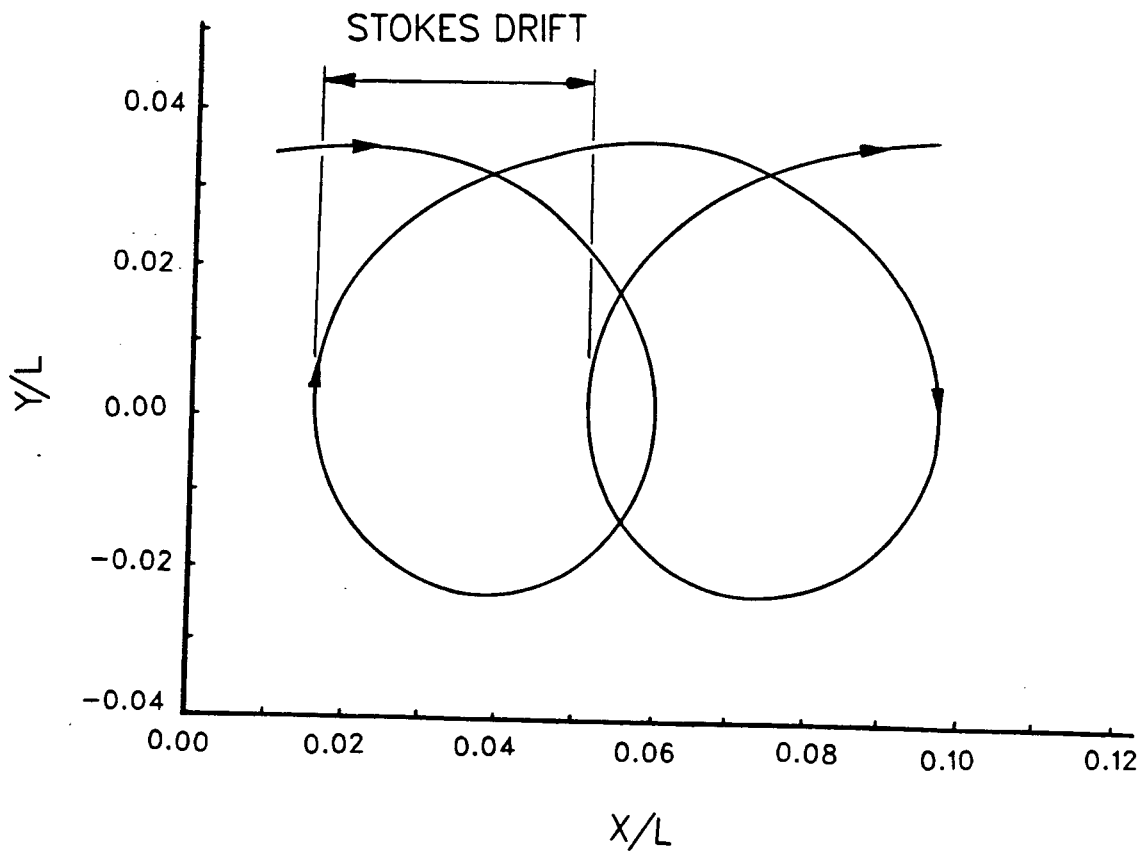

Figure 17. Trajectory of marked particle in Stokes fifth order wave H/L = 0. .

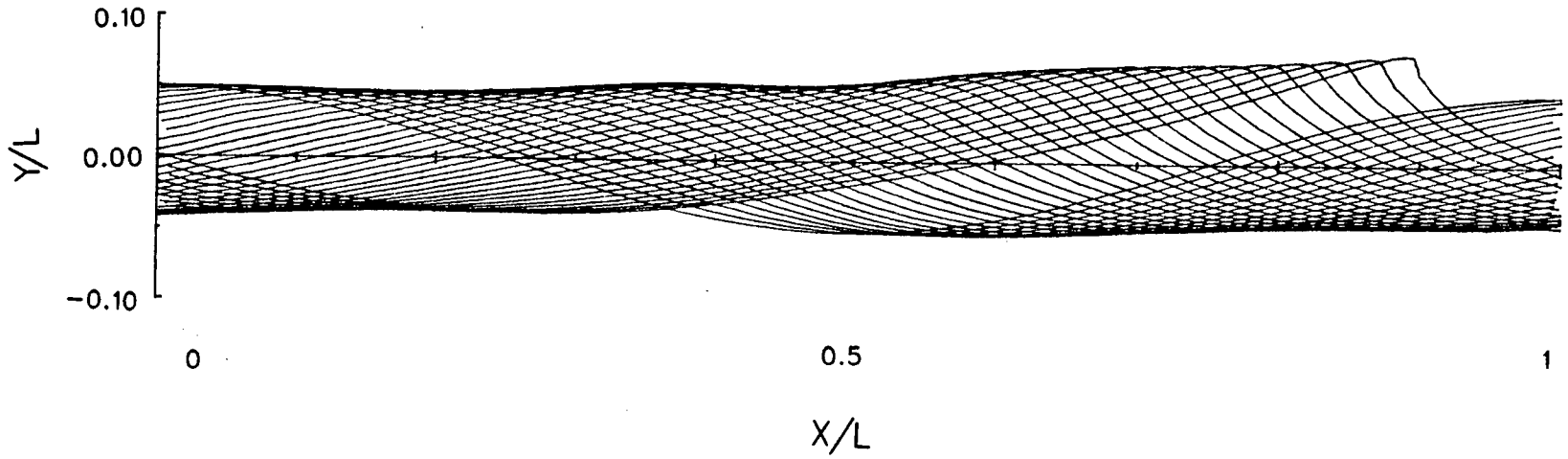

Figure 18. Deep water spilling breaker simulated from cosine initial condition H/L = 0.10.

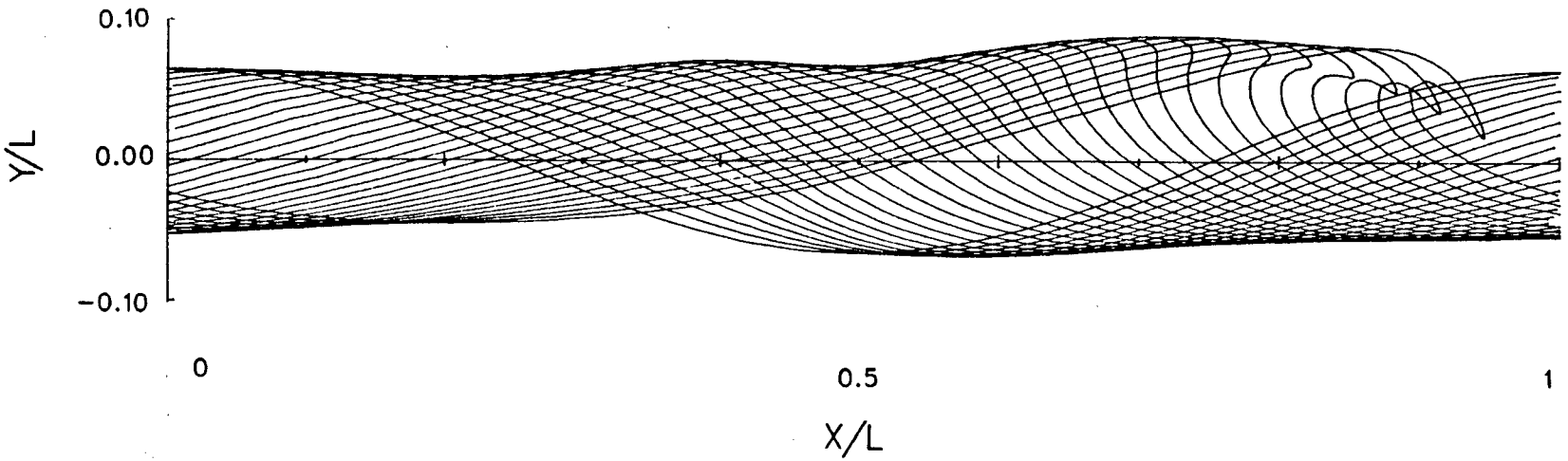

Figure 19. Deep water plunging breaker simulated from cosine initial condition H/L = 0.13.

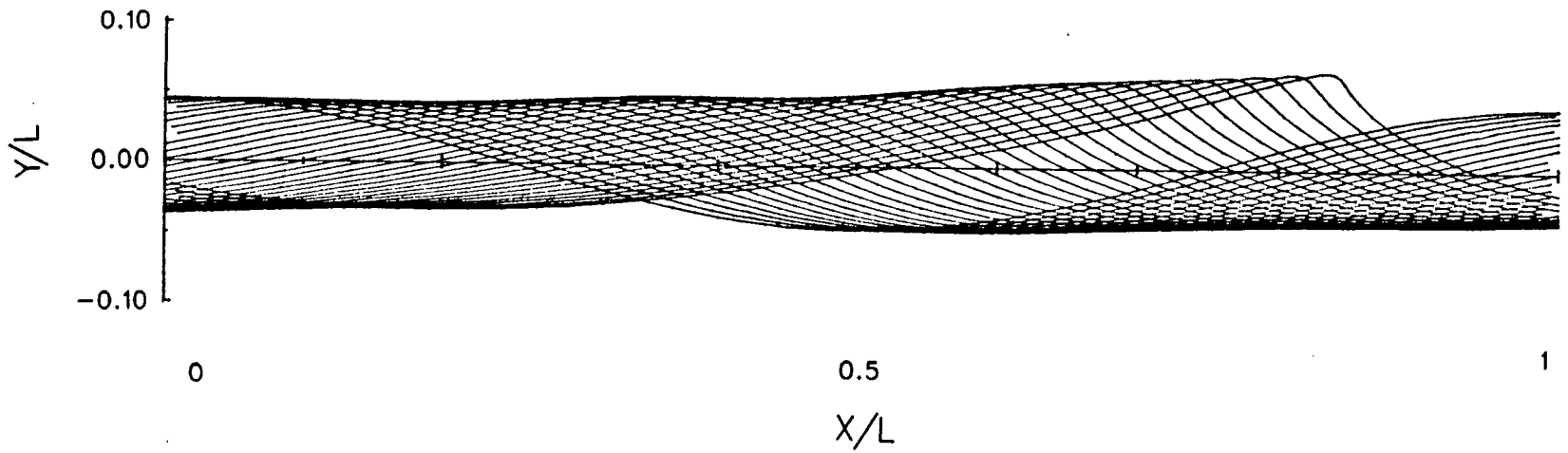

Figure 20. Shallow water spilling breaker simulated from cosine initial condition H/L = 0.10. Depth ratio d/L = 0.25.

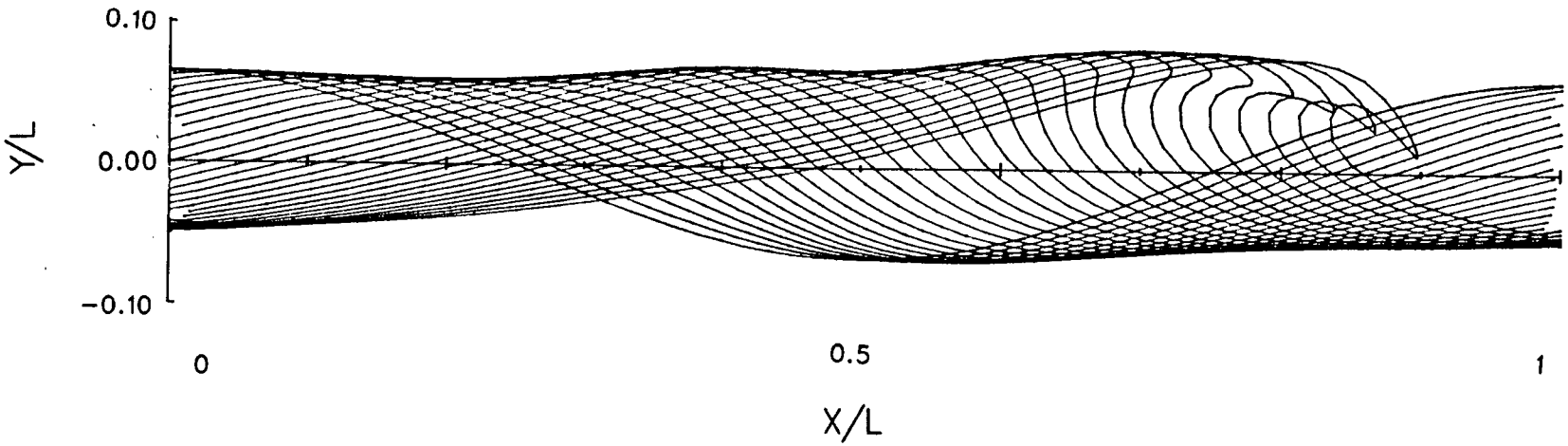

Figure 21. Shallow water plunging breaker simulated from cosine initial condition H/L = 0.13. Depth ratio d/L = 0.25.

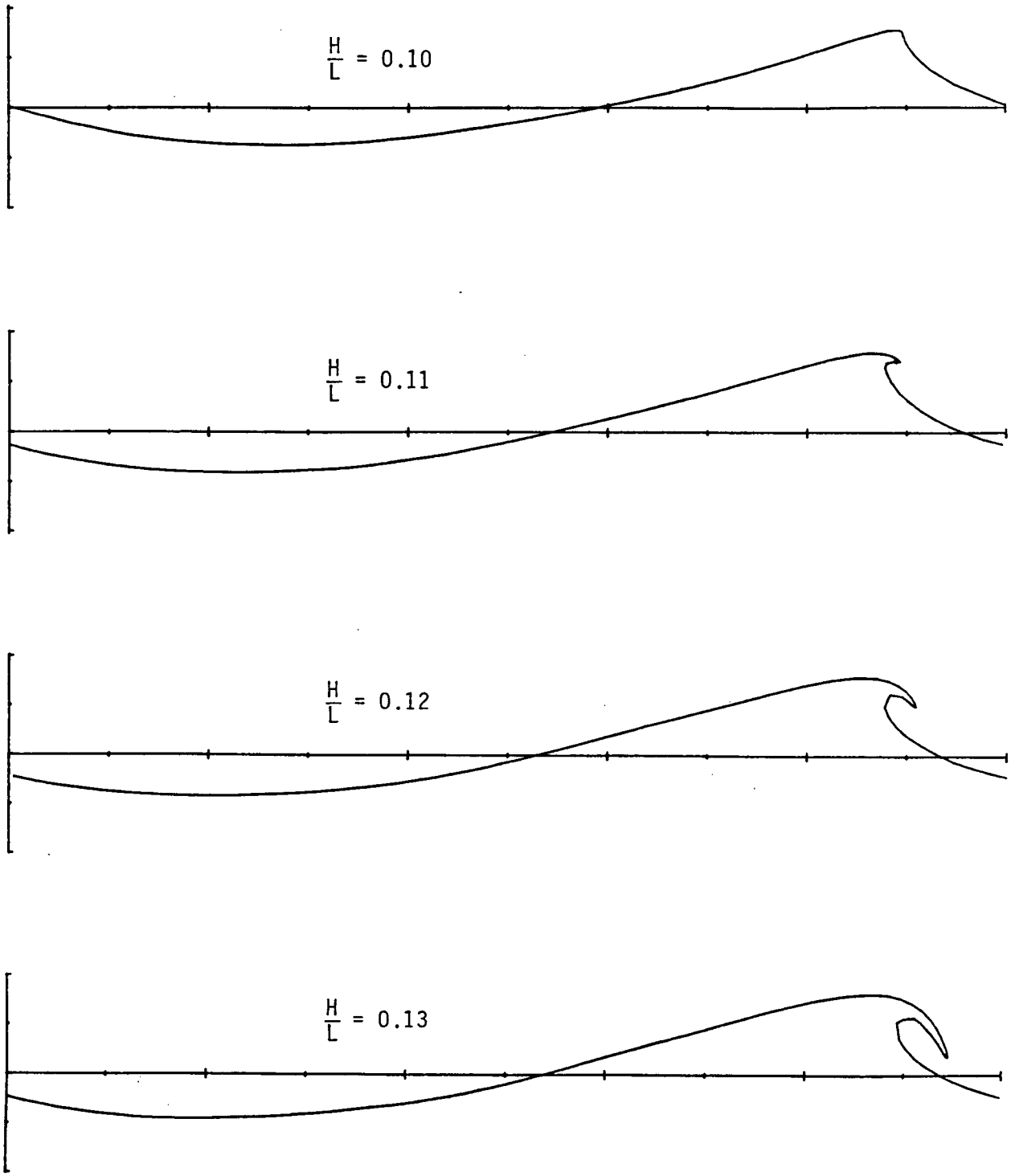

Figure 22. Last simulated step for deep water waves of varying height ratios showing transition from spilling to plunging breakers.

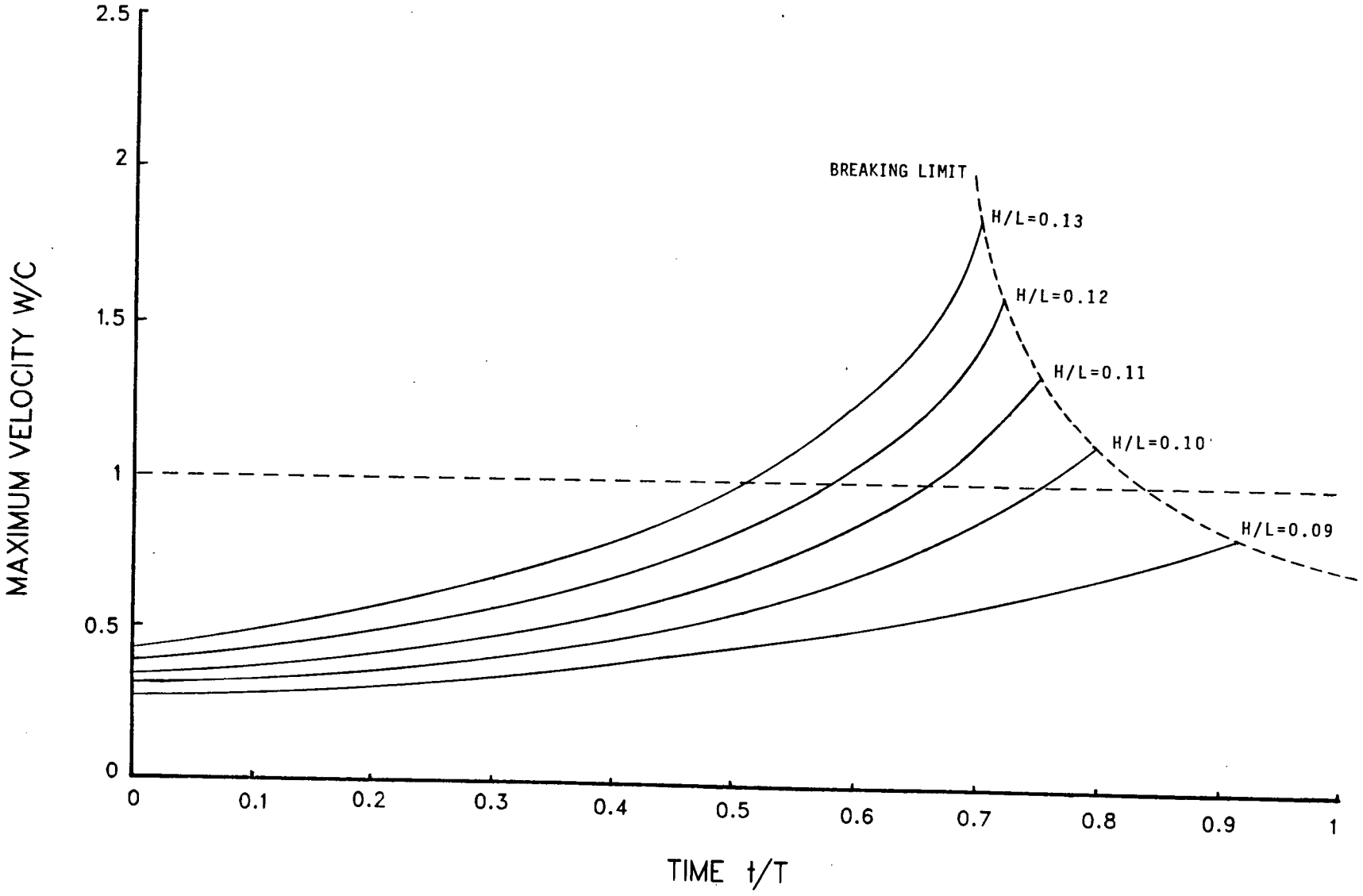

Figure 23. Maximum fluid particle velocities versus time for deep water waves from cosine initial conditions. Variables are normalized with values from linear theory.

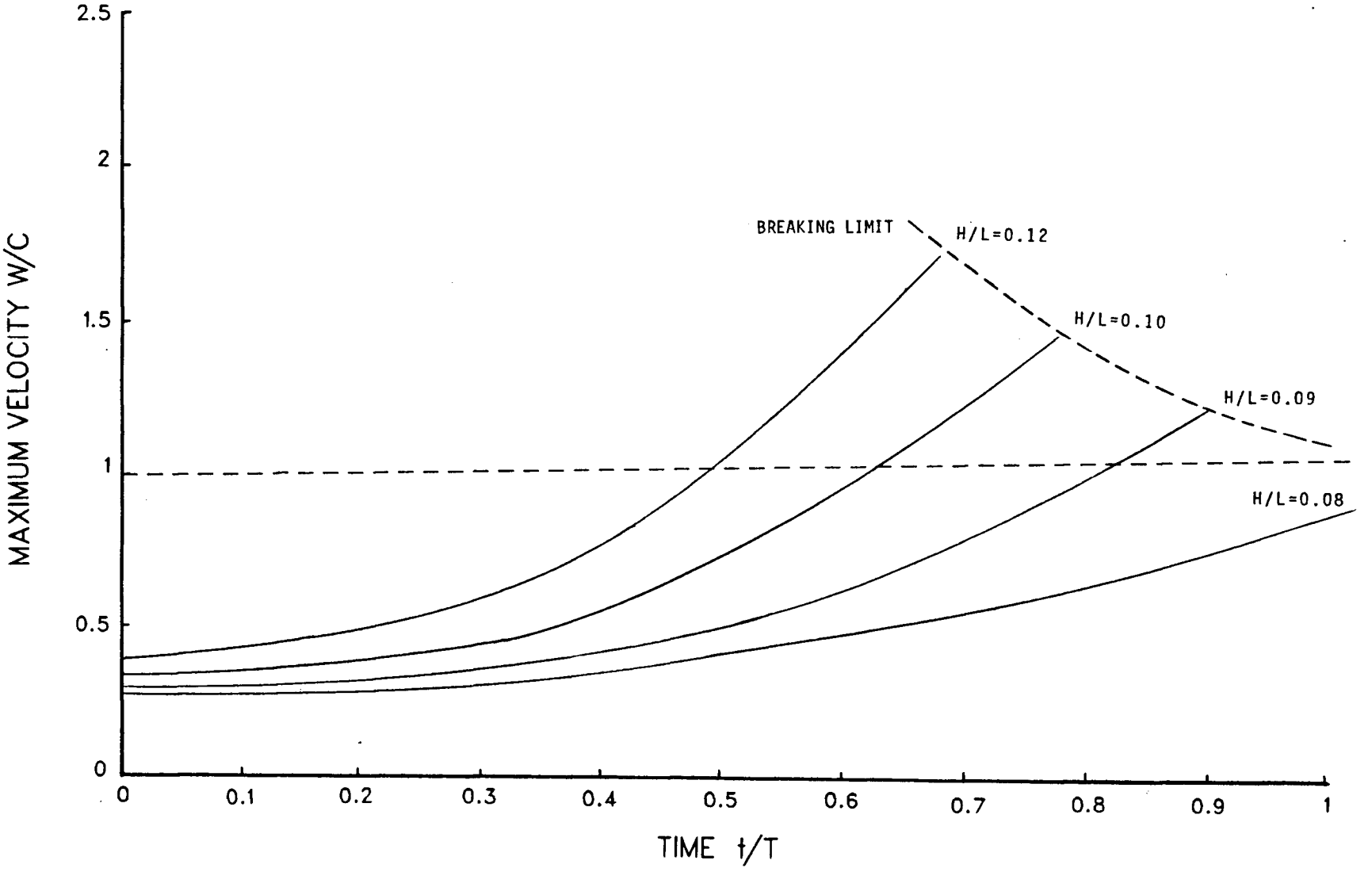

Figure 24. Maximum fluid particle velocities versus time for shallow water waves from cosine initial conditions. Variables are normalized with deep water linear theory.

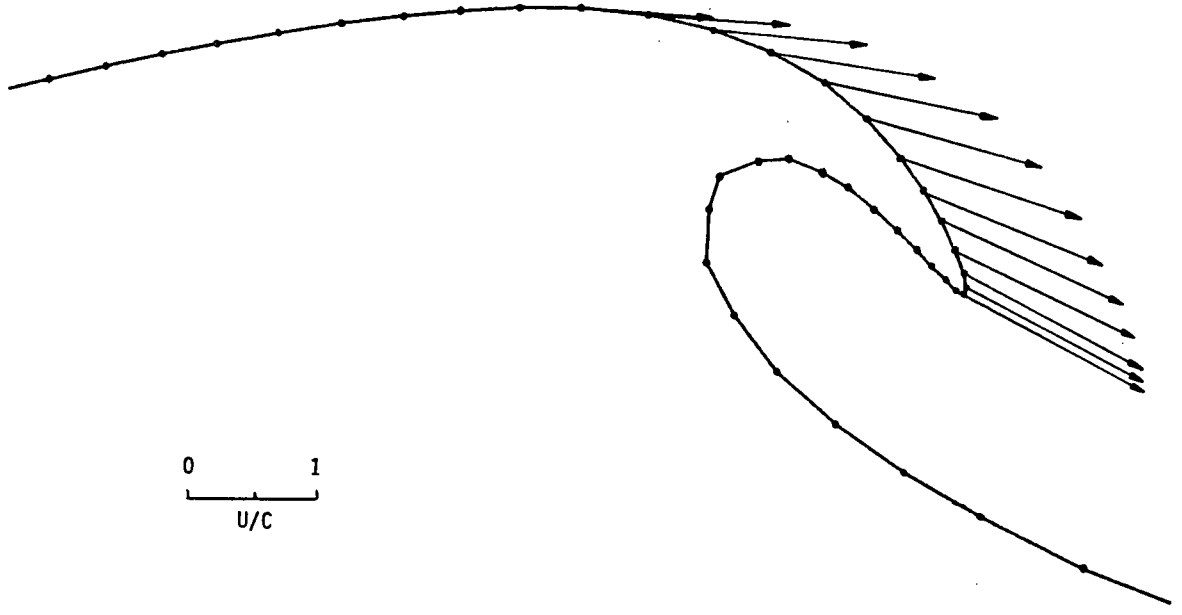

Figure 25. Fluid velocities around deep water plunging jet for case H/L = 0.13.

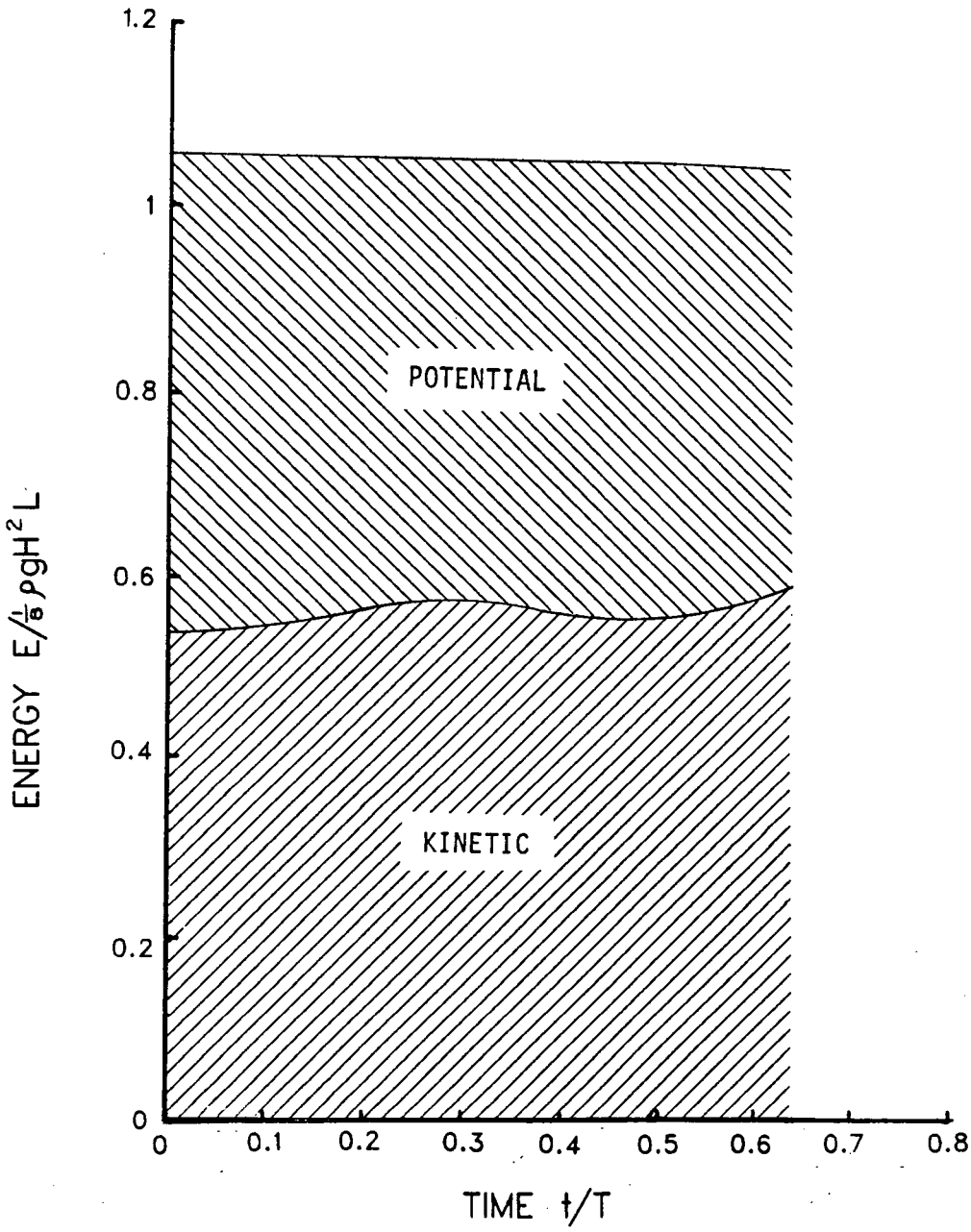

Figure 26. Control volume energy versus time for deep water breaking wave from cosine initial condition H/L = 0.13.

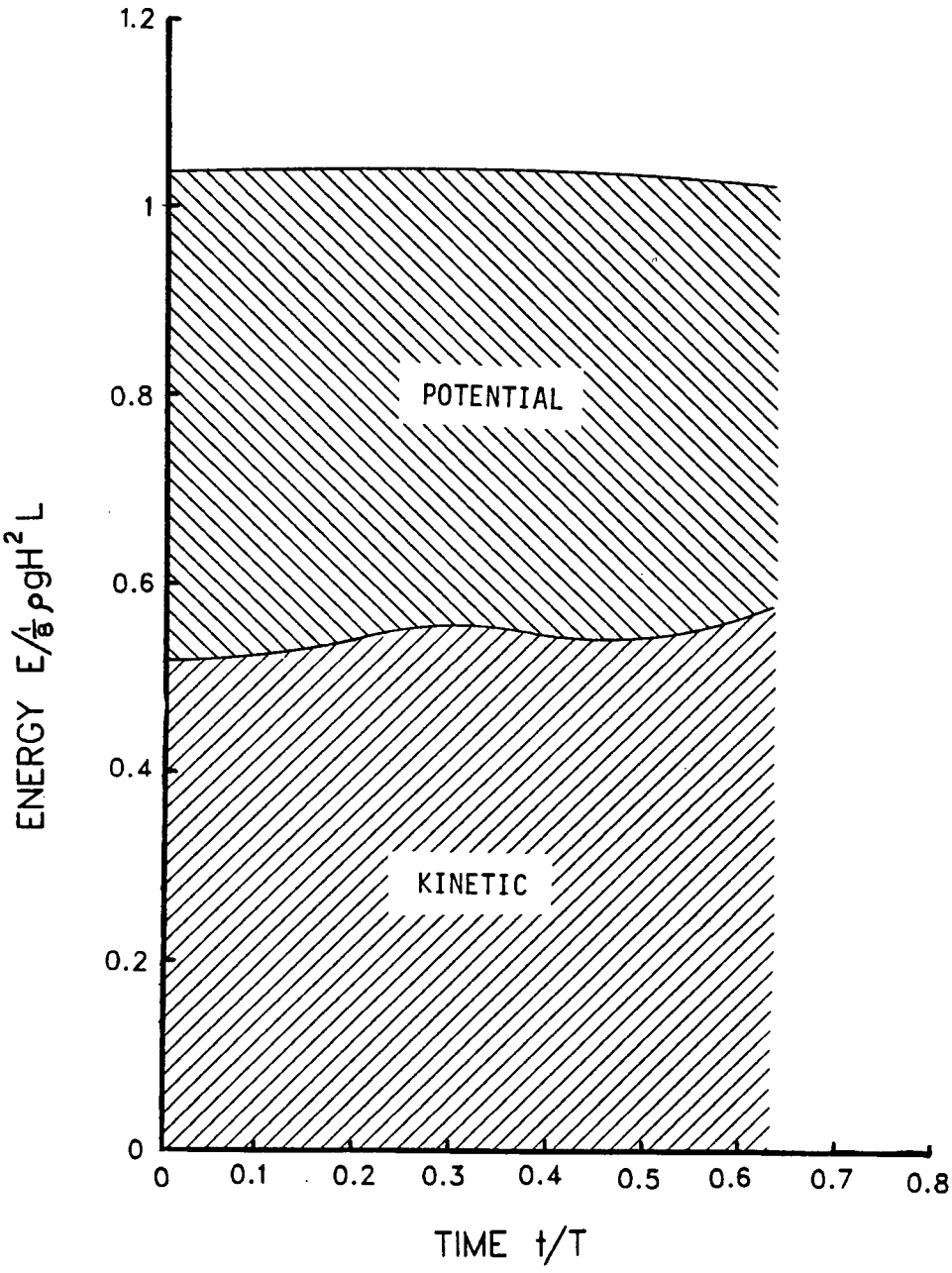

Figure 27. Control volume energy versus time for shallow water breaking wave from cosine initial condition H/L = 0.13. Depth ratio d/L = 0.25.

4. FLOATING BODY MOTION

4.1 INTRODUCTION

The formulation of a general two dimensional time stepping body motion simulation is presented. Development of such a simulation would permit extreme ship motions to be assessed in arbitrary steep nonlinear waves. Water on deck and capsizing could be modelled, and further extensions would allow breaking wave forces against the hull to be included.

4.2 NUMERICAL SOLUTION

4.2.1 FORMULATION

The control volume used for the wave simulation is modified to include an arbitrary two-dimensional surface piercing body in the contour of integration as shown in figure 28. The domain is again considered periodic with the free surface satisfying the kinematic and dynamic conditions discussed previously

$$\frac{\partial \eta}{\partial t} + \left(\frac{\partial \phi}{\partial x}\right)\left(\frac{\partial \eta}{\partial x}\right) = \frac{\partial \phi}{\partial y} \tag{4.1}$$

$$\frac{\partial \phi}{\partial t} + \frac{\rho}{2}\left[\left(\frac{\partial \phi}{\partial x}\right)^2 + \left(\frac{\partial \phi}{\partial y}\right)^2\right] + g\eta = f(t) \tag{4.2}$$

The stream function distribution on the body can be found by integrating the normal velocities along the surface giving

$$\psi = -\frac{\dot{\theta}R^2}{2} + u_G(y-y_G) - v_G(x-x_G) + \psi_o \qquad (4.3)$$

Details are described in Appendix VII. The constant of integration ψ_o can take on any value and is arbitrarily set to zero. The seabed is again a streamline, however, in this case the value cannot be chosen arbitrarily since ψ_o was fixed above and ψ here must be determined as part of the solution. The matrix for solving the complex potential is constructed such that terms involving ψ on the seabed are lumped together appropriately and ψ here is considered a single unknown.

Solution of the resulting boundary value problem using the Cauchy method provides velocities along the contour which are used to step the free surface nodal points as in the wave simulation

$$\frac{Dz}{Dt} = w^*$$

$$\frac{D\phi}{Dt} = \frac{ww^*}{2} - gy$$

The pressure distribution on the hull is found by applying Bernoulli's equation

$$P = -\rho\left(\frac{\partial\phi}{\partial t} + \frac{ww^*}{2} + gy\right) \qquad (4.4)$$

where $\partial\phi/\partial t$ remains to be determined. The obvious choice is to use a backwards finite difference approximation, however,

Vinje and Brevig (1981b) claim such a scheme is unstable and another technique must be used. An alternative method can be obtained by recognizing that since ϕ and ψ are harmonic functions, then so must be $\partial\phi/\partial t$ and $\partial\psi/\partial t$, consequently, $\partial\beta/\partial t$ is also an analytic function in the fluid domain. The Cauchy integral method is again applied in an identical fashion as for β using the time derivatives in this case. On the free surface $\partial\phi/\partial t$ is found from

$$\frac{\partial\phi}{\partial t} = -\frac{ww^*}{2} - gy$$

and on the body $\partial\psi/\partial t$ may be found by differentiating (4.3) giving

$$\frac{\partial\psi}{\partial t} = (y-y_G)a_x - (x-x_G)a_y - \frac{\ddot{\theta}R^2}{2}$$

$$+ u_G v - v_G u + [(x-x_G)(u_G-u) + (y-y_G)(v_G-v)]\dot{\theta} \quad (4.5)$$

The seabed has constant but unknown $\partial\psi/\partial t$ which comes out from the solution. The result yields $\partial\phi/\partial t$ on the body from which the pressure distribution can be found using (4.4) Body forces and moment about G are found as

$$F = -\int_S P\, n\, ds$$

$$M = -\int_S P\, r \times n\, ds$$

which are evaluated numerically as

$$F = -\sum_{i=N5}^{N6-1} i\left(\frac{P_{i+1}-P_i}{2}\right)(z_{i+1}-z_i)$$

$$M = -\sum_{i=N5}^{N6-1} \left(\frac{P_{i+1}-P_i}{2}\right) I_m\left\{i\left(\frac{z_{i+1}-z_i}{2} - z_G\right)(z_{i=1}-z_i)^*\right\}$$

Derivations are found in Appendix VIII. Accelerations are then determined from the equations of motion

$$a_x = \frac{F_x}{m}$$

$$a_y = \frac{F_y}{m}$$

$$\ddot{\theta} = \frac{M}{I}$$

which can then be integrated twice in time to find the heave, surge and roll motions.

4.2.2 THE CLOSURE PROBLEM

The technique outlined above suffers a closure problem in that the accelerations a_x, a_y and $\ddot{\theta}$ in (4.5) are unknown a priori and must come out as part of the solution. Fortunately Cauchy's theorem is linear and $\partial\beta/\partial t$ can be considered as being composed of four physically unreal components as

$$\frac{\partial\beta}{\partial t} = \left(\frac{\partial\beta}{\partial t}\right)_1 + a_x\left(\frac{\partial\beta}{\partial t}\right)_2 + a_y\left(\frac{\partial\beta}{\partial t}\right)_3 + \ddot{\theta}\left(\frac{\partial\beta}{\partial t}\right)_4$$

The problem is then decomposed into four independent solutions for the four contributing terms as shown schematically in figure 30. The boundary conditions on the surface are

$$\left(\frac{\partial\phi}{\partial t}\right)_1 = -\frac{ww^*}{2} - gy$$

$$\left(\frac{\partial\phi}{\partial t}\right)_2 = 0$$

$$\left(\frac{\partial\phi}{\partial t}\right)_3 = 0$$

$$\left(\frac{\partial\phi}{\partial t}\right)_4 = 0$$

while those on the body are

$$\left(\frac{\partial\psi}{\partial t}\right)_1 = u_G v - v_G u + \left[(x-x_G)(u_G-u) + (y-y_G)(v_G-v)\right]\dot{\theta}$$

$$\left(\frac{\partial\psi}{\partial t}\right)_2 = (y-y_G)$$

$$\left(\frac{\partial\psi}{\partial t}\right)_3 = (x-x_G)$$

$$\left(\frac{\partial\psi}{\partial t}\right)_4 = -\frac{\ddot{\theta}R^2}{2}$$

The body pressure distribution (4.4) can be written as

$$P = P_1 + P_2 a_x + P_3 a_y + P_4 \ddot{\theta}$$

where

$$P_1 = -\rho\left[\left(\frac{\partial\phi}{\partial t}\right)_1 - \frac{ww^*}{2} - gy\right]$$

$$P_2 = -\rho\left(\frac{\partial\phi}{\partial t}\right)_2$$

$$P_3 = -\rho\left(\frac{\partial\phi}{\partial t}\right)_3$$

$$P_4 = -\rho\left(\frac{\partial\phi}{\partial t}\right)_4$$

Forces and moments are then calculated for each individual problem using equations (4.5), and substituted into the equations of motion (4.7) which take on the form

$$F_{x_1} + F_{x_2} a_x + F_{x_3} a_y + F_{x_4} \ddot{\theta} = m a_x$$

$$F_{y_1} + F_{y_2} a_x \quad F_{y_3} a_y + F_{y_4} \ddot{\theta} - W = m a_y$$

$$M_1 + M_2 a_x + M_3 a_y + M_4 \ddot{\theta} = I \ddot{\theta}$$

These three equations can be solved for the three unknown accelerations a_x, a_y and $\ddot{\theta}$, thereby closing the problem.

Given accelerations at each time step, velocities and motions are determined by successive integrations. A simple finite difference Euler scheme is used for these integrations

$$u_{n+1} = u_n + a_x \Delta t$$

$$v_{n+1} = v_n + a_y \Delta t$$

$$\dot{\theta}_{n+1} = \dot{\theta}_n + \ddot{\theta} \Delta t$$

$$x_{n+1} = x_n + u_n \Delta t + \frac{a_x}{2} (\Delta t)^2$$

$$y_{n+1} = y_n + v_n \Delta t + \frac{a_y}{2} (\Delta t)^2$$

$$\theta_{n+1} = \theta_n + \dot{\theta}_n \Delta t + \frac{\ddot{\theta}}{2} (\Delta t)^2$$

A flow chart for the body motion simulation is presented in figure 31.

4.2.3 BODY POSITION

The body geometry is stored as a set of points defined in a ship coordinate system (x_s, y_s) attached to the body with the origin at G as shown in figure 29. Body position is specified by the location of G in the global frame (x, y) and the roll angle θ measured counterclockwise from the vertical. These three variables are known at each time step allowing the location of ship nodal points to be calculated in the global frame using the following transformation

$$x = x_s \cos\theta - y_s \sin\theta + x_G$$

$$y = x_s \sin\theta + y_s \cos\theta + y_G$$

The intersection points between the free surface and the body are difficult to determine due to the possible presence of singularities here and for practical purposes approximate methods must be used as discussed in a later section. Once the intersection points are located, nodes are placed there on each side and others added or removed at each time step to keep the same number of elements NH on the hull as the wetted surface changes throughout the simulation. Depending on the direction of fluid motion near the hull, a free surface nodal point may enter the body. This condition must

be checked at each time step and if necessary the offending point replaced outside the body. Conversely, if a nodal point migrates excessively far from the body, the resulting large free surface element should be subdivided appropriately.

4.2.4 INITIAL CONDITIONS

Initialization of the simulation requires a free surface profile $\eta(x)$ and potential $\phi(x)$, as well as body position (x_G, y_G, θ) and velocities (u_G, v_G, $\dot{\theta}$). There are consequently six free parameters to specify when placing the body on the wave. Unlike the wave simulation, however, these initial conditions cannot be chosen arbitrarily. The free surface velocity is specified by $\phi(s)$ and must match the body velocity at the intersection points to avoid erroneously forcing fluid into or away from the body. This condition is ensured by adjusting the potential distribution in the neighbourhood of the body to satisfy the relation

$$\frac{\partial \phi}{\partial s} = v_n \cdot \hat{\xi}$$

at the intersection point P, where $\hat{\xi}$ is the unit vector along the free surface. The ϕ distribution is adjusted by a quadratic polynomial extrapolation over a region of length Lc on either side of the body to match the derivatives at the intersection points.

4.2.5 INTERSECTION SINGULARITIES

The intersection points between the body and the free surface present special problems because the fluid velocity w(z) may be singular here. Yim (1985) describes the analytical solution to a semi-infinite flate plate moving downward on the free surface. The complex velocity has a square root singularity at the plate edge where the velocity becomes infinite. Greenhow and Lin (1985) describe a series solution to an impulsively moved vertical boundary that predicts a logarithmically infinite surface elevation next to the wall. These two idealized cases are analogous to the heave and surge of a floating body, which for general motions is obviously a much more complicated problem. Singularity behaviour at the free surface in the more general case is less clear. Lin et al (1984) describe experiments which closely examined the flow behaviour next to an impulsively moved wavemaker, suggesting that the singularity may actually have a physical interpretation. Photographs show a very small fluid jet being ejected perpendicularly from the paddle at the intersection. This peculiar phenomenon is an example of how potential flow modelling can break down in certain regions, where effects such as viscosity and surface tension keep the real fluid behaviour finite.

One further problem at the intersection points is that even in the absence of singularities, the variation of ϕ or ψ may be rapid close to the body. Maskell and Ursell (1970)

give a second order solution for a heaving cylinder which shows a steep gradient of ψ and high velocities near the body. High element density would be required here to achieve good resolution, though it is not clear if this is really necessary for a stable solution. Furthermore, excessive element density can cause additional numerical problems both in computational stability and further complication of element redistribution near the body. It has been found that reducing the number of free surface elements often improves numerical stability, though resolution is obviously the cost. One may have to be sacrificed for the other.

4.2.6 INTERSECTION SOLUTION

Several techniques were tried to handle the numerical solution in the intersection region, each requiring a separate simulation program. Boundary conditions for the three main versions are shown in figure 32. Version I was the same as that used by Vinje and Brevig (1981c) where a node is placed at the intersection point and the stream function specified as a boundary condition. The velocity potential here comes out from the solution and as such does not necessarily satisfy the free surface boundary condition. Experience with this formulation showed the complex potential to be poorly resolved near the body, and the velocity potential indeed did not satisfy the free surface boundary condition at the intersection. The discrepency was often large. Examination of the numerical solution at each

time step revealed that the fluid velocities were poorly calculated in the intersection regions, often yielding unrealistically large values that were not even of the correct sign.

Version II attempted to reduce the singularity problem by displacing nodes a small distance on either side of the true intersection points and thereby avoid integrating through the singularity. This method did not appear to offer any improvement. Since the small diagonal connecting elements are included in the contour integration, this formulation is really equivalent to version I with the nodes shifted appropriately. In the usual formulation each node is considered to have contributions from each of the adjacent elements. To avoid integrating through the singlarities, however, these small elements must be left out of the contour. As such, the matrix coefficients for these special points must be rederived considering the contribution to β from one element only.

Version III attempts to improve the solution by placing a node directly at each intersection and specifying both ϕ and ψ here. Lin et al (1984) used this formulation for modelling a wave maker in a basin and claimed greatly improved results. The number of unknowns in this case is two less and the matrix must be reconstructed accordingly. The actual equations used are given in Appendix IX. This formulation resulted in a more stable solution, although the fluid velocities near the intersections were still

questionable.

In all the above formulations the velocities at the intersection points could not be determined directly by the numerical procedure and the values calculated at these two points were discarded. Without these velocites, however, the free surface position at the next time step cannot be determined. This is certainly the most challenging problem in achieving a good simulation. For practical purposes, these velocities must be estimated by other means using some sort of approximation. The most obvious choice is to use a polynomial extrapolation into the body, however, since the immediately adjacent points are also under the influence of the singularities their positions are questionable as well. Furthermore, surface irreguarities can produce large errors, especially if the element nearest the body requires a long extrapolation. A more tenable solution is to simply extend the adjacent nodes horizontally into the body. This alternative works well provided the surface is not excessively steep and allows the simulation to proceed. For steeper waves three point smoothing must be used in the region next to the body. Results are presented in a later section.

4.2.7 A NUMERICAL PERTURBATION CORRECTION

Throughout the simulations both the fluid volume and total system energy were monitored as a measure of numerical stability. The volume was usually quite stable although the

total energy often grew significantly. These errors were no doubt due largely to the problems of accuracy in the intersection regions and the need to impose artificial values here. While these errors are obviously undesirable they do, however, provide a possible means for correcting the positions of the intersection points. Conservation of mass and energy can be considered as two equations for the two unknown intersection locations.

Referring to equations (3.7) and (3.8) it can be seen that the energy of the fluid is of the form

$$E = E_p(x,y) + E_k(\phi,\psi)$$

Unfortunately, this expression cannot be cast into a closed form solution for the unknown intersection positions since the contour geometry (x,y) and the complex potential (ϕ,ψ) are linked numerically. An iterative trial and error solution to satisfy the two constraints might be possible, however, computational time would become prohibitive with no guarantee of convergence.

An alternative is to consider a "numerical perturbation" method where small changes in system energy and volume can be derived as functions of small changes in the intersection positions. That is,

$$\Delta V = f(\Delta y_L, \Delta y_R, \ell_L, \ell_R)$$

$$\Delta E = f(\Delta y_L, \Delta y_R, \ell_L, \ell_R)$$

where Δy_L and Δy_R represent upward vertical displacements of the left and right intersection points and l_L and l_R are the lengths of the elements next to the body. These expressions take on the form

$$\Delta V = A(\Delta y_L) + B(\Delta y_R)$$

$$\Delta E = C(\Delta y_L) + D(\Delta y_R) + E(\Delta y_L)^2 + F(\Delta y_R)^2$$

where the coefficients are functions of known quantities. These equations can then be solved for Δy_L and Δy_R. Detailed derivations may be found in Appendix X. To implement the procedure, a preliminary solution is obtained by the previously described method and the changes in volume and energy noted. These are then used to calculate corrections to the intersection positions. As only two constraints are available, only the two elements adjacent to the body are involved. A more elaborate correction scheme involving adjacent points as well would be possible using polynomial segments, however, the derivation would be much more complicated. Only the first order approximation described above is considered in the present work. This self-correcting simulation is referred to as version IV.

4.3 RESULTS

For the purpose of testing the simulation a simple case is examined first of a rectangular body heeled over in calm water. Upon release the body should undergo roll oscillations while disturbance waves radiate outward removing energy from the body and damping the motion. The roll period in this case can be calculated theoretically from the standard formula for small angles found in any text such as Comstock (1967). For the present case the following conditions applied: beam = 10 feet, draft = 3 feet, weight = 1900 lb/ft, radius of gyration = 2.5 feet, and initial angle = 30°. The theoretical roll period for this body is 2.5 sec. For preliminary tests the sharp corners were rounded to keep velocities well-behaved and avoid creating unnecessary additional complications. Figure 33 shows the results of a simulation carried out using version III with L=100 feet, NS=25, NH=15, N=100, and Δt = 0.05 sec. Close inspection of the figure reveals very low disturbances radiating outward as the body oscillates. As expected, fluid velocities were poorly resolved in the intersection region, however, as the forces in this simple case were primarily hydrostatic the behaviour was good. The actual roll period was about 2.6 seconds during which the system gained energy causing an increase in roll amplitude of about five degrees over one cycle. The calculated motions are plotted in figure 34.

The second test case examines the motion of the same body on a low amplitude wave. Figures 35 and 36 show the

results of a motion simulation on a cosine wave of length L = 100 feet and height ratio H/L = 0.04 using version III. The initial conditions in this case were chosen carefully by placing the body at the midpoint of the trough where the velocity potential gradients on the free surface are equal on both sides of the body and match the initial horizontal body velocity. The initial roll angle was chosen arbitrarily to be 15°. As can be seen in the figure the nonlinear effects were large and the wave underwent considerable modification as the crest passed the body. Energy was imparted to the body resulting in an increased roll angle and water on deck after one cycle. Hull pressure distributions are shown in figure 37 for various positions on the wave and the motions for sway, heave, and roll are plotted in figure 38. Of particular interest are the rather large horizontal displacements. Accelerations in this case were as much as 0.5 g. These characteristics have also been noted in model experiments [26].

The third test case involved increasing the wave height further to H/L = 0.08 to invoke large nonlinear effects and examine the limitations of the model. Placing the body in the trough with an initial horizontal velocity to match the velocity potential gradient resulted in almost immediate water on deck. By giving the body an additional negative angular velocity of -0.15 rad/sec deck wetting was delayed and eventually came about from the downwave side as the body rolled too far back. Figures 39 and 40 show the actual

simulation. The resulting motions are plotted in figure 41.

One final test case is that of the body in a very steep wave of H/L = 0.12. Undisturbed, this initial condition would result in a distinct plunging breaker as shown earlier in chapter 3, however, as can be seen in figures 42 and 43 the presence of the body modified the wave considerably and breaking did not occur before water on deck terminated the simulation. Several initial conditions were tried for this wave and all resulted in water on deck in less than one second. The motions for this case are plotted in figure 44.

For steep waves one would expect the body to act somewhat as a wave damping device removing energy much like a floating breakwater. This wave energy, of course, is converted to body motion and, as a result, would tend to keep the wave from breaking. Achievement of a breaking wave next to the body will require some other type of initial wave configuration.

Version IV of the simulation employing the self-correction scheme met with limited success and was useful only for nearly calm water. It became apparent that correcting the positions and boundary conditions of only the intersection nodal points was insufficient, and really the method should be used in conjunction with polynomial segments to allow the adjacent free surface points to be corrected as well, both in position and velocity potential.

Having demonstrated the ability to simulate extreme body motions in steep nonlinear waves, the next step was to

use the simulation program to carry out numerical experiments under varying initial conditions. The current versions have been found to accumulate energy due to numerical problems at the intersection singularities and are therefore really only useful for short time periods. Furthermore, previous experience with a simpler linearized simulation [3] has shown that roughly two wave periods are required for transient effects to decay and allow the body to acheive steady state rolling in a wave train. Therefore, if capsizing is to be modelled with the present version of the simulation it must be induced in a short period of time. Bearing this in mind, the selection of initial conditions becomes very important. Initial position placement can be arbitrary, however, the choice of the three corresponding initial velocities and their relative phases will have a great influence on the subsequent motions. For example, figure 45 shows the effect of zero initial angular velocity. Water on deck is almost immediate due to rotational inertia. More likely, a ship at this point would have a negative angular velocity, although this would really depend on the prior unsteady response history.

It is clear now that conditions leading to water on deck or capsizing can indeed be simulated and one must now ask whether or not the chosen initial conditions are likely to occur in nature.

4.4 EXTENSION TO THREE DIMENSIONS

Comparisons made with a constant element Green's function method used by other investigators [3], to simulate a breaking wave produced somewhat differing results. The Cauchy integral method remained remarkably constant in both energy and volume and therefore for two dimensional free surface problems appears to be the preferred technique. Unfortunately, because the method uses complex variables it cannot be extended to three dimensions. For some cases, however, one may be able to make an approximation. Since ship motions and stability are dominated by the midbody, end effects would be expected to be of minor significance, especially for short time periods involved in ship capsizing. If in addition the beam/length ratio is reasonably low one can use a "slender ship" approximation where the crossflow term $\partial^2\phi/\partial^2 z$ in Laplace's equation is assumed small enough to neglect and the flow is locally two dimensional. Strip theory can then be used where the ship is considered equivalent to a composite of representative prismatic sections as shown in figure 46 and independent simulations are carried out for each. The forces and moments can then summed over each section to obtain the total body accelerations and resulting motions.

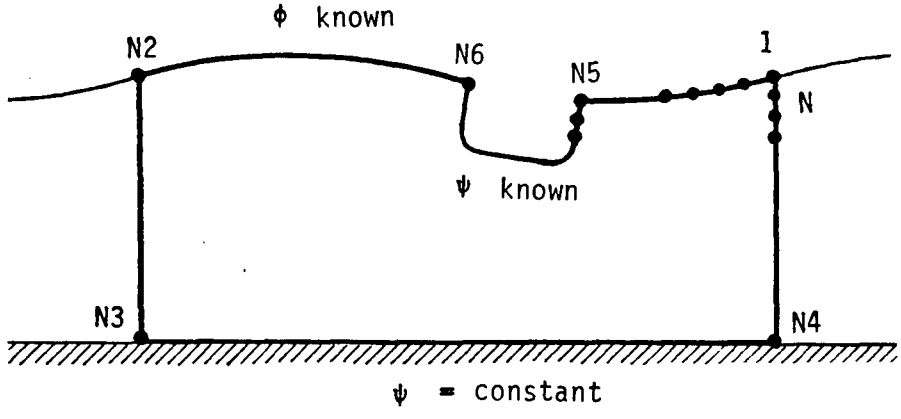

Figure 28. Control volume for body motion simulation.

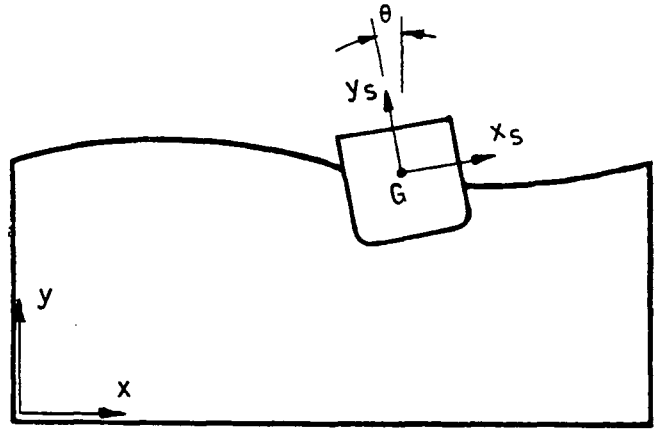

Figure 29. Definition of coordinate systems.

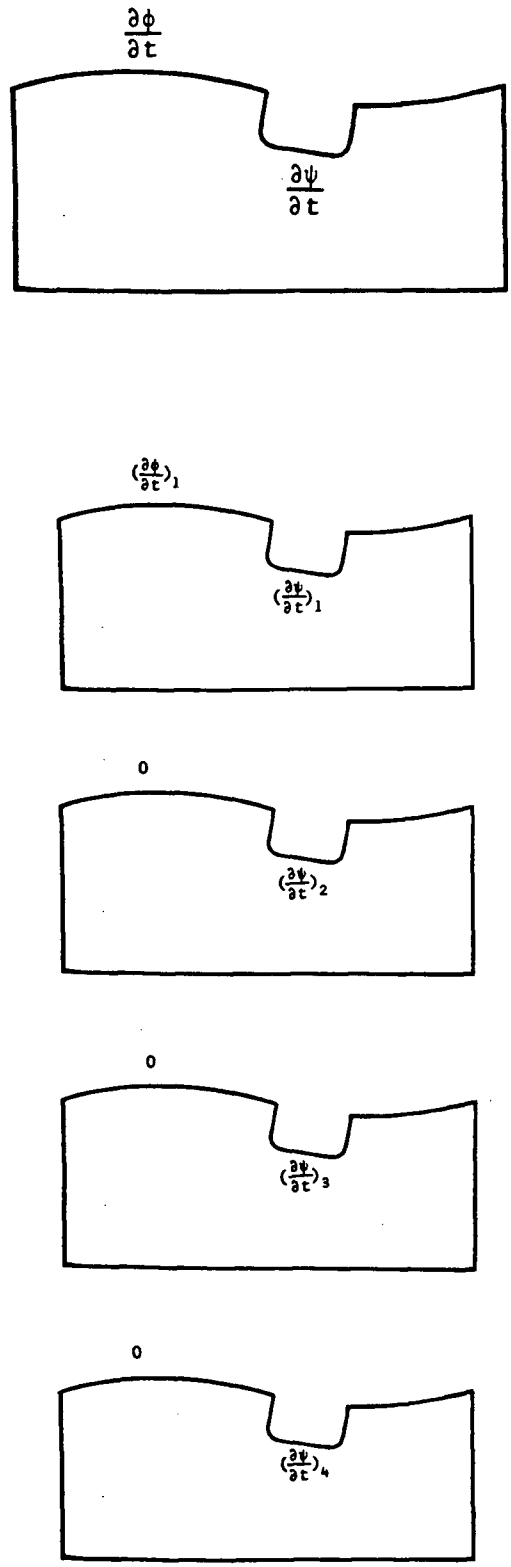

Figure 30. Decomposition of time derivatives into four independent problems.

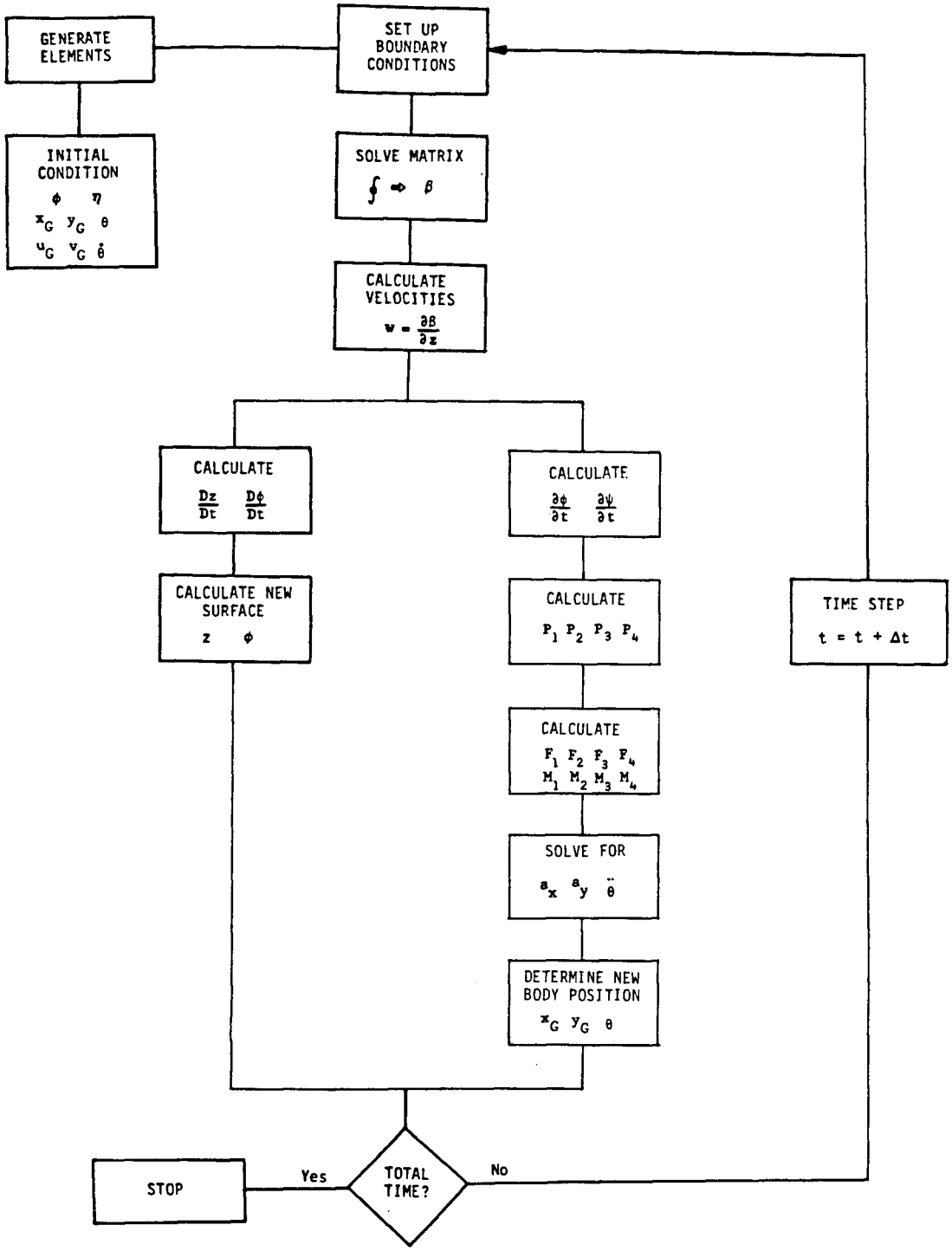

Figure 31. Flow chart for body motion simulation algorithm.

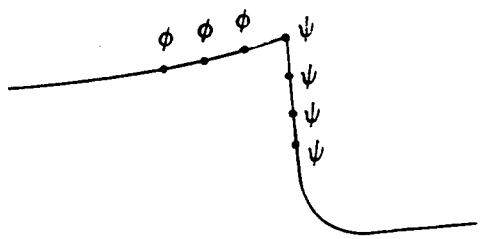

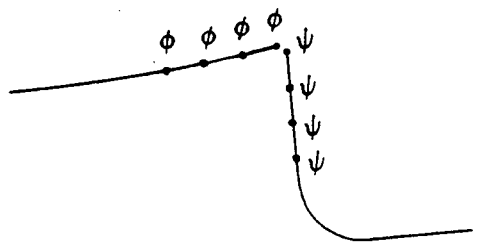

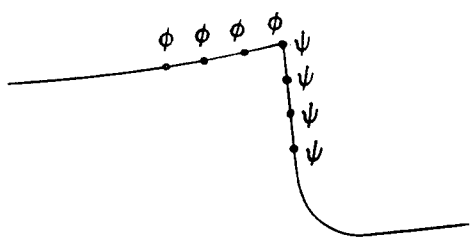

Figure 32. Boundary conditions tested.

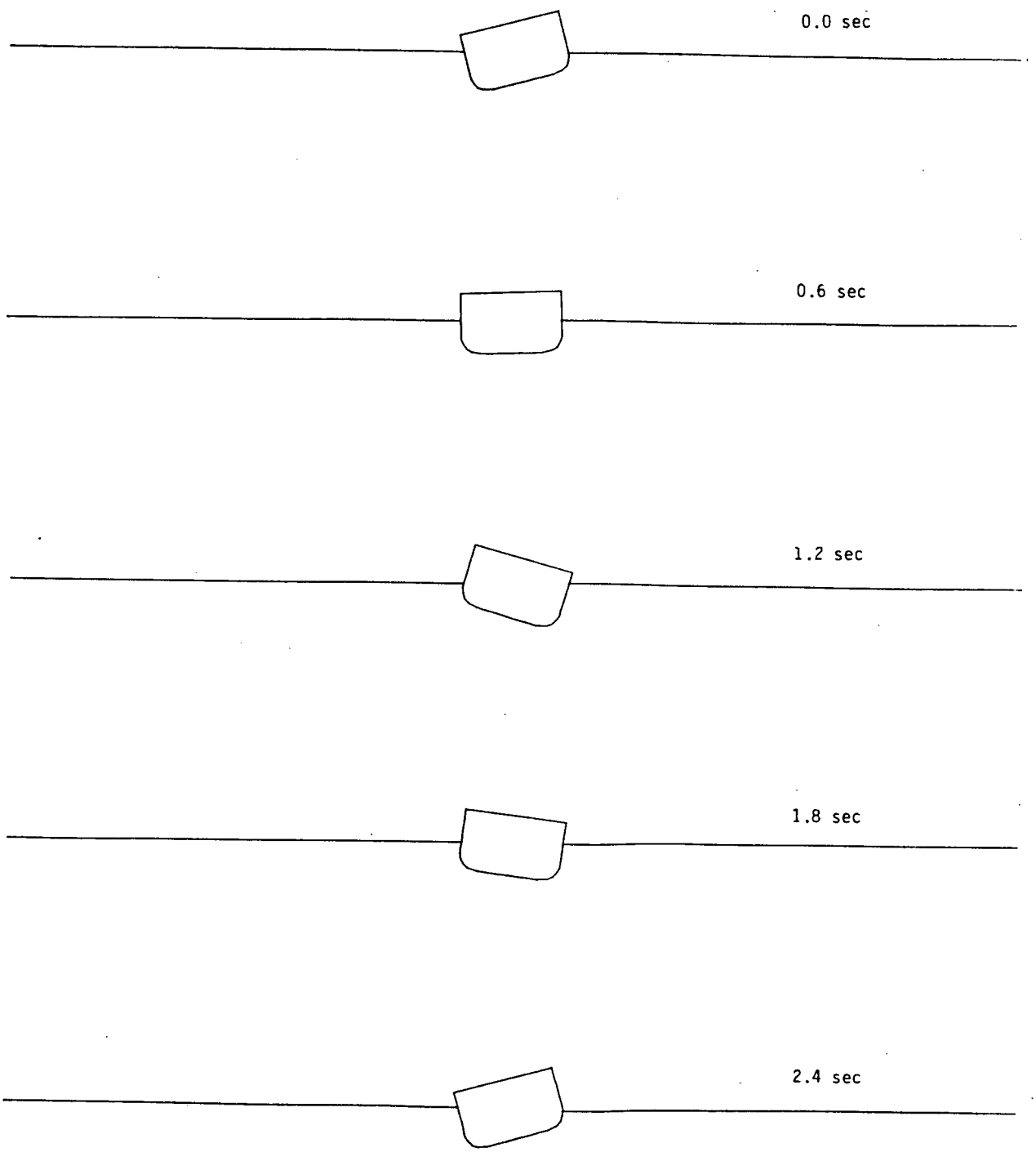

Figure 33. Simulation of roll motion in calm water.

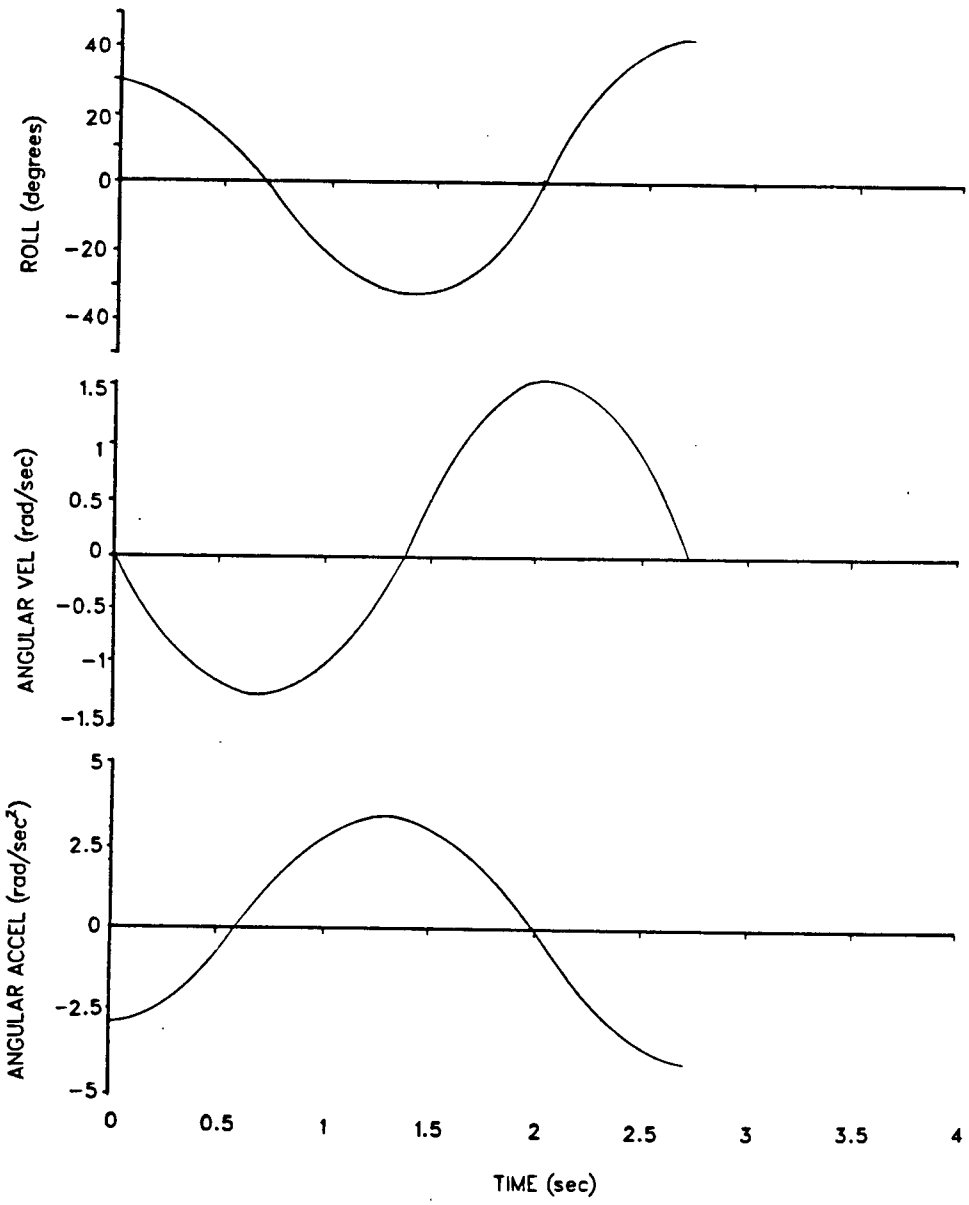

Figure 34. Roll motion for calm water case.

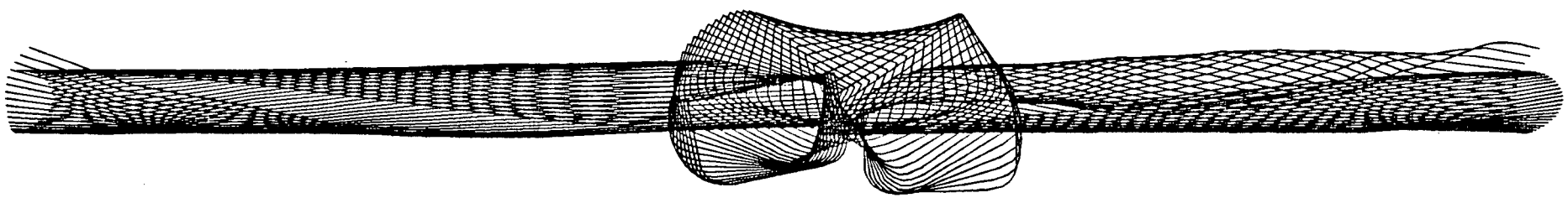

Figure 35. Simulation of motion in wave H/L = 0.04.

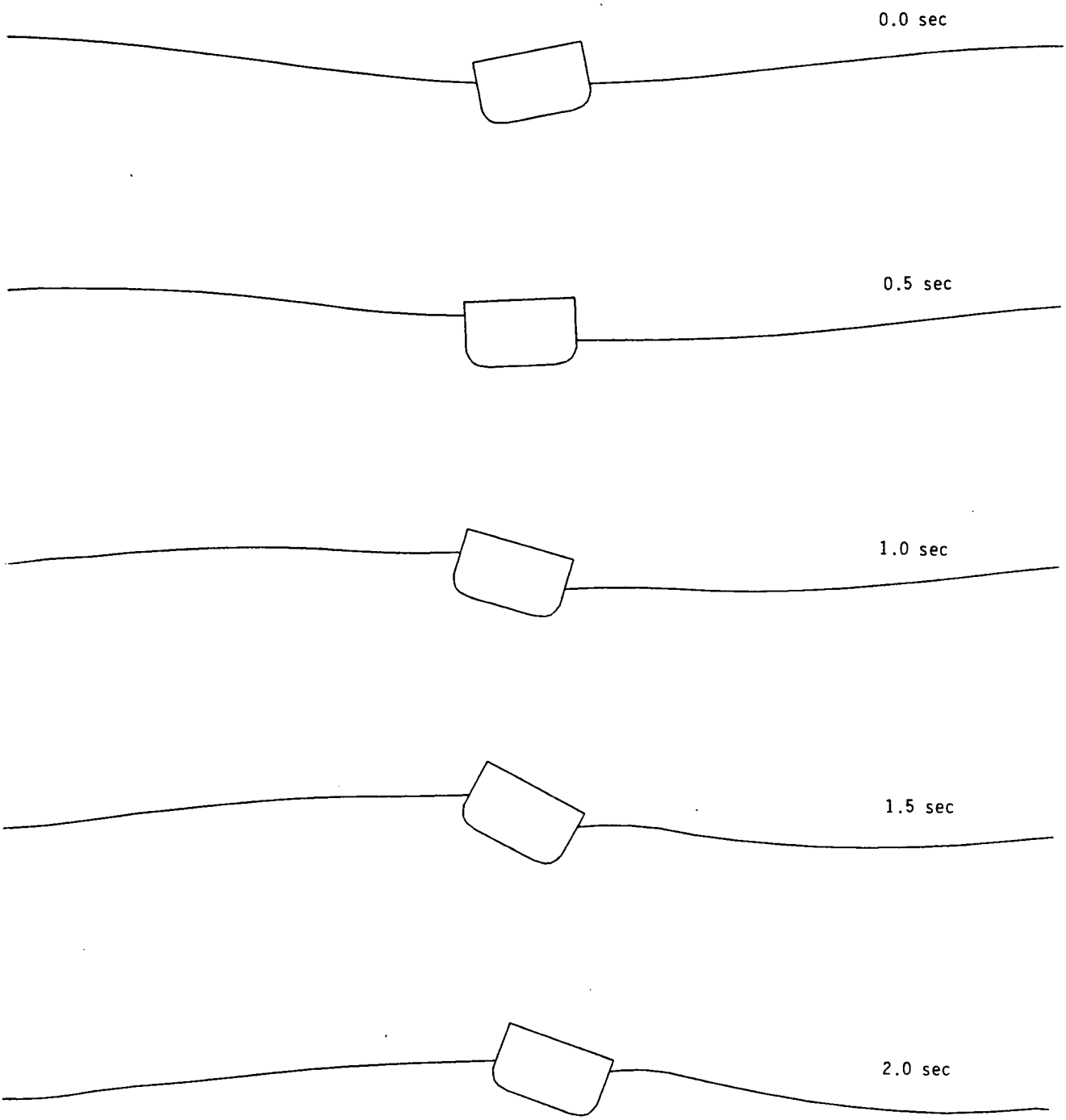

Figure 36. Simulation of motion in wave H/L = 0.04.

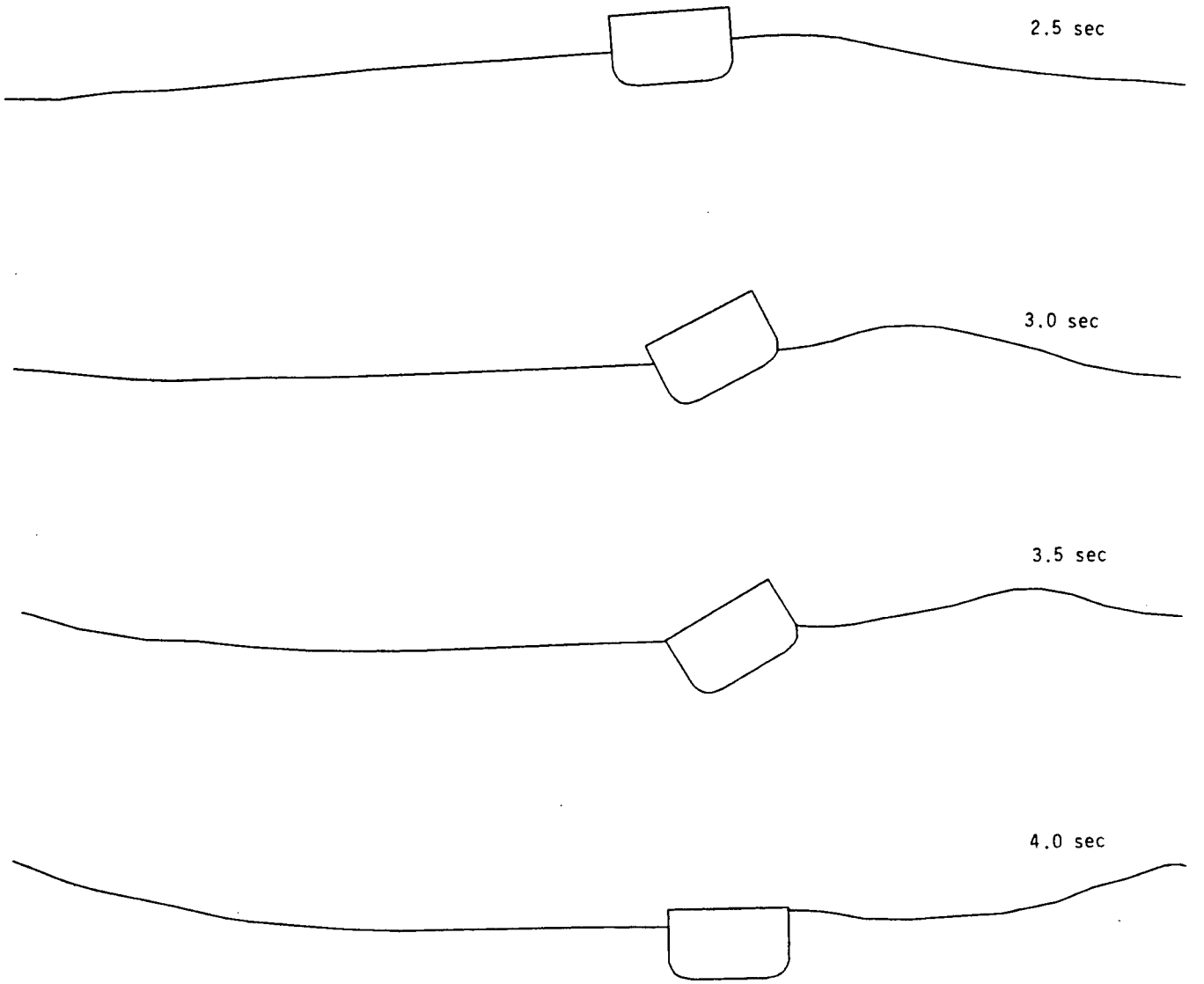
2.5 sec
3.0 sec
3.5 sec
4.0 sec

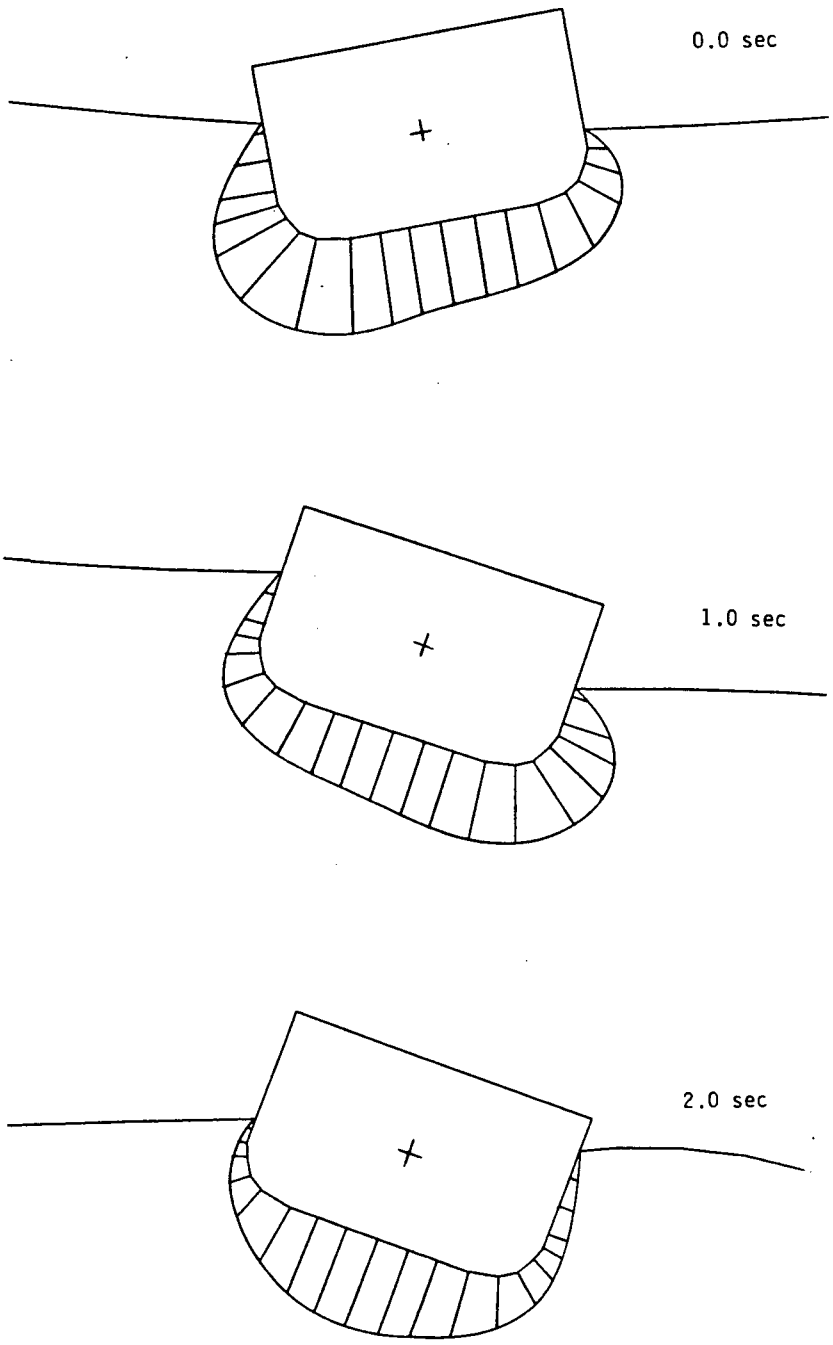

Figure 37. Hull pressure distributions for H/L = 0.04.

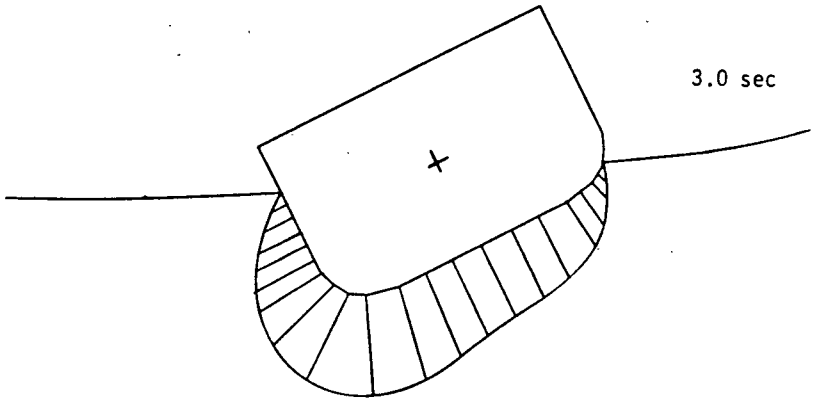
3.0 sec

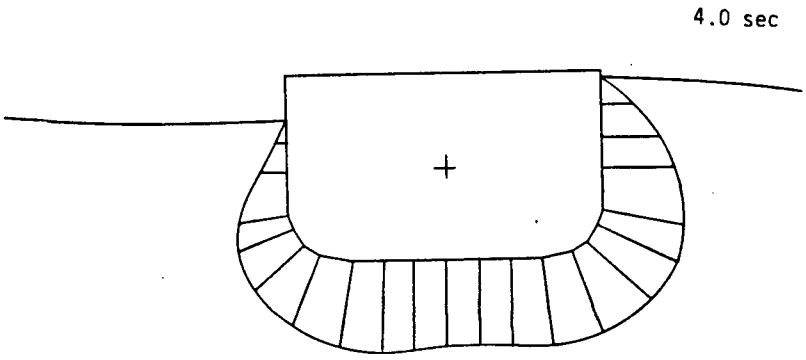
4.0 sec

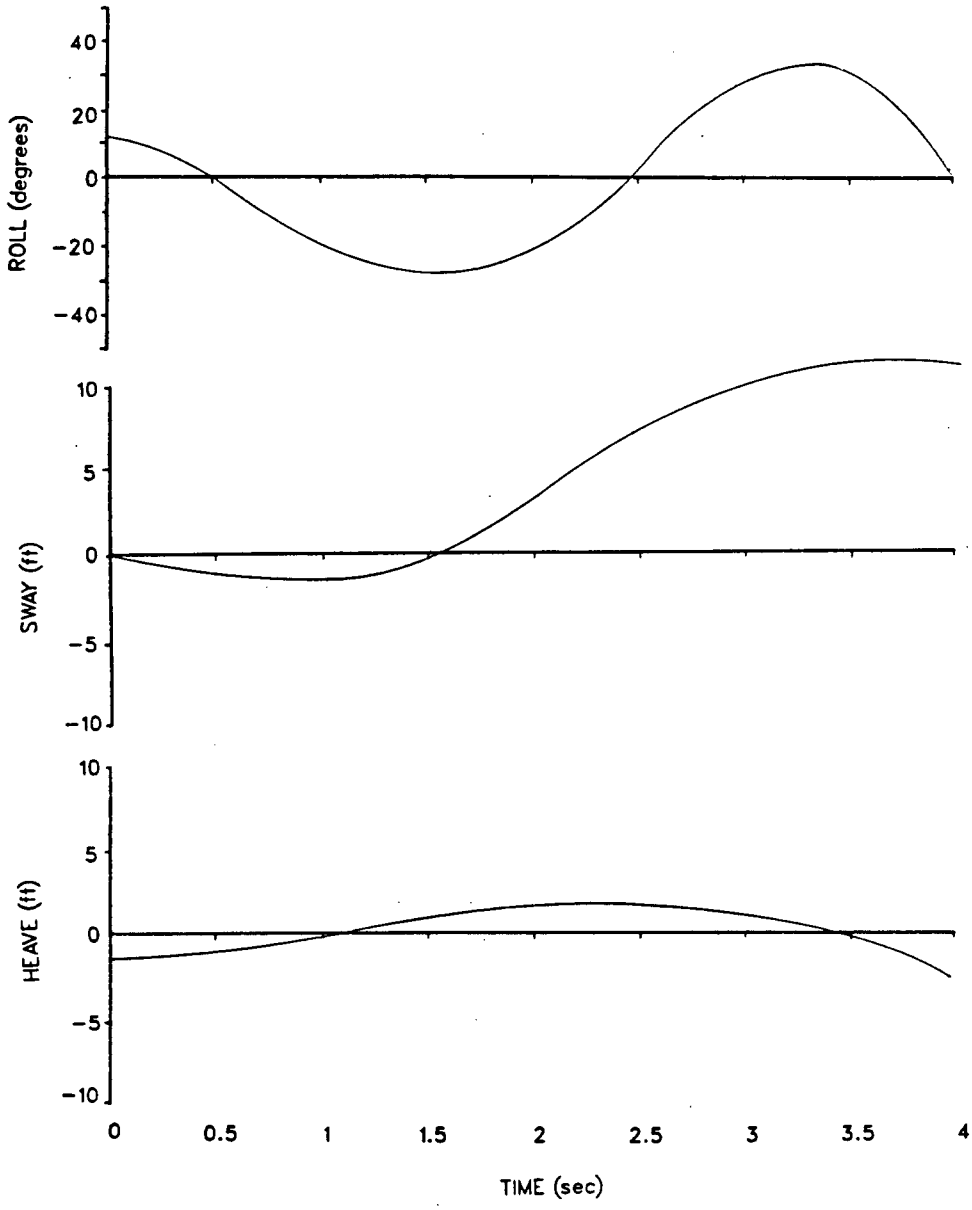

Figure 38. Motions for case H/L = 0.04.

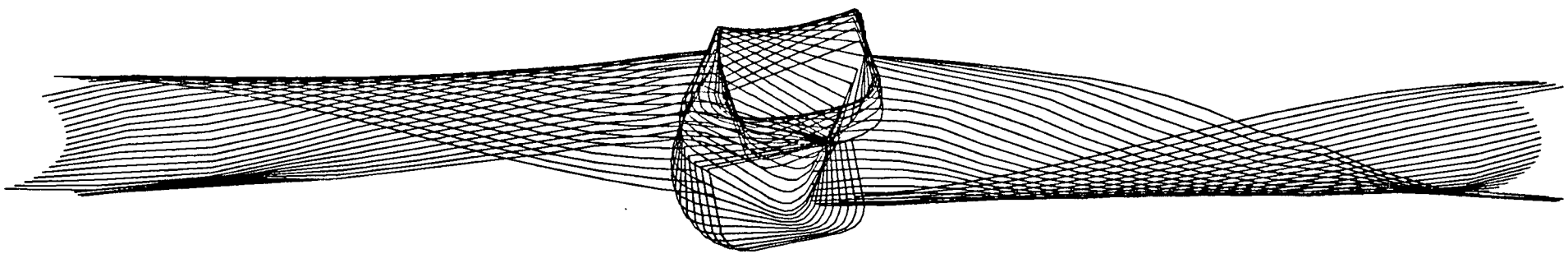

Figure 39. Simulation of motion in wave H/L = 0.08.

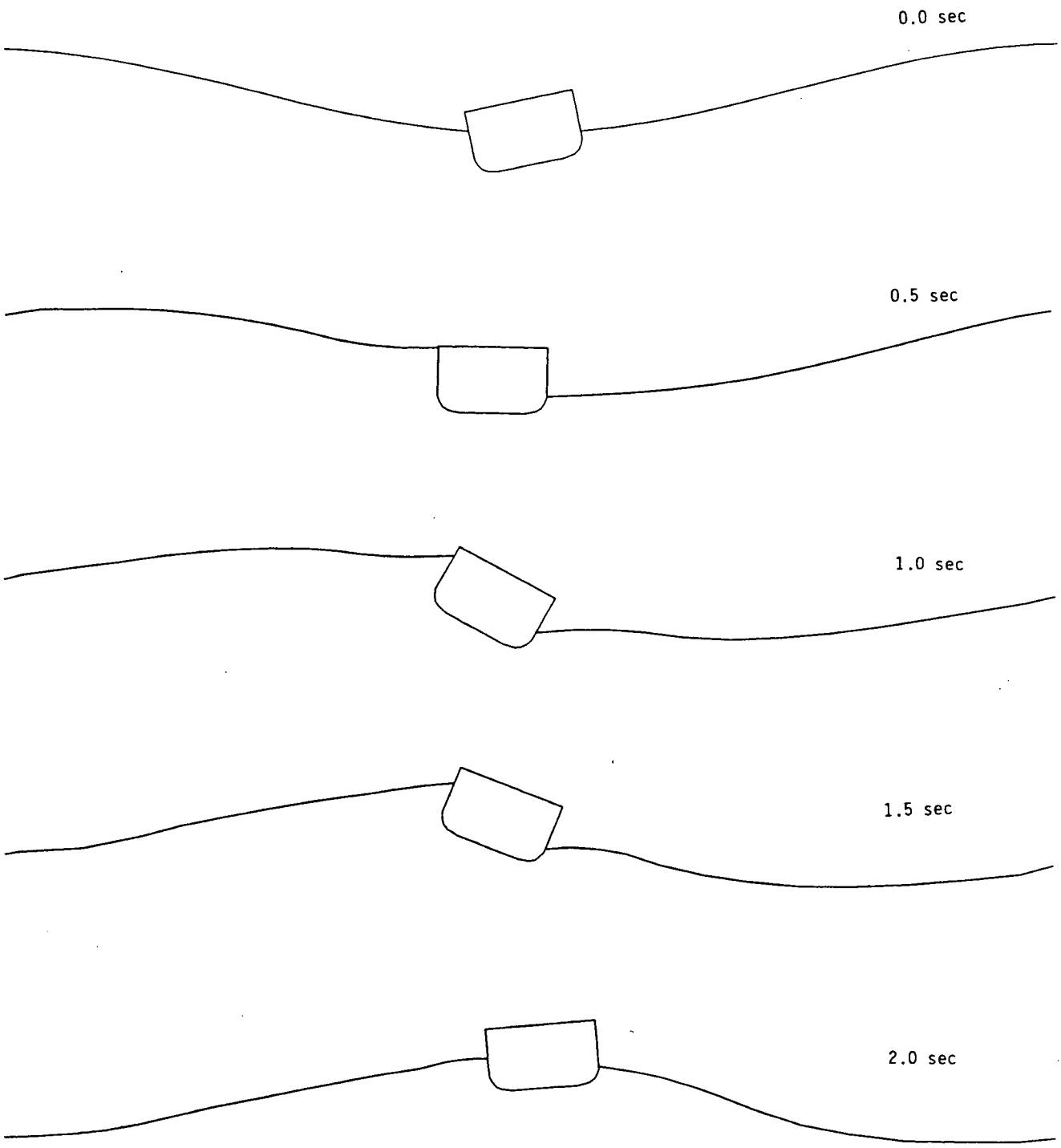

Figure 40. Simulation of motion in wave H/L = 0.08.

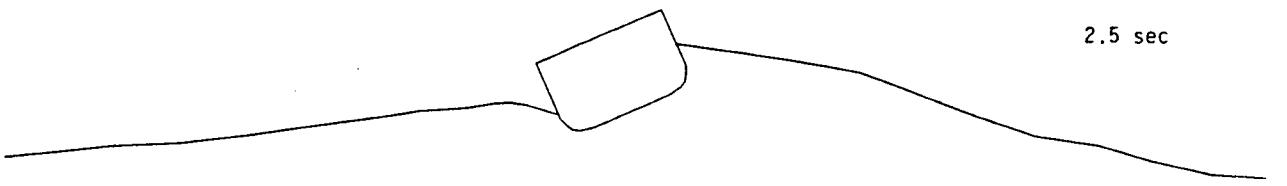
2.5 sec

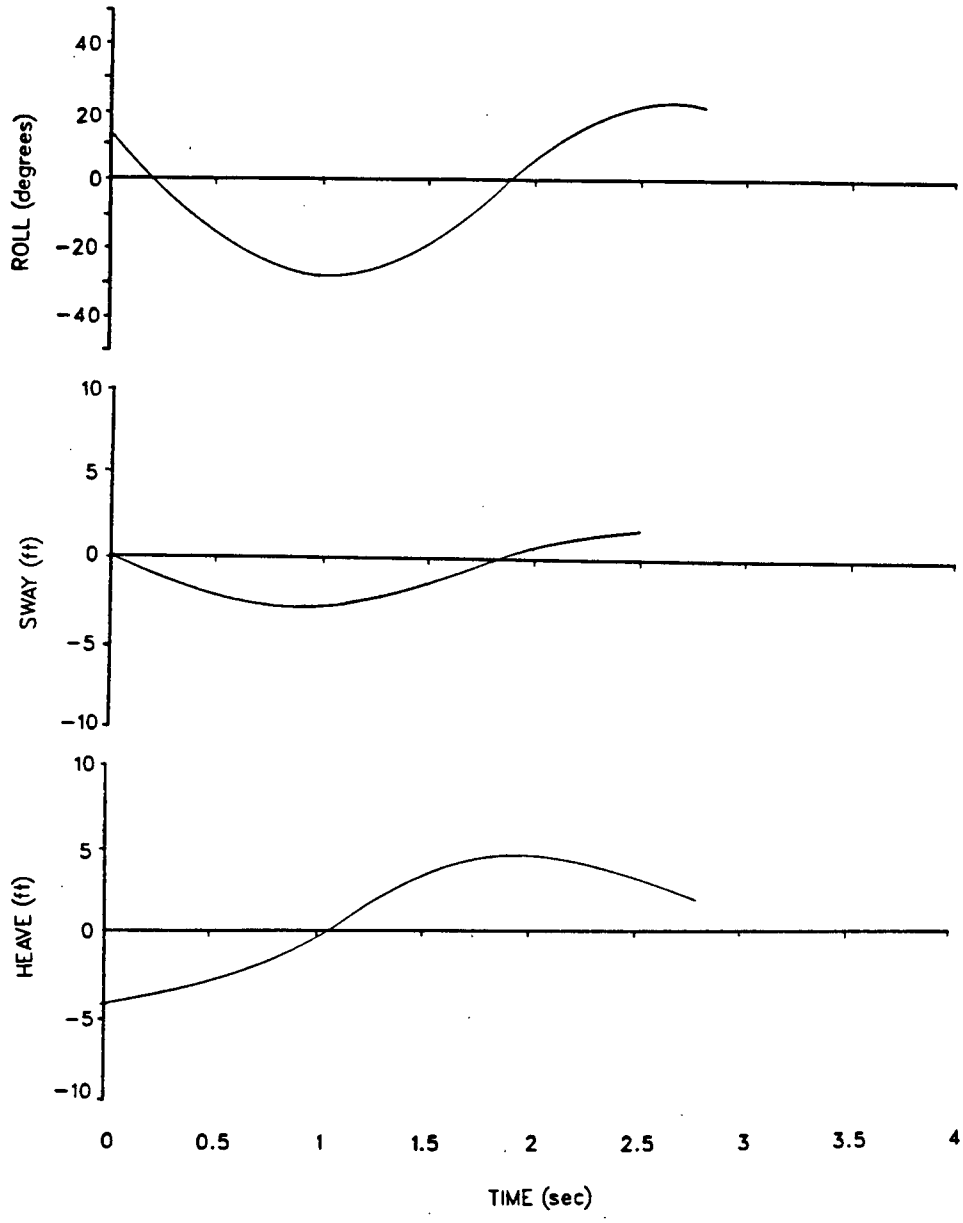

Figure 41. Motions for case H/L = 0.08.

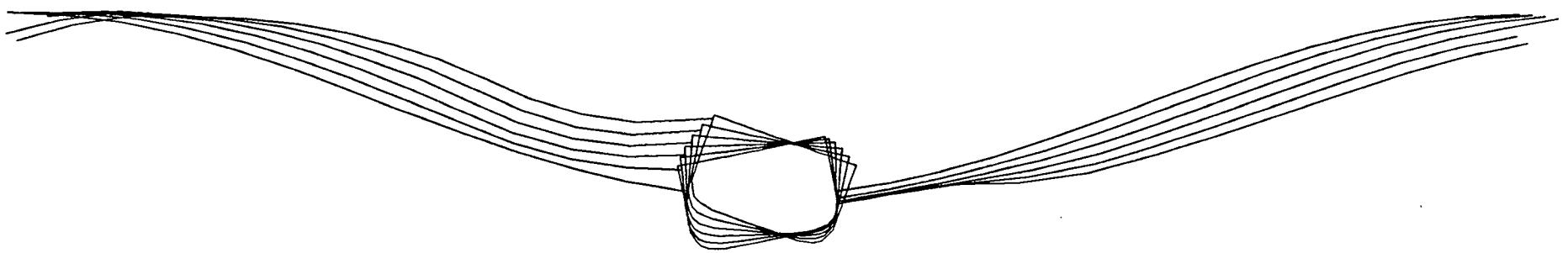

Figure 42. Simulation of motion in wave H/L = 0.12.

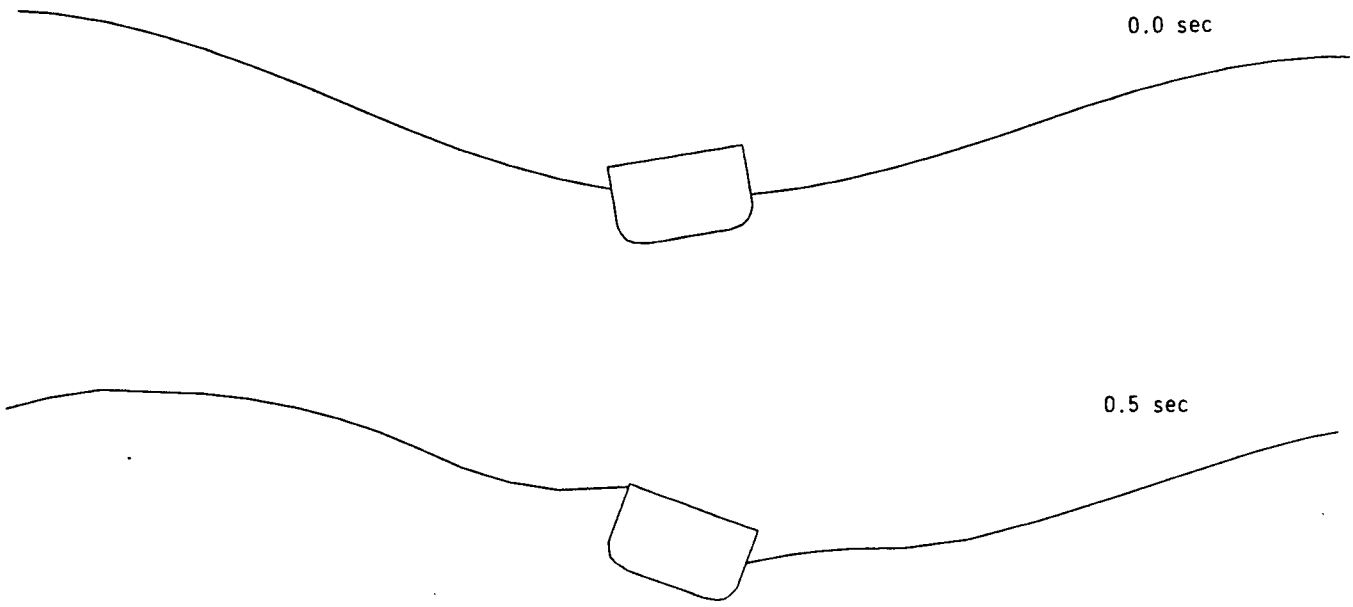

Figure 43. Simulation of motion in wave H/L = 0.12.

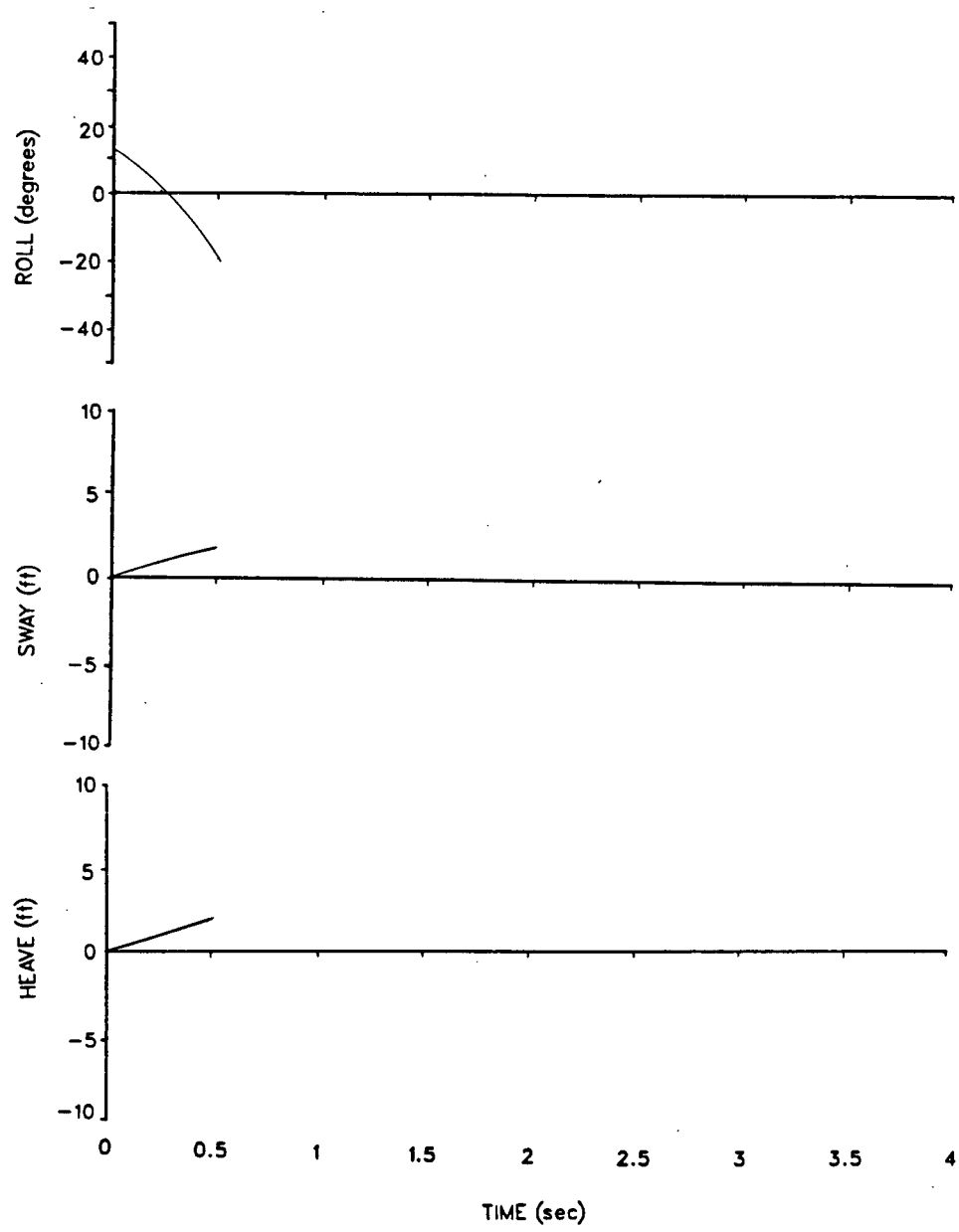

Figure 44. Motions for case H/L = 0.12.

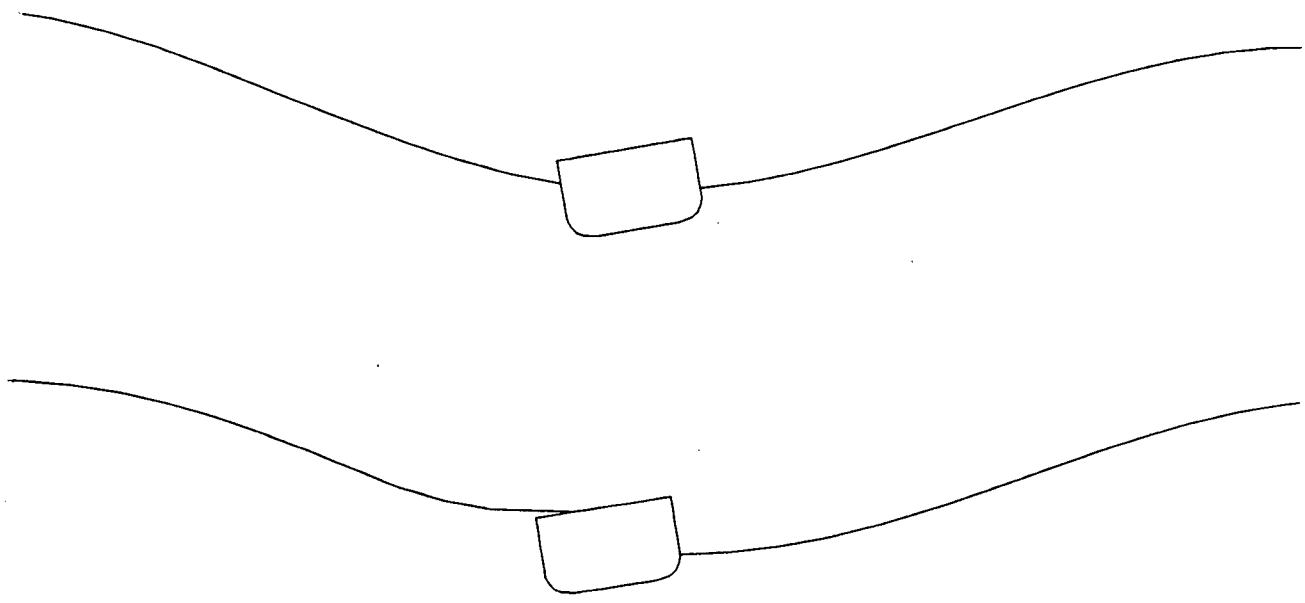

Figure 45. Result of zero initial angular velocity.

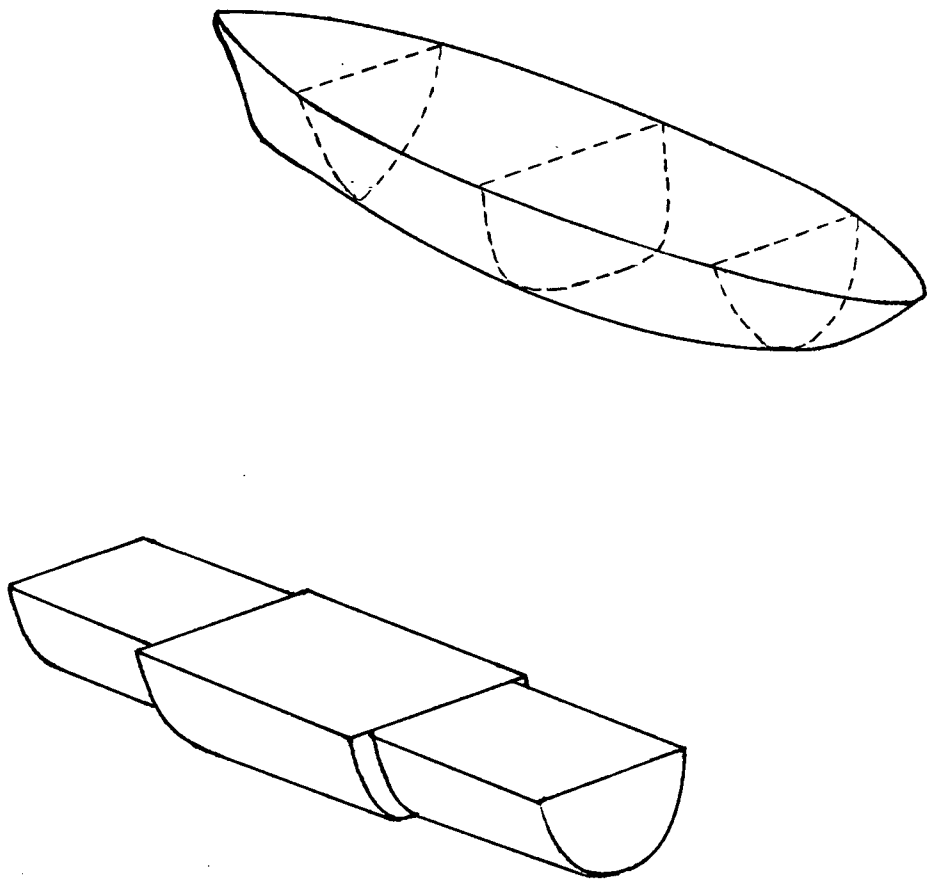

Figure 46. Equivalent prismatic representation of ship.

5. CONCLUSIONS AND RECOMMENDATIONS

A complex variable boundary integral method has been used to numerically simulate the behaviour of nonlinear free surface waves. Breaking waves in deep and shallow water have been simulated and profile velocities determined. The method has proven to be powerful and robust. Virtually any continuous smooth wave can be simulated provided initial conditions can be assigned.

The method was extended to include the nonlinear motions of a body on the free surface, and simulations were carried out for several test cases. The presence of singularities at the free surface intersection points prevented the direct determination of velocities in the surrounding regions, limiting accuracy of the simulation. No accurate solutions to this intersection problem have been developed to date.

A two step perturbation correction procedure was introduced to force the additional constraints of mass and energy conservation. This first order correction was used for locating the two intersection points. The accuracy of the immediately adjacent points, however, was also questionable and work is needed to make the correction procedure more robust to allow these additional points to be included. Local smoothing of function distributions may be required. Free surface smoothing may be helpful as well, however, care must be taken that important details of the surface behaviour are not lost in the process. Empirical

information would be useful here as a guide.

There is wide scope for further work on the body motion problem. One possible alternative solution method that has so far not been attempted is to reformulate the problem as an inner and outer solution. The outer solution would involve the usual Cauchy integral around a path that is clear of the singular points and well behaved, while inner solutions on each side of the body could utilize additional information such as conservation of mass, momentum flux, and energy while ensuring matched values of complex potential and velocities along the common boundaries. Polynomial distributions of functions could be assumed close to the body provided their coefficients could be determined.

The forces due to a wave breaking on the side of a vessel are of great interest in studying the safety of ships at sea. These forces could be estimated by a simulation either by means of applying an explicit boundary condition on the recipient surface, or more simply by considering the breaking wave jet to be approximately equivalent to an idealized jet whose force on a flat plate can be calculated from momentum considerations knowing the fluid velocity and effective flow rate as a function of time.

Empirical input is still required to define the free surface behaviour near the intersections, but is lacking. It is recommended that experiments be carried out on two dimensional bodies in a wave basin under both small and large amplitude waves so that detailed empirical results may

be obtained as a baseline for numerical experiments. Strobe photographs and floating marker particles are needed to accurately obtain the free surface profiles and fluid velocities. This information would be useful for establishing realistic initial conditions and assessing the progress of numerical simulations as various formulations are tried.

The importance of viscous effects such as boundary layer development and vortex shedding remain to be determined and may be quite significant, especially in cases where the hull geometry is not smooth. Flow visualization studies should be carried out using dye injection to elucidate the flow structure. Such experiments would also provide a useful assessment of the validity of strip theory by allowing observation of the longitudinal crossflow component.

REFERENCES

1. Bhattacharyya, R. (1979) *Dynamics of Marine Vehicles.* John Wiley & Sons, New York.
2. Carnahan, B. (1969) *Applied Numerical Methods.* John Wiley & Sons, New York.
3. Chan, J.L.K. (1986) Unpublished results. Dep't of Mechanical Engineering, University of British Columbia, Vancouver, Canada.
4. Chan, R.K.C. & Street, R.L. (1970) "A Computer Study of Finite Amplitude Water Waves", *J. Comp. Phys.*, Vol. 6, pp. 68-79.
5. Chapman, R.B. (1979) "Large Amplitude Transient Motion of Two Dimensional Floating Bodies", *J. Ship Res.*, Vol. 23, No. 1, pp. 20-31.
6. Cokelet, E.D. (1977) "Breaking Waves," *Nature*, Vol. 267, pp. 769-774.
7. Comstock, J.P. (1967) *Principles of Naval Architecture*, Soc. of Naval Architects and Marine Engineers., New York.
8. Faltinsen, O.M. (1977) "Numerical Solutions of Transient Nonlinear Free Surface Motion Outside or Inside Moving Bodies", *2nd Int. Conf. Numerical Ship Hydrodynamics*, Univ. of California, Berkeley.
9. Flanigan, F.J. (1972) *Complex Variables: Harmonic and Analytic Functions*. Dover Publications Inc., New York.
10. Garrison, C.J. (1975) "Hydrodynamics of Large Objects in the Sea. Part II: Motion of Free-Floating Bodies", *J. Hydronautics*, Vol. 9, pp.58-63.
11. Greenhow, M., Brevig, P. & Taylor. J. (1982) "A Theoretical and Experimental Study of the Capsize of Salter's Duck in Extreme Waves", *J. Fluid Mech.* Vol 118, pp. 221-239.
12. Greenhow, M. & Woei-Min, L. (1985) "Numerical Simulation of Nonlinear Free Surface Flows Generated by Wedge Entry

and Wavemaker Motions", Preprint, *4th Int. Conf. Numerical Ship Hydrodynamics*, Washington, D.C.

13. Isaacson, M. de S. Q. (1982) "Nonlinear Wave Effects on Fixed and Floating Bodies", *J. Fluid Mech.* Vol. 120, pp. 267-281.
14. Kim, W.D. (1966) "On a Free Floating Ship in Waves", *J. Ship Res.* Vol. 10, pp.182-191.
15. Kjeldsen, P. (1981) "Shock Pressures from Deep Water Breaking Waves", *Int. Symp. Hydrodynamics in Ocean Eng.*, Norwegian Inst. Tech., pp. 567-584.
16. Kjeldsen, S.P. & Myrhaug, D. (1979) "Breaking Waves in Deep Water and Resulting Wave Forces", OTC 3646, *11th Offshore Tech. Conf.*, Houston, Texas, pp. 2515-2522.
17. Korvin-Kroukovsky, B.V. (1955) "Investigations of Ship Motions in Regular Waves", *Trans. SNAME*, Vol. 63, pp. 386-435.
18. Lee, C.M. (1969) "The Second Order Theory of Heaving Cylinders in a Free Surface", *J. Ship Res.* Vol. 12, pp. 313-327.
19. Lin, W.M., Newman, J.N., & Yue, D.K. (1984) "Nonlinear Forced Motions of Floating Bodies", *15th Symp. on Naval Hydrodynamics*, Hamburg, Germany, pp. 33-49.
20. Longuet-Higgins, M.S. (1977) "Advances in the Calculation of Steep Surface Waves and Plunging Breakers", *2nd Int. Conf. Numerical Ship Hydrodynamics*, Univ. of California, Berkeley.
21. Longuet-Higgins, M.S. & Cokelet, E.D. (1976) "The Deformation of Steep Surface Waves on Water, I. A Numerical Method of Computation", *Proc. R. Soc. Lond. Series A.* Vol 350, pp. 1-26.
22. MacCamy, R.C. (1964) "The Motion of Cylinders of Shallow Draft", *J. Ship Res.* Vol. 7, No. 3, pp. 1-11.
23. Maskell, S.J. & Ursell, F. (1970) "The Transient Motion of a Floating Body", *J. Fluid Mech.* Vol. 44, pp. 303-313.
24. Newman, J.N. (1980) *Marine Hydrodynamics*. MIT Press, Cambridge, Mass.

25. Rawson, K.J. & Tupper, E.C. (1968) *Basic Ship Theory.* Longmans, London.
26. Rohling, G.F. (1986) "Experimental Investigation of Fishing Vessel Stability in a Transverse Seaway", *M.A.Sc. Thesis*, Dept. of Mechanical Engineering, University of British Columbia, Vancouver, Canada.
27. Sarpkaya, T. & Isaacson, M. (1981) *Mechanics of Wave Forces on Offshore Structures.* Van Nostrand Reinhold Co., New York.
28. Schultz, W.W., Ramberg, S.E. & Griffin, O.M. (1986) "Steep and Breaking Deep Water Waves", Preprint *16th Symp. Naval Hydrodynamics*, Berkeley, California.
29. Schwartz, L.W. (1974) "Computer Extension and Analytic Continuation of Stoke's Expansion for Gravity Waves", *J. Fluid Mech.* Vol. 62, pp. 553-578.
30. Skjelbreia, L. & Hendrickson, J. (1960) "Fifth Order Gravity Wave Theory", *Proc. 7th Coastal Eng. Conf.*, The Hague, pp.184-196.
31. Stokes, G.G. (1847) "On the Theory of Oscillatory Waves", *Trans. Camb. Phil. Soc.* Vol. 8, pp. 441-455.
32. Ursell, (1964) "The Decay of the Free Motion of a Floating Body", *J. Fluid Mech.* Vol. 19, pp. 305-319.
33. Vinje, T. & Brevig, P. (1980) "Breaking Waves on Finite Water Depth - A Numerical Study", *SIS Report*, Norwegian Hydrodynamic Laboratories.
34. Vinje, T. & Brevig, P. (1981a) "Numerical Calculation of Forces from Breaking Waves", *Int. Symp. Hydrodynamics in Ocean Eng.*, Norwegian Inst. Tech., pp. 547-565.
35. Vinje, T. & Brevig, P. (1981b) "Nonlinear Ship Motions", *3rd Int. Conf. Numerical Ship Hydrodynamics*, Paris, pp. 257-266.
36. Vinje, T. & Brevig, P. (1981c) "Nonlinear Two Dimensional Ship Motions", Study", *SIS Report*, Norwegian Hydrodynamic Laboratories.
37. Wehausen, J.V. (1971) "The Motion of Floating Bodies", *Ann. Rev. Fluid Mech.* Vol. 3, pp.237-268.
38. Wiegel, R.L. (1964) *Oceanographical Engineering.*

Prentice-Hall, Englewood Cliffs, N.J.

39. Yim, B. (1985) "Numerical Solution for Two Dimensional Wedge Slamming With a Nonlinear Free Surface Condition", Preprint, *4th Int. Conf. Numerical Ship Hydrodynamics*, Washington, D.C.

APPENDIX I

THE CAUCHY INTEGRAL THEOREM

According to the Cauchy Theorem the path integral of an analytic function around a closed contour is zero

$$\oint f(z)\, dz = 0$$

therefore

$$\oint_C \frac{\beta}{z-z_0}\, dz = 0 \qquad \text{(A1.1)}$$

so long as z_0 is outside the enclosed region

For the purpose of numerical solution z_0 must take on the values of the nodal points on the contour and hence must be allowed to approach C. The contour C can be considered as composed of C_1 and C_2 where C_2 subtends z_0 with a circular arc of radius ϵ.

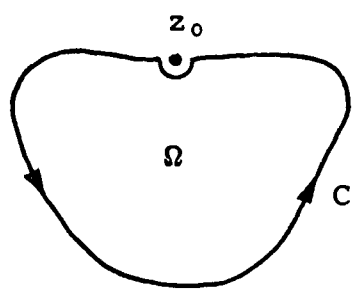

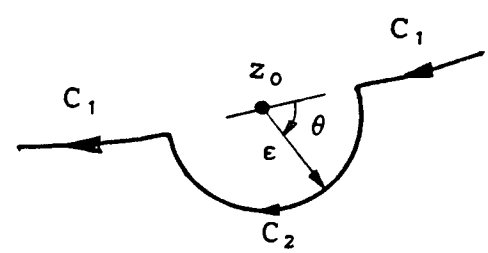

In this case Cauchy's Theorem can be written as

$$\int_{C_1} \frac{\beta}{z-z_0}\, dz + \int_{C_2} \frac{\beta}{z-z_0}\, dz = 0 \qquad \text{(A1.2)}$$

On C_2

$$z = z_0 + \varepsilon\, e^{i\theta}$$

$$dz = i\, \varepsilon\, e^{i\theta}\, d\theta$$

so equation (A1.2) reduces to

$$\int_{C_1} \frac{\beta}{z-z_0}\, dz + \int_{o}^{\alpha} \frac{\beta}{\varepsilon\, e^{i\theta}}\, i\, \varepsilon\, e^{i\theta}\, d\theta = 0$$

where α is the interior angle at z_o equal to π when C is smooth and $\pi/2$ at a corner. Evaluating in the limit as $\epsilon \longrightarrow 0$, C_1 becomes C and

$$\oint_{C} \frac{\beta}{z-z_0}\, dz = i\, \alpha\, \beta(z_0)$$

APPENDIX II

FORMULATION OF INTEGRAL EQUATION

The contour is discretized into N elements and the values of $\beta(z)$ are calculated at the nodes joining each. The integral equation (2.2) can then be reduced to a linear equation for numerical solution, as described below.

As outlined in Chapter 2, Cauchy's theorem can be written

$$\oint_C \frac{\beta}{z-z_0}\,dz = i\,\alpha\,\beta(z_0) \qquad \text{(A2.1)}$$

$$\sum_{j=1}^{N} \left\{ \int_{z_j}^{z_{j+1}} \frac{\beta}{z-z_0}\,dz \right\} = i\,\alpha\,\beta(z_0) \qquad \text{(A2.2)}$$

$$\sum_{j=1}^{N} \gamma_{ij}\,\beta_j = i\,\alpha\,\beta_i$$

To evaluate the integral in (A2.2), and hence calculate $\gamma_{i,j}$, a linear distribution of β is assumed over each element. $\beta(z)$ can then be expressed by the linear interpolation formula

$$\beta = \left(\frac{z-z_j}{z_{j+1}-z_j}\right)\beta_{j+1} + \left(\frac{z_{j+1}-z}{z_{j+1}-z_j}\right)\beta_j \qquad z_j \leq z \leq z_{j+1}$$

which is then substituted into (A2.2). Integration is then carried out as .

$$\int_{z_j}^{z_{j+1}} \frac{\beta(z)}{z-z_0}\,dz = \int_{z_j}^{z_{j+1}} \left\{\left(\frac{z_{j+1}-z}{z_{j+1}-z_j}\right)\beta_j + \left(\frac{z-z_j}{z_{j+1}-z_j}\right)\beta_{j+1}\right\} \frac{dz}{z-z_0}$$

$$= \frac{\beta_j}{(z_{j+1}-z_j)} \int_{z_j}^{z_{j+1}} \left(\frac{z_{j+1}-z}{z-z_0}\right) dz + \frac{\beta_{j+1}}{(z_{j+1}-z_j)} \int_{z_j}^{z_{j+1}} \left(\frac{z-z_j}{z-z_0}\right) dz$$

$$= \frac{\beta_j}{(z_{j+1}-z_j)} I_1 + \frac{\beta_{j+1}}{(z_{j+1}-z_j)} I_2$$

where

$$I_1 = \int_{z_j}^{z_{j+1}} \frac{z_{j+1}}{z-z_0} dz - \int_{z_j}^{z_{j+1}} \frac{z}{z-z_0} dz$$

$$= (z_{j+1}-z_0) \ln \left(\frac{z_{j+1}-z_0}{z_j-z_0}\right) - (z_{j+1}-z_j)$$

$$I_2 = \int_{z_j}^{z_{j+1}} \frac{z}{z-z_0} dz - \int_{z_j}^{z_{j+1}} \frac{z_j}{z-z_0} dz$$

$$= (z_{j+1}-z_j) - (z_j-z_0) \ln \left(\frac{z_{j+1}-z_0}{z_j-z_0}\right)$$

Substituting I_1 and I_2 back into (A2.4) gives

$$\int_{z_j}^{z_{j+1}} \frac{\beta(z)}{z-z_0} dz = \beta_j \left[\left(\frac{z_{j+1}-z_0}{z_{j+1}-z_j}\right) \ln \left(\frac{z_{j+1}-z_0}{z_j-z_0}\right) - 1\right]$$

$$+ \beta_{j+1} \left[\left(\frac{z_0-z_j}{z_{j+1}-z_0}\right) \ln \left(\frac{z_{j+1}-z_0}{z_j-z_0}\right) + 1\right]$$

Returning to (A2.2) and using the above result one obtains

$$i \alpha \beta(z_0) = \oint_C \frac{\beta}{z-z_0} dz$$

$$i \alpha \beta_i = \sum_{j=1}^{N} \gamma_{ij} \beta_j$$

where

$$\gamma_{i,j} = \left(\frac{z_i - z_{j-1}}{z_j - z_{j-1}}\right) \ln\left(\frac{z_j - z_i}{z_{j-1} - z_i}\right) + \left(\frac{z_{j+1} - z_i}{z_{j+1} - z_j}\right) \ln\left(\frac{z_{j+1} - z_i}{z_j - z_i}\right) \tag{A2.3}$$

This expression represents the influence coefficient for β_j at any z_j away from the control point z_i. It can be seen however that problems arise when the control point is in the neighbourhood of z_j and these special cases must be examined separately.

<u>i=j-1</u>

In this case, $\gamma_{j-1,j}$ equals the expression (A2.) in the limit as $z_i \to z_{j-1}$. The first term becomes

$$\lim_{z_i \to z_{j-1}} \left[\left(\frac{z_i - z_{j-1}}{z_j - z_{j-1}}\right) \ln\left(\frac{z_{j-1} - z_i}{z_{j+1} - z_i}\right)\right]$$

which is of the form $\lim_{z \to 0} [z \ln(1/z)] = 0$, and hence vanishes leaving only the second term

$$\gamma_{j-1,j} = \left(\frac{z_{j+1} - z_{j-1}}{z_{j+1} - z_j}\right) \ln\left(\frac{z_{j+1} - z_{j-1}}{z_j - z_{j-1}}\right)$$

<u>i=j</u>

The quantities premultiplying the ln terms in (A2.) reduce to 1 in the limit $i \to j$ leaving .

$$\gamma_{j,j} = \lim_{i \to j} \left[\ln\left(\frac{z_j - z_i}{z_{j-1} - z_i}\right) + \ln\left(\frac{z_{j+1} - z_i}{z_j - z_i}\right)\right]$$

$$= \lim_{i \to j} \left[\ln \left(\frac{z_{j+1} - z_i}{z_{j-1} - z_i} \right) \right]$$

$$= \ln \left(\frac{z_{j+1} - z_j}{z_{j-1} - z_j} \right)$$

<u>i=j+1</u>

Here $\gamma_{j+1,j}$ equals (A2.3) in the limit as $i \to j+1$. The second term becomes

$$\lim_{z_i \to z_{j+1}} \left[\left(\frac{z_{j+1} - z_i}{z_{j+1} - z_j} \right) \ln \left(\frac{z_{j+1} - z_i}{z_j - z_i} \right) \right]$$

which is of the form $\lim_{z \to 0} [z \ln(z)] = 0$, and hence vanishes leaving only the first term

$$\gamma_{j+1,j} = \left(\frac{z_{j+1} - z_{j-1}}{z_j - z_{j-1}} \right) \ln \left(\frac{z_j - z_{j+1}}{z_{j-1} - z_{j+1}} \right)$$

The lefthand side of (A2.3) has actually been taken care of when the limit was taken of $i \to j$ and is set to zero to prevent duplication, resulting in the final form for solution .

$$\sum_{j=1}^{N} \Gamma_{ij} \beta_j = 0$$

where

$$\Gamma_{ij} = \left(\frac{z_i - z_{j-1}}{z_j - z_{j-1}}\right) \ln \left(\frac{z_j - z_i}{z_{j-1} - z_i}\right) + \left(\frac{z_{j+1} - z_i}{z_{j+1} - z_j}\right) \ln \left(\frac{z_{j+1} - z_i}{z_j - z_i}\right)$$

$$= \left(\frac{z_{j+1} - z_{j-1}}{z_{j+1} - z_j}\right) \ln \left(\frac{z_{j+1} - z_{j-1}}{z_j - z_{j-1}}\right) \qquad i = j-1$$

$$= \ln \left(\frac{z_{j+1} - z_j}{z_{j-1} - z_j}\right) \qquad i = j$$

$$= \left(\frac{z_i - z_{j-1}}{z_j - z_{j-1}}\right) \ln \left(\frac{z_j - z_{j+1}}{z_{j-1} - z_{j+1}}\right) \qquad i = j+1$$

APPENDIX III

CALCULATION OF Γ_{ii} TERM

Calculation of the Γ_{ij} terms is straight forward using the Cauchy principle values for the complex logarithm function. Calculating Γ_{ii}, however, requires special attention since it contains the term $-i\alpha$ from equation (2.3) as its imaginary part. To clarify the problem Γ_{ii} can be written in polar form as

$$\ln\left(\frac{z_A}{z_B}\right) = \ln\left|\frac{z_A}{z_B}\right| + i(\theta_A - \theta_B)$$

where $(\theta_A - \theta_B)$ should equal $-\alpha$.

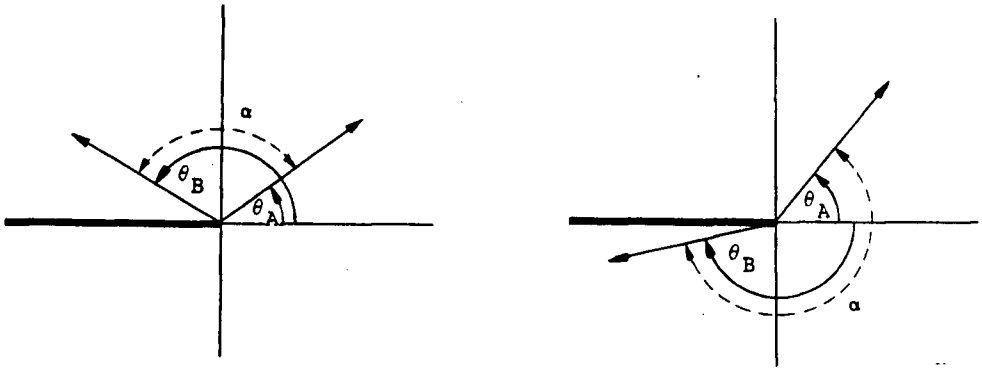

The figure on the left above shows the angle that results when the branch cut at $-\pi$ is inside α. Here $(\theta_A - \theta_B)$ erroneously yields the exterior angle. If the branch cut is outside α, as in the figure on the right, then there is no problem. In general, this error occurs whenever the

branch cut of the log function lies inside the included angle α. In these cases $2\pi i$ must be subtracted from the imaginary part of Γ_{ii}.

Alternatively, since α is by definition a positive number, an equivalent rule is that if $\mathrm{Im}(\Gamma_{ii}) < 0$ then subtract $2\pi i$ to ensure that it is equal to $-i\alpha$.

APPENDIX IV

CALCULATION OF VELOCITIES

The velocity of each point on the contour is found as

$$w = \frac{\partial \beta}{\partial z}$$

The complex potential β has been assumed piecewise linear so $\partial\beta/\partial z$ is discontinuous at each node. Provided elements are small, $\partial\beta/\partial z$ can be approximated by

$$\left(\frac{\partial \beta}{\partial z}\right)_j = a_{j-1}\beta_{j-1} + a_j\beta_j + a_{j+1}\beta_{j+1} \qquad (A4.1)$$

where the coefficients are to be determined. β_{j+1} and β_{j-1} can be written as Taylor series expansions away from β_j

$$\beta_{j-1} = \sum_{n=0}^{\infty} \frac{\beta_j^{(n)}}{n!} (z_{j-1} - z_j)^n$$

$$\beta_{j+1} = \sum_{n=0}^{\infty} \frac{\beta_j^{(n)}}{n!} (z_{j+1} - z_j)^n$$

which are then substituted into (A4.1) giving

$$\left(\frac{\partial \beta}{\partial z}\right)_j = (a_{j-1} + a_j + a_{j+1})\beta_j$$

$$+ [a_{j-1}(z_{j-1} - z_j) + a_{j+1}(z_{j+1} - z_j)]\beta'_j$$

$$+ \frac{1}{2} [a_{j-1}(z_{j-1} - z_j)^2 + a_{j+1}(z_{j+1} - z_j)^2]\beta''_j + \ldots$$

Coefficients can be equated giving three linear equations for the three unknown quantities

$$a_{j-1} + a_j + a_{j+1} = 0$$

$$a_{j-1}(z_{j-1} - z_j) + a_{j+1}(z_{j+1} - z_j) = 1$$

$$a_{j-1}(z_{j-1} - z_j)^2 + a_{j+1}(z_{j+1} - z_j)^2 = 0$$

Solution yields

$$a_{j-1} = \frac{Z_{j+1} - Z_j}{(Z_{j-1} - Z_j)(Z_{j+1} - Z_{j-1})}$$

$$a_{j+1} = \frac{Z_{j-1} - Z_j}{(Z_{j+1} - Z_j)(Z_{j-1} - Z_{j+1})}$$

$$a_j = -a_{j-1} - a_{j+1}$$

APPENDIX V

EQUATIONS FOR WAVE SIMULATION

The set of linear equations to be solved to obtain the unknown quantities X_j which are either ϕ_j or ψ_j, can be written as

$$\sum_{j=1}^{N} h_{ij} X_j = g_j$$

There are N nodal points in the contour, however, there are actually N-2 unknowns since points 1 and N2 are identical as are N3 and N4. The number of linear equations is therefore also N-2.

The actual equations are:

$1 \leqslant i \leqslant N2$

$N4 < i \leqslant N$

$$\sum_{j=1}^{N2-1} a_{ij}\psi_j + \sum_{j=N2+1}^{N3-1} (b_{ij}+b_{ik})\phi_j + \sum_{j=N3}^{N4-1} b_{ij}\phi_j$$

$$+ \sum_{j=N4+1}^{N} (a_{ik}+a_{ij})\psi_j = - \sum_{j=1}^{N2} b_{ij}\phi_j$$

$N2 < i \leq N4$

$$-\sum_{j=1}^{N2-1} b_{ij}\psi_j + \sum_{j=N2+1}^{N3-1} (a_{ij}+a_{ik})\phi_j + \sum_{j=N3}^{N4-1} a_{ij}\phi_j$$

$$-\sum_{j=N4+1}^{N} (b_{ik}+b_{ij})\psi_j = -\sum_{j=1}^{N2} a_{ij}\phi_j$$

where k represents the nodal point on the vertical boundary exactly opposite j and is equal to

$$k=N+NS+2-j$$

By periodicity the following relations also hold

$$\phi_k = \phi_j \qquad \psi_{N2} = \psi_1$$

$$\psi_k = \psi_j \qquad \phi_{N4} = \phi_{N3}$$

APPENDIX VI

CALCULATION OF ENERGY

The kinetic energy for a fluid volume is

$$E_K = \frac{\rho}{2} \int\int_{\Omega} V^2 \, dV$$

In order to evaluate this expression the volume integral must be rewritten as a contour integral involving function values on the boundary. The fluid velocity at any point can be expressed as

$$V^2 = \nabla\phi \cdot \nabla\phi$$

which can be substituted into Green's first identity

$$\int\int_{v} [\phi\nabla^2\phi + \nabla\phi \cdot \nabla\phi]dv = \int_{c} [\phi\nabla\phi] \cdot n \, ds$$

yeilding

$$= \frac{\rho}{2} \int_{c} \phi \left(\frac{\partial\phi}{\partial n}\right) ds$$

$$= \frac{\rho}{2} \int_{c} \phi \left(\frac{\partial\psi}{\partial s}\right) ds$$

$$= \frac{\rho}{2} \int_{c} \phi \, d\psi$$

Since the normal velocity component is zero on the seabed and cancels on the vertical boundaries, this integral need only be evaluated on the free surface. Considering the surface to be piecewise linear the integral becomes

$$= \frac{\rho}{2} \sum_{i=1}^{N2} \phi \, \Delta\psi$$

$$= \frac{\rho}{2} \sum_{i=1}^{N2} \left(\frac{\phi_{i+1} + \phi_i}{2}\right)(\psi_{i+1} - \psi_i)$$

which by periodicity reduces to

$$E_K = \frac{\rho}{4} \sum_{i=1}^{N2} (\phi_i \psi_{i+1} - \phi_{i+1} \psi_i)$$

The potential energy for the fluid volume is

$$E_P = \frac{\rho g}{2} \int_0^L \eta^2 \, dx$$

By considering the volume to be made up of trapezoidal sections under each element this expression becomes

$$= \frac{\rho g}{2} \sum_{i=1}^{N2} \int_{x_i}^{x_{i+1}} y^2 \, dx$$

$$= \frac{\rho g}{2} \sum_{i=1}^{N2} \left[\frac{y^3}{3}\right]_{x_i}^{x_{i+1}} \frac{\Delta x}{\Delta y}$$

yielding finally

$$E_P = \frac{\rho g}{6} \Sigma (x_i - x_{i+1})(y_{i+1}y_i + y_{i+1}^2 + y_i^2)$$

Again only free surface values are required.

The floating body kinetic energy includes both translational and rotational contributions. Potential energy can be measured from any arbitrary datum with the still water level being chosen for convenience. The total body energy is therefore

$$E_B = \frac{m}{2} (u_G^2 + v_G^2) + \frac{I}{2} \dot{\theta}^2 + mg\, y_G$$

APPENDIX VII

CALCULATION OF BODY BOUNDARY CONDITIONS

The position and velocities of the body are assumed known at each time step hence the velocity component normal to the body can be written as

$$v_n = \frac{\partial \phi}{\partial n} = \frac{\partial \psi}{\partial s}$$

This expression is then integrated numerically to determine ψ as

$$\psi = \int_s v_n \, ds + \psi_o$$

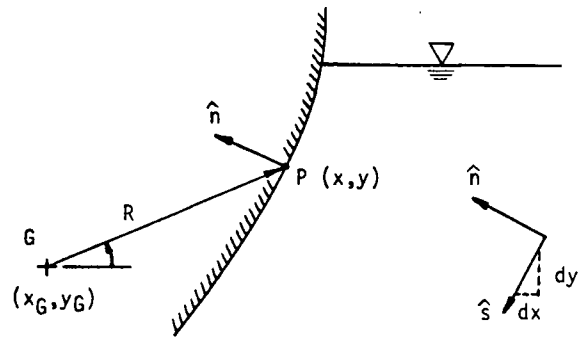

The normal velocity component V_n is found as follows. The velocity of a point P on the hull is

$$\vec{v}_p = \vec{v}_G + \vec{v}_{P/G}$$

where

$$\vec{v}_G = u_G i + v_G j$$

$$\vec{v}_{P/G} = \dot{\theta}\ k \times \vec{R}$$

$$\vec{R} = (x-x_G)i + (y-y_G)j$$

The unit normal vector $\hat{n} = k \times \hat{s}$ where

$$\hat{s} = \frac{dx\ i + dy\ j}{ds}$$

The velocity at P is therefore

$$\vec{v}_p = \{u_G\ i + v_G\ j\} + \dot{\theta}\ [-(y-y_G)i + (x-x_G)]] \qquad (A7.1)$$

and the normal component is

$$\frac{\partial \psi}{\partial s} = \vec{v}_p \cdot \hat{n}$$

The stream function is found by integrating

$$d\psi = u_G\ dy - v_G\ dx - \dot{\theta}[(y-y_G)dy + (x-x_G)dx]$$

to finally obtain

$$\psi = -\frac{\dot{\theta}R^2}{2} + u_G(y-y_G) - v(x-x_G) + \psi_o \qquad (A7.2)$$

where

$$R^2 = (x-x_G)^2 + (y-y_G)^2$$

For time stepping purposes the time derivative $\partial\psi/\partial t$ is needed. Equation (A7.2) represents ψ on the moving fluid boundary so the material derivative must be taken following the fluid particles.

$$\frac{D\psi}{Dt} = (y-y_G)a_x - (x-x_G)a_y - \frac{\ddot{\theta}R^2}{2}$$

$$+ u_G \frac{D}{Dt}(y-y_G) - v_G \frac{D}{Dt}(x-x_G)$$

where

$$\frac{D}{Dt}(x-x_G) = \frac{Dx}{Dt} - u_G = -\dot{\theta}(y-y_G)$$

$$\frac{D}{Dt}(y-y_G) = \frac{Dy}{Dt} - v_G = \dot{\theta}(x-x_G)$$

The last step was obtained by referring to equation (A7.1) since Dx/Dt and Dy/Dt are just the velocity components of points on the boundary V_P. Therefore,

$$\frac{D\psi}{Dt} = (y-y_G)a_x - (x-x_G)a_y - \frac{\ddot{\theta}R^2}{2}$$

$$+ \dot{\theta}[u_G(x-x_G) + v_G(y-y_G)]$$

For applying a boundary condition in the numerical solution,

however, the derivative is needed as seen by the instantaneous boundary. That is,

$$\frac{\partial \psi}{\partial t} = \frac{D\psi}{Dt} - v \cdot \nabla\psi$$

where the advective term in this case is due to motion of the rigid body and its velocity must be used for v giving

$$\nabla\psi = (\frac{\partial \psi}{\partial x})i + (\frac{\partial \psi}{\partial y})j = -v\ i + u\ j$$

$$v = [u_G - \dot{\theta}(y-y_G)]i + [v_G + \dot{\theta}(x-x_G)]j$$

Completing the algebra yields for the final boundary condition

$$\frac{\partial \psi}{\partial t} = (y-y_G)a_x - (x-x_G)a_y - \frac{\ddot{\theta}R^2}{2}$$

$$+ u_G v - v_G u + [(x-x_G)(u_G-u) + (y-y_G)(v_G-v)]\dot{\theta}$$

APPENDIX VIII

CALCULATION OF BODY FORCES AND MOMENTS

The body force vector is determined by integrating the pressures over the wetted hull as

$$F = -\int_s P\,\hat{n}\cdot ds$$

or, for numerical evaluation, as the sum of the contributions over each element.

$$F = -\sum_s P\,\hat{n}\,\Delta s$$

The pressure is taken as the average of the values at the bounding nodal points and acts in the directon normal to the hull.

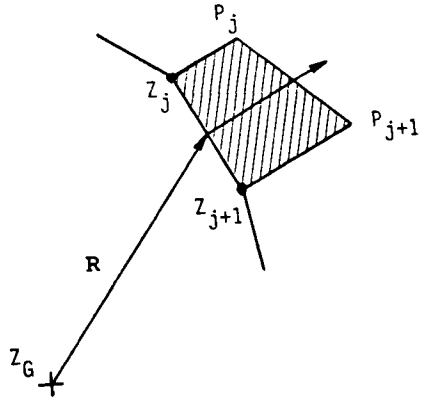

The unit normal vector is found $\hat{n} = i\hat{s}$ where

$$\hat{s} = \frac{\Delta z}{\Delta s}$$

The total force $F_x + iF_y$ can therefore be computed as

$$F = - \sum_{i=N5}^{N6-1} i\left(\frac{P_{i+1}-P_i}{2}\right)(z_{i+1}-z_i)$$

The moment acting on the hull about G is equal to

$$M = - \int_s P\, r x \hat{n}\, ds$$

where the pressure over each element is again taken as the average of the bounding nodal values and considered to act at the centroid of the pressure distribution. $\bar{R}$ is the radius vector from G to the body surface point where the pressure is acting

$$M = - \sum_s P(r \times \hat{n})\Delta s$$

The cross product is evaluated by considering $\bar{R}$ and $\hat{n}$ to be complex numbers and using the identity $Z_A \times Z_B = Im(Z_A^* Z_B)$. The moment is therefore computed as

$$M = - \sum_{i=N5}^{N6-1} \left(\frac{P_{i+1}-P_i}{2}\right) I_m\left\{i\left(\frac{z_{i+1}-z_i}{2} - z_G\right)(z_{i-1}-z_i)^*\right\}$$

APPENDIX IX

EQUATIONS FOR BODY MOTION SIMULATION

The set of linear equations used in version III of the body motion simulation are given below. In this version both ϕ and ψ are specified at the intersection points N5 and N6 hence there are two less unknowns than in the wave simulation. The stream function on the seabed is an unknown constant evaluated at N3. There are consequently N-3 equations.

The actual equations are:

$1 \leqslant i < N5$

$N5 < i \leqslant N2$

$N4 < i \leqslant N$

$i = N3$

$$\sum_{j=1}^{N5-1} a_{ij}\psi_j + \sum_{j=N5+1}^{N6-1} b_{ij}\phi_j + \sum_{j=N6+1}^{N2-1} a_{ij}\psi_j$$

$$+ \sum_{j=N2+1}^{N3-1} (b_{ij}+b_{ik})\phi_j + \sum_{j=N3}^{N4-1} b_{ij}\phi_j + \sum_{j=N4+1}^{N} (a_{ik}+a_{ij})\psi_j + \sum_{j=N3}^{N4-1} a_{ij}\psi_{N3}$$

$$= -\sum_{j=1}^{N5} b_{ij}\phi_j - \sum_{j=N5}^{N6} a_{ij}\psi_j - \sum_{j=N6}^{N2} b_{ij}\phi_j$$

$\underline{N5 < i < N6}$

$\underline{N2 < i < N3}$

$\underline{N3 \leqslant i < N4}$

$$- \sum_{j=1}^{N5-1} b_{ij}\psi_j + \sum_{j=N5+1}^{N6-1} a_{ij}\phi_j - \sum_{j=N6+1}^{N2-1} b_{ij}\psi_j$$

$$+ \sum_{j=N2+1}^{N3-1} (a_{ij}+a_{ik})\phi_j + \sum_{j=N3}^{N4-1} a_{ij}\phi_j - \sum_{j=N4+1}^{N} (b_{ik}+b_{ij})\psi_j - \sum_{j=N3}^{N4-1} b_{ij}\psi_{N3}$$

$$= - \sum_{j=1}^{N5} a_{ij}\phi_j + \sum_{j=N5}^{N6} b_{ij}\psi_j - \sum_{j=N6}^{N2} a_{ij}\phi_j$$

where k represents the nodal point on the vertical boundary exactly opposite j and in this case is equal to

$$k=N+NS+NH+2-j$$

By periodicity the following relations also hold

$$\phi_k = \phi_j \qquad \psi_{N2} = \psi_1$$

$$\psi_k = \psi_j \qquad \phi_{N4} = \phi_{N3}$$

The stream function on the seabed is a constant evaluated at N3 so

$$\psi_j = \psi_{N3} \qquad j = N3,\ N4$$

APPENDIX X

NUMERICAL PERTURBATION CORRECTION

The control volume energy for the first approximate solution is E and the volume is $\forall$. The two intersection points are then displaced upward on the body by Δy_L and Δy_R resulting in new values for the energy and volume of E' and $\forall'$. The total change in energy including the known change in body energy is

$$\Delta E = \Delta E_B + \Delta E_K + \Delta E_P$$

while the change in volume is

$$\Delta V = V' - V$$

The problem is to find the position corrections Δy_L and Δy_R required to offset the errors in energy and volume resulting from the numerical solution at each time step. The two elements adjacent to the body are adjusted accordingly.

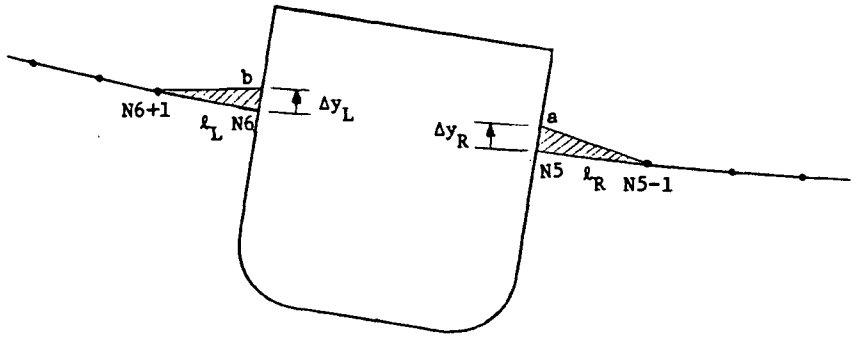

Referring to the above figure the change in volume is the area of the two triangles

$$\Delta V = \frac{1}{2}(\ell_R \Delta y_R + \ell_L \Delta y_L)$$

where l_L and l_R are the left and right element lengths. This is the first constraint. Using equation (3.8)

$$E_P = \frac{\rho g}{6} \sum_{i=1}^{N2} (x_i - x_{i+1})(y_{i+1} y_i + y_{i+1}^2 + y_i^2)$$

the potential energy for the preliminary configuration can be expanded and subtracted from the expansion for the displaced configuration. The difference is then

$$\Delta E_P = \frac{\rho g}{6} \{(3\ \ell_R\ y_{N5})(\Delta y_R) + \ell_R(\Delta y_R)^2$$

$$+ (3\ \ell_L\ y_{N6})(\Delta y_L) + \ell_L(\Delta y_L)^2\}$$

Similarly, using equation (3.7)

$$E_K = \frac{\rho}{4} \sum_{i=1}^{N2} (\phi_i \psi_{i+1} - \phi_{i+1} \psi_i)$$

the kinetic energy before displacement is subtracted from the expression resulting after displacement. By using the following Cauchy Riemann approximations

$$\frac{\phi_a - \phi_{N5}}{\Delta y_R} = \frac{\psi_{N5} - \psi_{N5-1}}{\ell_R}$$

$$\frac{\psi_a - \phi_{N6}}{\Delta y_R} = \frac{\phi_{N5-1} - \phi_{N5}}{\ell_R}$$

$$\frac{\phi_b - \phi_{N6}}{\Delta y_L} = \frac{\psi_{N6+1} - \psi_{N6}}{\ell_L}$$

$$\frac{\psi_b - \psi_{N6}}{\Delta y_L} = \frac{\phi_{N6+1} - \phi_{N6}}{\ell_L}$$

and carrying out the algebra, the difference works out to

$$\Delta E_K = \frac{\rho}{4}\left\{\frac{\Delta y_R}{\ell_R}\left[\phi^2_{N5-1} - \phi^2_{N5} + (\psi_{N5} - \psi_{N5-1})^2\right]\right.$$

$$\left. + \frac{\Delta y_L}{\ell_L}\left[\phi^2_{N6} - \phi^2_{N6+1} + (\psi_{N6+1} - \psi_{N6})^2\right]\right\}$$